Basic Study on Long-Span Bridge Management System by means of Reliability Analysis(Dissertation_全文)

AUTHOR(S):

Yamada, Ikuo

BASIC STUDY ON LONG-SPAN BRIDGE MANAGEMENT SYSTEM BY MEANS OF RELIABILITY ANALYSIS

by

Ikuo Yamada

January 20, 2005

Acknowledgement

I am deeply indebted to Professor Eiichi Watanabe, my Doctor adviser for his constant encouragement, friendship and guidance throughout my research studies associated with the reliability analysis in bridge engineering.

I would like to express my appreciation to Honorary Professor Yoshiji Niwa for his constant concerns and suggestions about my research after graduation of Kyoto University in 1983.

Also, I would to like to express my appreciation to Professor Masaru Matsumoto and Professor Hirokazu Iemura for their encouragement and advice.

Finally, I want to thank my wife Junko and two daughters Mariko and Minako for their patience.

Contents

Appendix

1. Introduction

1.1 Overview and Objectives

Long-span bridges, including suspension bridges, consist of various members and have a high degree-of-freedom. Generally, safety factor is determined, considering the importance and feature of each member on those bridges. For instance, the suspension bridge consists of stiffening girder, main towers and main cables. Usually, the safety factors are 1.7 for stiffening girder and main towers against the yield stress or buckling stress, and 2.5 for main cables against the tensile stress, respectively.

In the maintenance for long-span bridges, the preventive maintenance works are carried out, considering the importance of structures. For instance, repaint works for steel structures and coating works for concrete structures are generally used. However, health on structural members is conventionally evaluated by results of visual checks or coating inspections. In this manner, health on overall system is not evaluated by a quantitative method nor predicted.

Therefore, the aim of this study is to analyze the structural safety of the long-span bridges by the reliability analysis, to evaluate the health the long-span bridges, and to examine the preventive maintenance in consideration of the life-cycle cost.

1.2 Organization of the Study

Firstly, short-span bridges, which are geometrically linear systems, are calculated by reliability analysis, considering the time-dependence on strength and load. Based on these results, reliability indexes on representative members are obtained, and long-term safety are evaluated for steel bridges with statically determinate structures.

Secondly, long-span bridges, which are geometrically nonlinear systems, are calculated by reliability analysis, considering the time-dependence on strength and load. Based on these results, the reliability indices on various members are obtained, and long-term safety are evaluated for steel bridges with statically indeterminate structures.

Finally, the conventional bridge management system, which is identified with essential maintenance, is replaced and a new bridge management system, which is identified with a quantitative and preventive maintenance by reliability analysis, is proposed, based on the results of long-term reliability analyses associated with the long-span bridges.

2. Structural Reliability Analysis

2.1 Introduction

Nature contains randomness and human knowledge involves uncertainty. In order to overcome this difficulty, basic and advanced studies on reliability analysis have been continued since the twenty century.

The Classical Reliability theory for structures was introduced by Freudental in 1940s, and the Extended Reliability theory was introduced by A.H-S.Ang in 1960s. The Second Moment method was proposed by C.A.Cornell in 1960s. Moreover, the Monte Carlo techniques and Fuzzy Set theory were developed in 1980s. The history of structural reliability is shown in Table 2.1.

In this chapter, basic techniques of structural reliability analysis are reviewed.

Table 2.1 History of structural reliability

Year	Establishment	Random Vibration	System Stochasticity
1940s	Probabilistic load and strength		Freudental
1950s	Full-distribution theory	Random excitation and response	
1960s	FOSM Methods (First Order Second Moment Methods)	Stationary → Non-stationary; SDOF→ MDOF	Spatial variability of material properties and strength
1970s	AFOSM Method (Advanced FOSM)	Linear →Nonlinear	Monte Carlo Techniques
1980s	Randomness and Uncertainty; Fuzzy Set Theory; Human Error; Risk Assessment ANS158.1A-1982 PRA and Margin Study	Monte Carlo Techniques; System identification	Stochastic Finite Element Analysis

2.2 Reliability Analysis

In general, the reliability analysis, which is featured by the reliability index and the probability of failure, can be given in the following process.

Expressing that S is the load on the structure and R is the resistance of the structure, the probability of failure P_f is given as the following equations. (Fig. 2.1)

$$P_f = P\ (S > R) = P\ (R/S < 1)$$

$$= \int_{-\infty}^{\infty} g_S(\eta)d\eta \int_{-\infty}^{\eta} f_R(\xi)d\xi \quad \cdots\cdots (2.1)$$

$$= \int_{-\infty}^{\infty} g_S(\eta)F_R(\eta)d\eta \quad \cdots\cdots (2.2)$$

Or

$$P_f = \int_{-\infty}^{\infty} f_R(\xi)d\xi \int_{\xi}^{\infty} g_S(\eta)d\eta \quad \cdots\cdots (2.3)$$

$$= \int_{-\infty}^{\infty} f_R(\xi)[1-G_S(\xi)]\ d\eta \quad \cdots\cdots (2.4)$$

where, f_R is the density function of resistance, F_R is the cumulative function of resistance, g_S is density function of load, G_S is cumulative density function of load.

The probability of safety P_s or the probability of reliability P_r is expressed as follows.

$$P_s = P_r = P\ (R/S \geqq 1)$$

$$= 1 - P_f \quad \cdots\cdots (2.5)$$

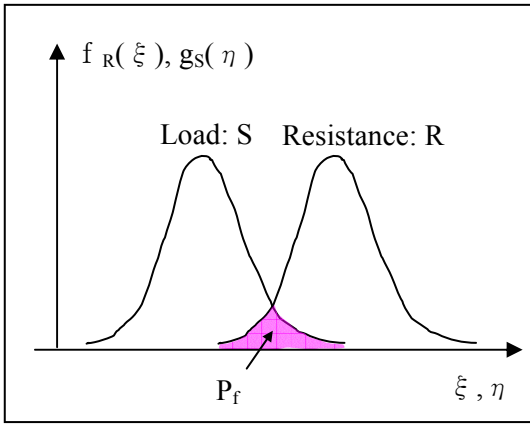

Fig.2.1 Probability density function of load and resistance

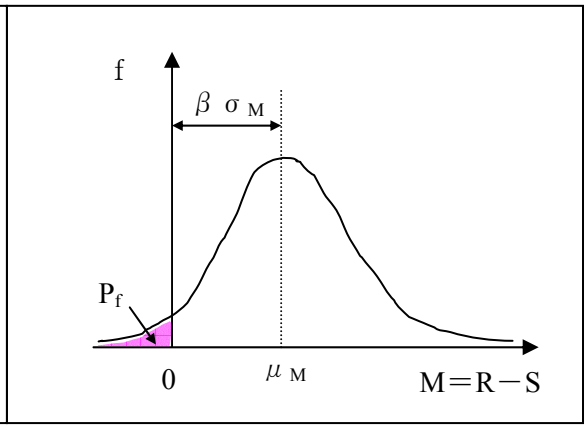

Fig.2.2 Relation between marginal distribution M and reliability index β

The reliability index β is expressed by using the marginal distribution M, which equal to R－S, can be expressed as follows.(Fig. 2.2)

$$\mu_M = \beta \sigma_M \quad \cdots\cdots (2.6)$$

Or

$$\beta = 1 / (\sigma_M / \mu_M) = 1 / \delta_M \quad \cdots\cdots (2.7)$$

where, β is reliability index, μ_M is average of marginal distribution, σ_M is standard deviation of marginal distribution, and δ_M is coefficient of variation of marginal distribution.

Assuming that the resistance and load are independent and have the normal distributions, the probability of failure is given by the Second Moment Method as follows.

$$P_f = \frac{1}{\sqrt{2\pi}} \int_{\frac{\mu R - \mu S}{\sqrt{\sigma R^2 + \sigma S^2}}}^{\infty} \exp(-\frac{t^2}{2}) dt \quad \cdots\cdots (2.8)$$

The reliability is given as follows.

$$P_r = 1 - P_f$$

$$= \frac{1}{\sqrt{2\pi}} \int_{-\infty}^{\frac{\mu R - \mu S}{\sqrt{\sigma R^2 + \sigma S^2}}} \exp(-\frac{t^2}{2}) dt \quad \cdots\cdots (2.9)$$

where, μ_R is the average of resistance R, μ_S is the average of load S, σ_R is coefficient of variation of resistance R, and σ_S is coefficient of variation of load S.

The central average γ_0 can be expressed

$$\gamma_0 = \frac{\mu_R}{\mu_S} = \frac{1 - k_{pf} \sqrt{\delta_R^2 + \delta_S^2 + \delta_R^2 \delta_S^2 k_{pf}^2}}{1 - \delta_R^2 k_{pf}^2} \quad \cdots\cdots (2.10)$$

where, δ_R is coefficient of variation of resistance R, δ_S is coefficient of variation of load S, and k_{pf} is $\phi^{-1}(1 - P_f)$.

Assuming that the resistance and load are independent and have the normal distributions, the reliability index can be expressed as follows.

$$\beta = \frac{\mu_R - \mu_S}{\sqrt{\sigma_R^2 + \sigma_S^2}} \quad \cdots\cdots (2.11)$$

$$= \frac{\gamma_0 - 1}{\sqrt{\gamma_0 \delta_R^2 + \delta_S^2}} \quad \cdots\cdots (2.12)$$

2.3 System Reliability Analysis

2.3.1 Material Modeling

The material behavior in structural engineering can be classified to a) elastic, b) elastic-brittle, c) elastic-plastic, d) elastic-residual strength, e) elastic-hardening, f) curvilinear (inelastic). In design for the structure, the steel members and the concrete members are usually assumed to a) elastic, c) elastic-plastic or f) curvilinear.

In this paper, the small damages in each structural element, including the local yield or the local buckling, are focused on, the material behavior is assumed to be an elastic model in the structural reliability analysis.

2.3.2 System Modeling

(1) Series systems

In general, a statically determinate structure is a series system since the failure of any one of its members implies the failure of the structure. Therefore, each member in the series system is a possible failure mode. A typical example of series systems is a "chain," which is also called a "weakest link" system (Fig.2.3). The system failure probability for a weakest link which is composed of *m* members is given by

$$P_f = P(F_1 \cup F_2 \cup F_3 \cup \ldots \cup F_m) = \int_{D \in X} \ldots \int f_X(x)dx \quad \cdots\cdots\cdots\cdots\cdots\cdots\cdots\cdots \quad (2.13)$$

where F_i (i=1,m) is each failure mode, X represents the vector of all basic random variables and D is the domain in X defining failure of the system.

On the other hand, if the safe (or survival) region is denoted $\bar{D}$, the probability of survival for a weakest link structure which is composed of *m* members is given by

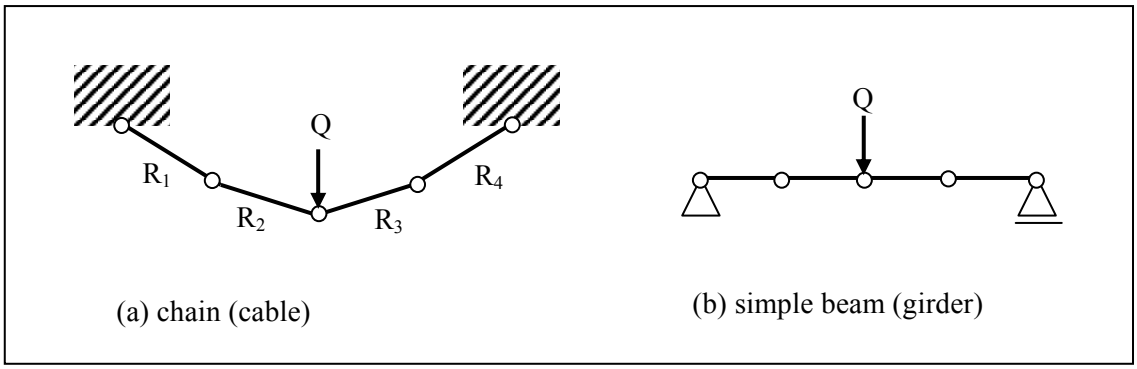

(a) chain (cable) (b) simple beam (girder)

Fig. 2.3 Examples of series systems

$$P_s = P(\bar{F}_1 \cap \bar{F}_2 \cap \bar{F}_3 \cap \ldots \cap \bar{F}_m) = \int_{\bar{D}} \ldots \int f_X(x)dx \quad \cdots\cdots\cdots\cdots\cdots\cdots\cdots\cdots\cdots\cdots \quad (2.14)$$

If $F_{Ri}(r_i)$ is the cumulative distribution function for strength of the *i*-th link, then the cumulative distribution function for a chain as a whole system is given by

$$F_R(r) = P(R \leqq r) = 1 - P(R > r) = 1 - P(R_1 > r_1 \cap R_2 > r_2 \cap \cdots \cap R_m > r_m) \quad \cdots\cdots\cdots\cdots \quad (2.15)$$

which becomes for independent strength properties

$$F_R(r) = P(R \leqq r) = 1 - [1 - F_{R1}(r_1)][1 - F_{R2}(r_2)] \ldots [1 - F_{Rm}(r_m)] = 1 - \prod_{i=1}^{m} [1 - F_{R_{1i}}(r_i)] \quad \cdots\cdots\cdots \quad (2.16)$$

(2) Parallel systems

The structural system, which has the elements in the system are so interconnected that the limit state in any one or more elements does not necessarily mean the failure of the whole system, is called a “parallel” or “redundant” system (Fig.2.4).

The system failure probability for a parallel system which is composed of *n* members is given by

$$P_f = P(F_1 \cap F_2 \cap F_3 \cap \ldots \cap F_n) = \int_{D_1 \in X} \ldots \int f_X(x)dx \quad \cdots\cdots\cdots\cdots\cdots\cdots\cdots\cdots\cdots\cdots \quad (2.17)$$

The parallel system can fail only when all contributory elements have reached their limit states, which means the characteristics of the system elements are considerable important to define the “system failure.”

In a complicated parallel system, it is very difficult to evaluate the failure mode and the probability of failure. Consequently, in this paper, the small damages in each element are focused on , assuming an elastic model in the structural reliability analysis.

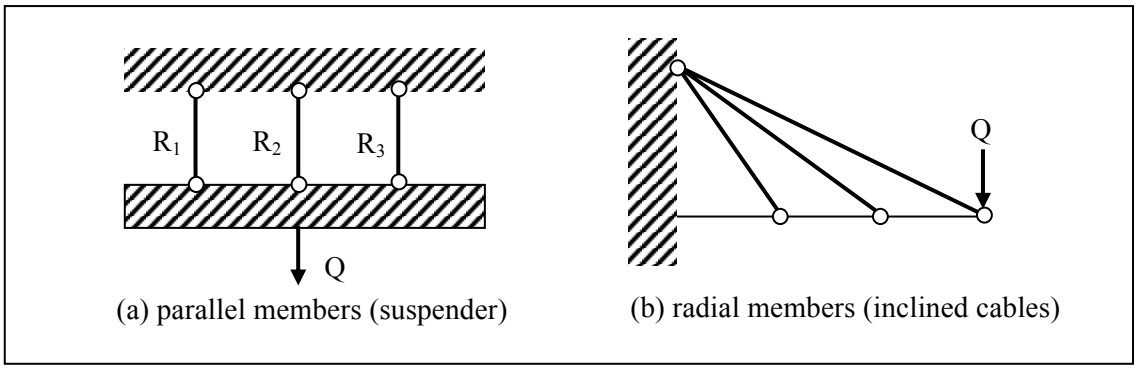

(a) parallel members (suspender) (b) radial members (inclined cables)

Fig. 2. 4 Examples of parallel systems

2.4 Monte Carlo Simulation

One of the most effective calculation methods is the Monte Carlo analysis in order to perform a statistical analysis of the uncertainty in structural engineering problems. It is often helpful to use the Monte Carlo analysis as an experiment, which is performed by a computer rather than by a laboratory

The fundamental step in the Monte Carlo analysis is to make a set of random numbers. Today, these numbers can be mechanically or electronically generated by using digital personal computers. Uniform random numbers have the property so that the generated number equally occurs anywhere in the selected range of values (e.g., 0.0-1.0). These random number can be used for any range of uniform probability density function (hereafter referred to as PDF) if scaled properly. These random number can be transformed to any distribution, including the normal distribution, the log-normal distribution, etc.

The uniform PDF is defined as follows. The general shape is shown in Fig.2.5.

$$\left.\begin{array}{ll} p(x) = 1/(b-a) & a \leqq x \leqq b \\ = 0 & \text{otherwise} \end{array}\right\} \quad \cdots\cdots\cdots\cdots\cdots\cdots\cdots\cdots\cdots\cdots\cdots\cdots \quad (2.18)$$

The normal PDF is defined as follows, and is shown in the Fig.2.6.

$$p(x) = \frac{1}{\sigma_x \sqrt{2\pi}} \exp\left\{ -\frac{1}{2}\left(\frac{x-\mu_x}{\sigma_x} \right)^2 \right\} \quad \cdots\cdots\cdots\cdots\cdots\cdots\cdots\cdots\cdots\cdots\cdots\cdots \quad (2.19)$$

where μ_x is the mean value, and σ_x is the standard deviation.

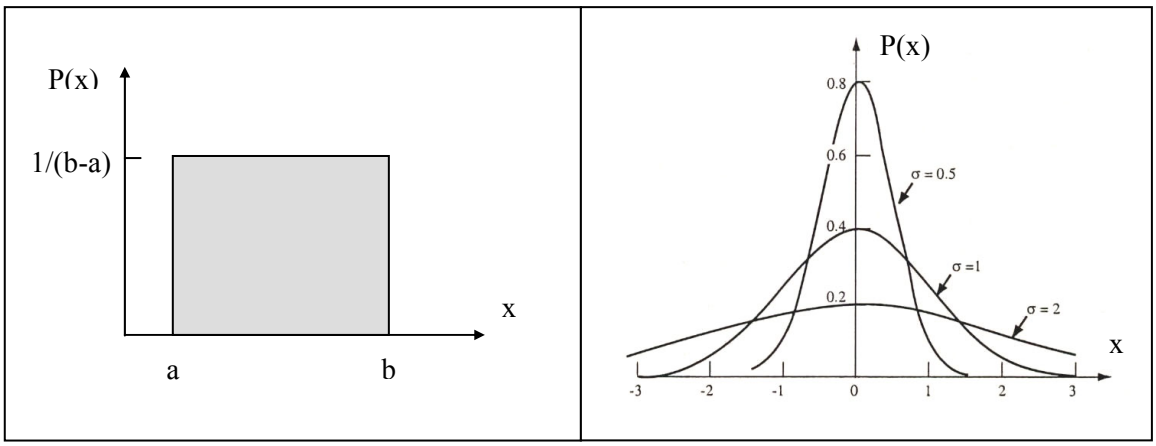

Fig.2.5 Uniform probability density function Fig.2.6 Normal probability density function

As an example of the Monte Carlo analysis, consider a simply supported beam shown in Fig.2.7 with a concentrated loading at the midspan and a distributed loading at the full span. From the fundamental knowledge of the structural engineering, the flexural stress at the midspan of the beam can be given as follows.

$$\sigma = PL/(4W) + qL^2/(8W) \quad \cdots\cdots (2.20)$$

where σ : flexural stress at midspan of the beam

P: concentrated load (variable)

q: distributed load (constant)

L: length of beam

W: modulus of section

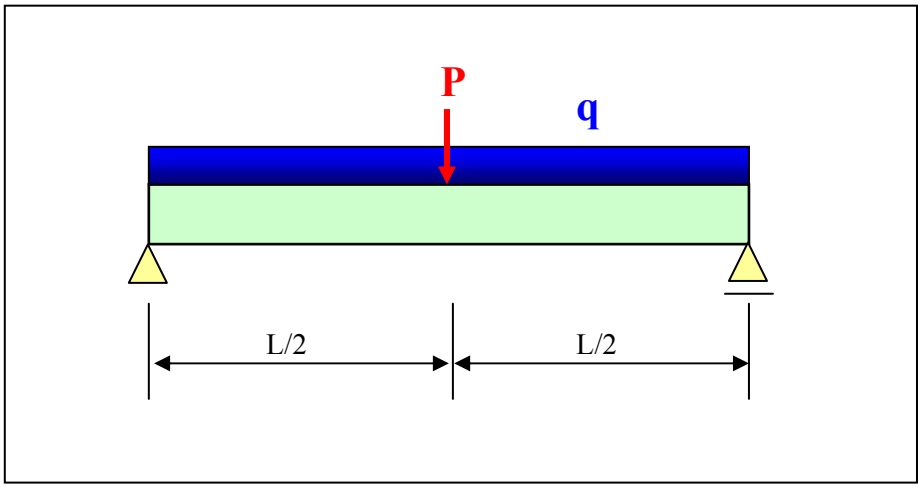

Fig. 2.7 Simply supported beam applied to a concentrated load at midspan and distributed load at full span

Fig.2.8 shows the flowchart for the Monte Carlo analysis of simply supported beam with one random variable. The Monte Carlo analysis involves the generation of one set of n random numbers for each random parameter in the response equation. The response equation is then solved by using each random number in the set. The response equation is solved n times, whichever the response equation is linear or nonlinear with respect to the variables. Finally, these values of response are analyzed by using the techniques, including histograms and sample statistics.

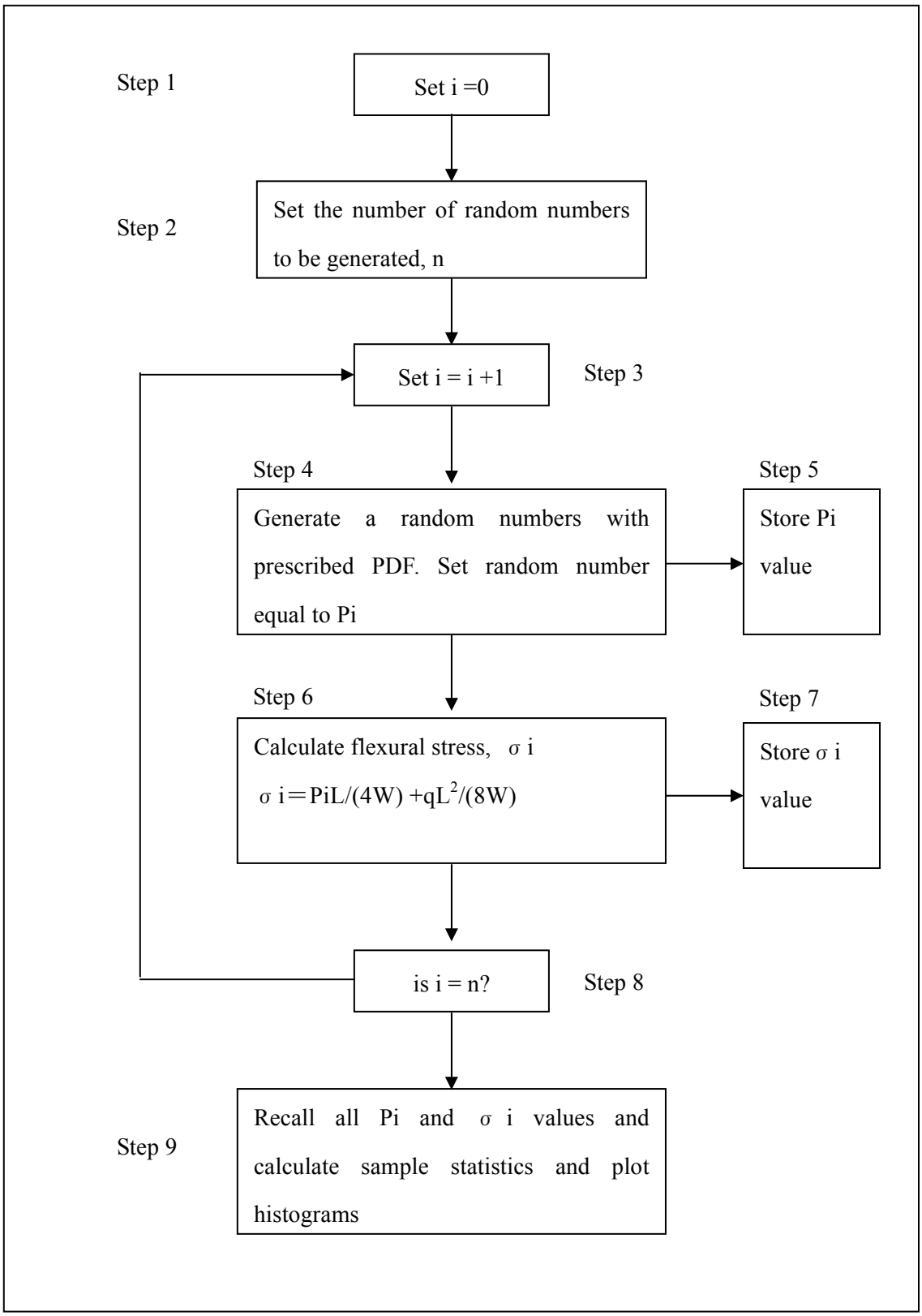

Fig. 2.8 Flowchart for the Monte Carlo analysis of simply supported beam with one random variable

2.5 Example of Analytical Computation

By using the same structural model as Fig.2.7 and the same techniques as Fig. 2.8, the reliability analysis can be performed. The example of analytical computation is shown in Fig. 2.9-2.12.

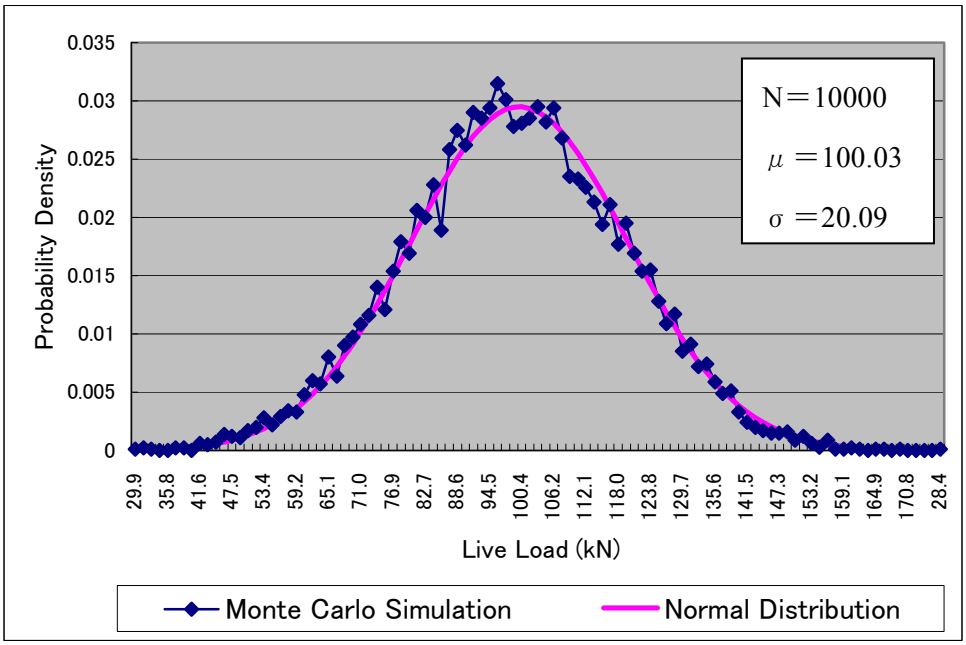

Fig. 2.9 Generated live load by Monte Carlo simulation

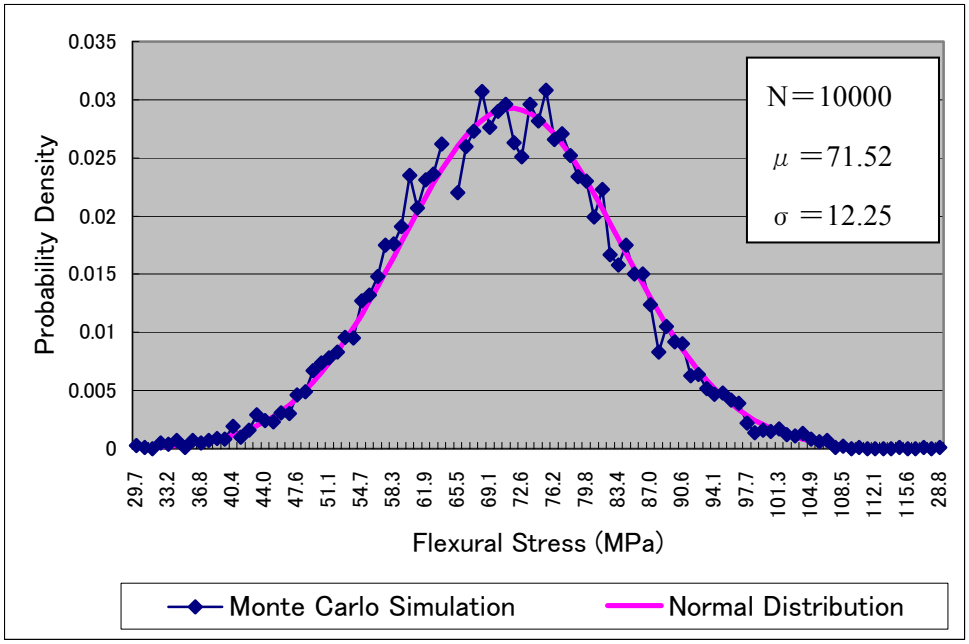

Fig. 2.10 Calculated flexural stress of beam by Monte Carlo simulation

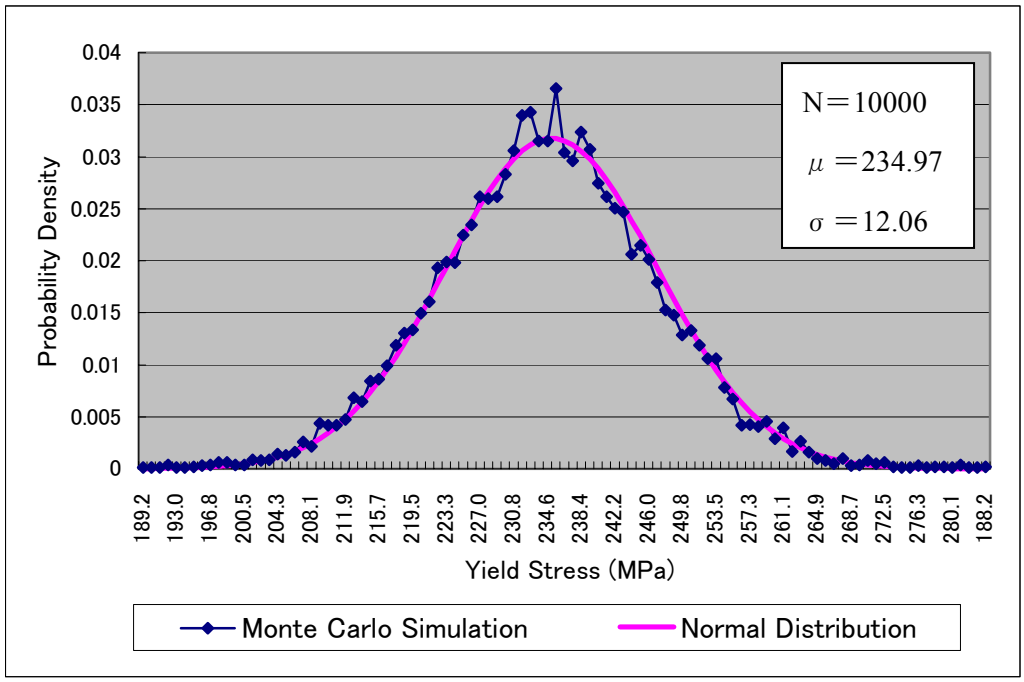

Fig. 2.11 Generated yield stress of by Monte Carlo simulation

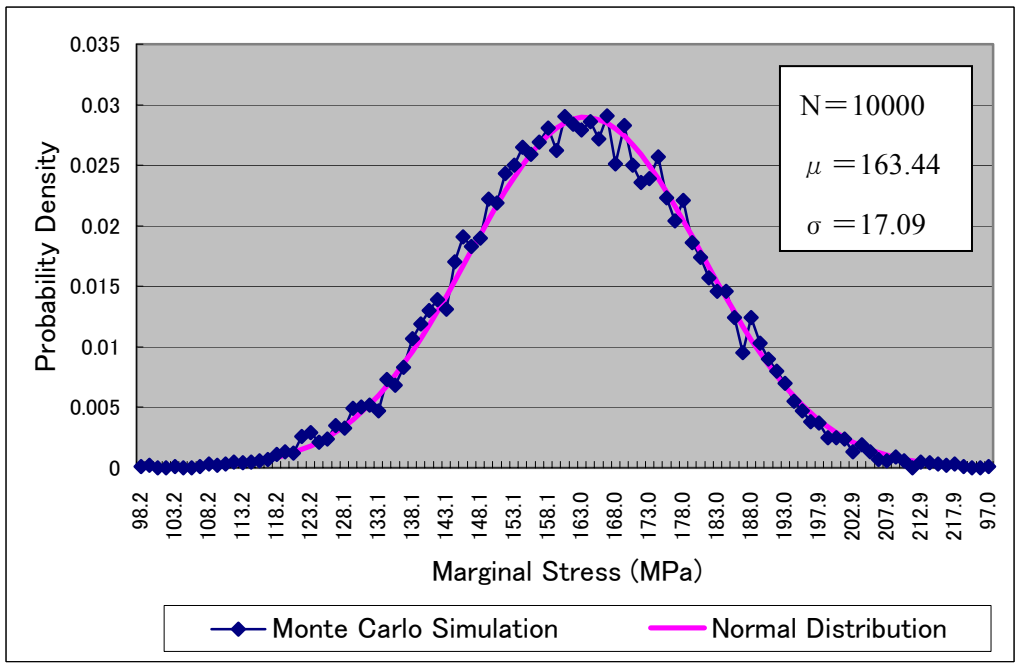

Fig. 2.12 Calculated marginal stress of beam by Monte Carlo simulation

2.6 Summary

The basic theory of reliability analysis was reviewed in this chapter. Especially, the Monte Carlo techniques is very convenient for reliability analysis even if the function has a complicated distribution, since the computer easily generates a lot of random numbers.

This technique can be used in the reliability analysis for various bridges, including the long-span bridges.

3. Time-dependence on Load and Strength

3.1 Introduction

In Japan, design loads are classified dead load, live load, impact, effect of thermal change, effect of earthquake and wind force in the Design Specification for Highway Bridges, which is hereafter referred to as “DSHB.”

In this chapter, the live load and the wind force are considered to be variable in time. On the other hand, steel structures and concrete structures are considered to be variable in time because of material deterioration.

3.2 Increasing Model for Live Load

The live load is mainly discussed since the live load is one of the most influent to superstructure of bridges and one of the most variable when time passes.

There is little data for traffic conditions on the Honshu-Shikoku Highways between Honshu Island and Shikoku Island in Japan. The first traffic investigation was carried out on the Seto-Ohashi Bridges for a weekday and a weekend in 1990, two years after completion of these bridges. All vehicles are classified to 22 vehicles. As the primary classification, the traffic volumes on the investigation days were 60 passenger cars (2.1%), 177 small trucks (6.3%), 1922 ordinary trucks (68.5%), 225 large trucks (8.0%), and 423 buses (15.1%).

Especially, the axis distributions and the vehicle weight distributions of the ordinary trucks are shown in Table 3.1 and 3.2, respectively. The ordinary trucks are secondarily classified to 9 trucks according to the number plates and the axis number. In the ordinary trucks, the middle class 3 (total weight of 8-20 tons, with 3 axes) was selected as the representative vehicle because it has a significant number of data, the maximum average of axis weight and the maximum average/standard deviation of total weight. The weight distribution of the middle truck 3 is shown in Fig.3.1. The weight distribution is similar to the normal distribution, which has the average of 16.4 tons, standard deviation of 4.2 tons, and the coefficient of variation of 0.25.

In 1994, the DSHB was revised and the design live load was changed in order to take countermeasure against the enlargement of vehicles and to enhance the durability of bridges.

Currently, the live load B, which constitutes of the load T for decks and the load L for girders, is applied to the first class bridges on national highways.

Fig.3.2 shows the change of the design live load for the first class bridges, which is specified in the DSHB from 1926 to 2002. According to the social and economical development of Japan, the design live load for highway bridges has increased and expected to increase in future. Therefore, the long-term change of the live load is one of the most important issues for maintenance of highway bridges. In this paper, the long-term change is referred to as "time-dependent load."

Table 3.1 Axis distributions of ordinary trucks on the Seto-Ohashi Bridges in 1990

(Unit: ton)

No.	Vehicle Type	Axis	Data	Average	S. Deviation	Minimum	Maximum
9	Ordinary Truck (small 2)	2	1238	3.01	1.381	1.0	12.2
10	Ordinary Truck (small 3)	3	90	4.86	1.794	1.8	11.1
11	Ordinary Truck (small 4)	4	24	3.33	0.850	2.2	5.2
12	Ordinary Truck (middle 2)	2	170	4.02	1.838	1.2	12.4
13	Ordinary truck (middle 3)	3	2973	5.45	2.049	1.0	15.9
14	Ordinarry truck (middle 4)	4	672	4.20	1.501	1.0	12.4
15	Ordinarry truck (middle 5)	5	0	0.00	0.000	0.0	0.0
16	Ordinarry truck (large 4)	4	80	4.51	2.164	1.4	11.6
17	Ordinary truck (large 5)	5	15	4.07	0.647	3.3	5.5

Table 3.2 Weight distributions of ordinary trucks on the Seto-Ohashi Bridges in 1990

(Unit: ton)

No.	Vehicle Type	Axis	Data	Average	S. Deviation	Minimum	Maximum
9	Ordinary Truck (small 2)	2	619	6.01	2.265	2.0	15.8
10	Ordinary Truck (small 3)	3	30	14.57	3.885	7.0	24.1
11	Ordinary Truck (small 4)	4	6	13.33	2.273	10.3	16.1
12	Ordinary Truck (middle 2)	2	85	8.05	2.900	2.8	17.7
13	Ordinary truck (middle 3)	3	991	16.35	4.136	6.8	31.5
14	Ordinarry truck (middle 4)	4	168	16.81	4.363	7.7	34.8
15	Ordinarry truck (middle 5)	5	0	0.00	0.000	0.0	0.0
16	Ordinarry truck (large 4)	4	20	18.03	7.231	7.4	37.5
17	Ordinary truck (large 5)	5	3	20.33	0.544	19.6	20.9

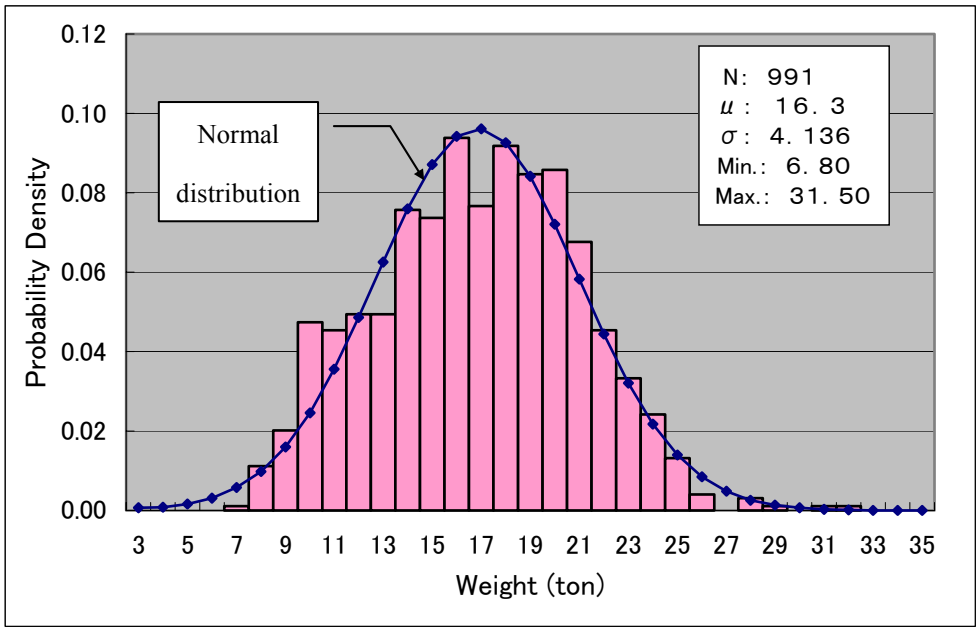

Fig.3.1 Weight distribution (ordinary truck (middle class 3))

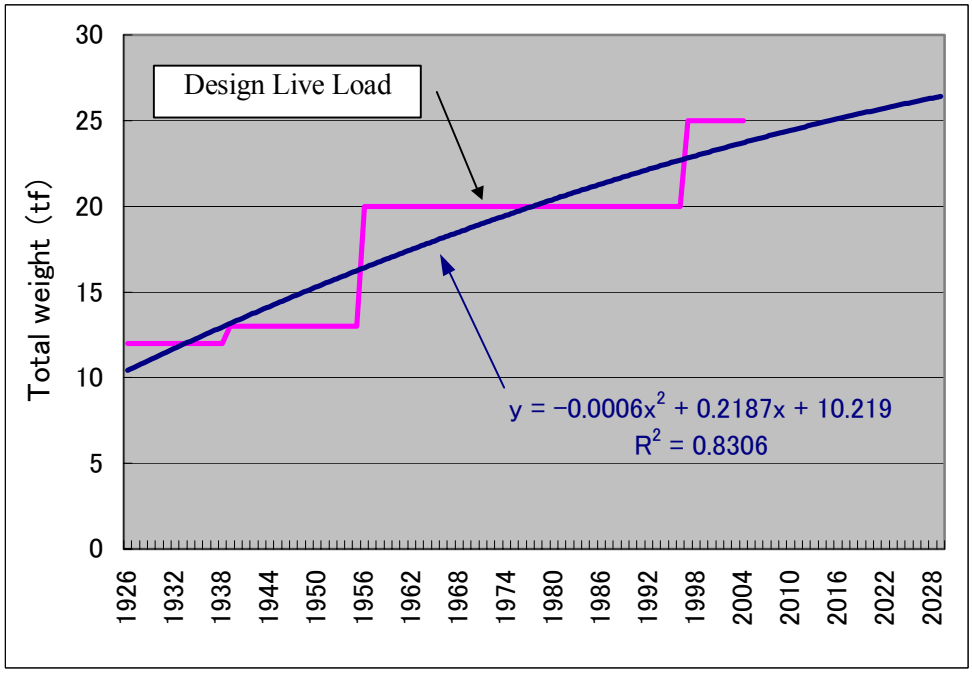

Fig.3.2 Long-term change of design live load for girder of the first class bridges in DSHB)

3.3 Maximum Model for Wind Load

For the long-span bridges, the wind load is one of the most influent loads for the superstructure. According to the wind proof design standard of Honshu-Shikoku Bridge Authority, the static design wind load for the main cable and stiffening girder in suspension bridge are given as follows.

$$P_D = \frac{1}{2}\rho C_D \nu_4 (\nu_1 \nu_2 V_{10})^2 A_n \quad \cdots\cdots (3.1)$$

where P_D is design wind load, ρ is air density, C_D is drag coefficient, ν_4 is correction factor due to the gust effect, ν_1 is correction factor due to the elevation of the structure, ν_2 is correction factor due to the special wind variation of the structure, V_{10} is basic wind velocity, and A_n is projection area.

The basic wind velocity V_{10} is expected value of ten-minute mean wind velocity for 150-year return period at the elevation of ten meters above sea level. For instance, the basic wind velocity for the Akashi Kaikyo Bridge is 43 meters in original standard in 1976, and 46 meters in current standard 1990. The basic wind velocity for the Ohnaruto Bridge is 50 meters. Fig.3.3 shows the flowchart of wind resistance design for long-span bridges

The static design wind load in Eq. (3.1) is associated with many uncertainties. The maxim wind velocity can be determined by using the extreme type I distribution as follows.

$$\Phi^{(1)}(V_{10}) = \alpha \exp\left[-\alpha(V_{10}-u) - \exp\left\{-\alpha(V_{10}-u)\right\}\right] \quad \cdots\cdots (3.2)$$

where u is μ_{V10} -0.455005 σ_{V10}, α is 1.28255/ σ_{V10}, μ_{V10} is mean of V_{10}, and σ_{V10} is standard deviation of V_{10}.

For the uncertainty in the basic wind velocity, the maxim wind velocity can be calculated by Eq. (3.2) with regard to the basic wind velocity for more than 150-year return period.

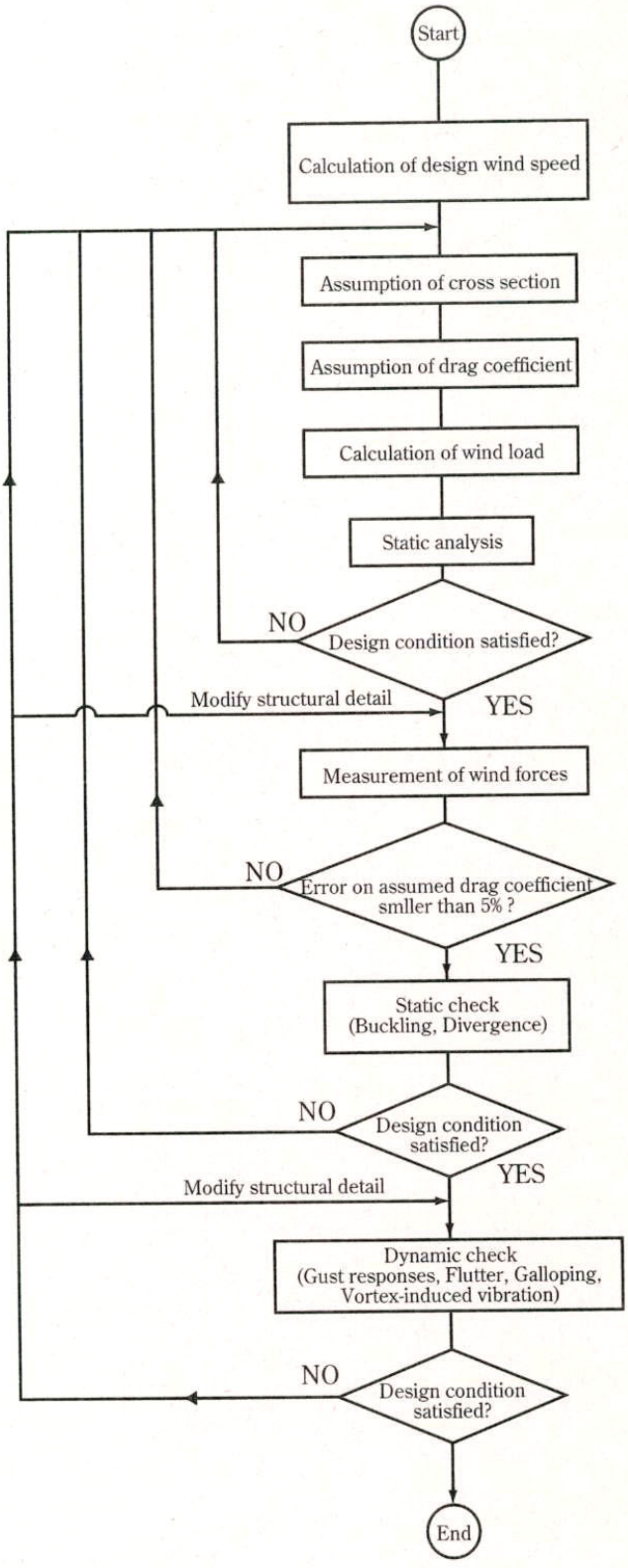

Fig.3.3 Flowchart of wind resistance design for long-span bridges

3.4 Aging Model of Steel Structures

The yield stress distribution and tensile strength distribution of SM490 as the representative material for steel bridges are shown in Fig.3.4 and Fig.3.5, respectively. The yield stress is similar to the normal distribution with the average of 420 MPa, the standard deviation of 20.6 MPa, and the coefficient of variation of 0.049. The tensile strength is similar to the normal distribution with the average of 554MPa (N/mm^2), the standard deviation of 12.4 MPa, and the coefficient of variation of 0.022.

In general, the surrounding conditions are more severe onshore than offshore, high-durability coating systems are applied to the onshore steel bridges. For example, phthalic resin and polyurethane resin are used for the offshore bridges, and chlorinated rubber paint, polyurethane paint, and fluoropolimer paint are used for onshore steel bridges on the Honshu-Shikoku Highways.

The periodical coating observation at fixed points, which is applied to onshore steel bridge, is shown in Fig.3.6. The thickness of polyurethane resin paint due to the ultraviolet rays decreases at the average of 7 -10 μ m/year in the sunshine, the average of 5 μ m/year in the sunshade. The required thickness of surface coat is more than 30 μ m, and that of middle coat is also more than 30 μ m. If the surrounding condition is very severe, the surface coat and the middle coat will disappear in approximately ten years. Since the epoxy resin is applied to the lower coat, which has a low durability, the deterioration progresses rapidly in the whole coating system.

On the Honshu-Shikoku Highways, all steel bridges are appropriately maintained, including repair coating and overall recoating. For example, the onshore steel bridges are overall repainted before disappearing the middle coating for the preventive maintenance.

However, in real steel bridges, the thickness of coating system reduces uncertainly and corrosions may occur at joint parts or lower flanges of girders. Fig.3.7 shows the deteriorating curve for coating and corrosion, considering the thickness variation of total coating system. After loss of the surface coat and the middle coat, the lower coat rapidly degreases. In this thesis, the long-term change is referred to as “time-dependent strength.”

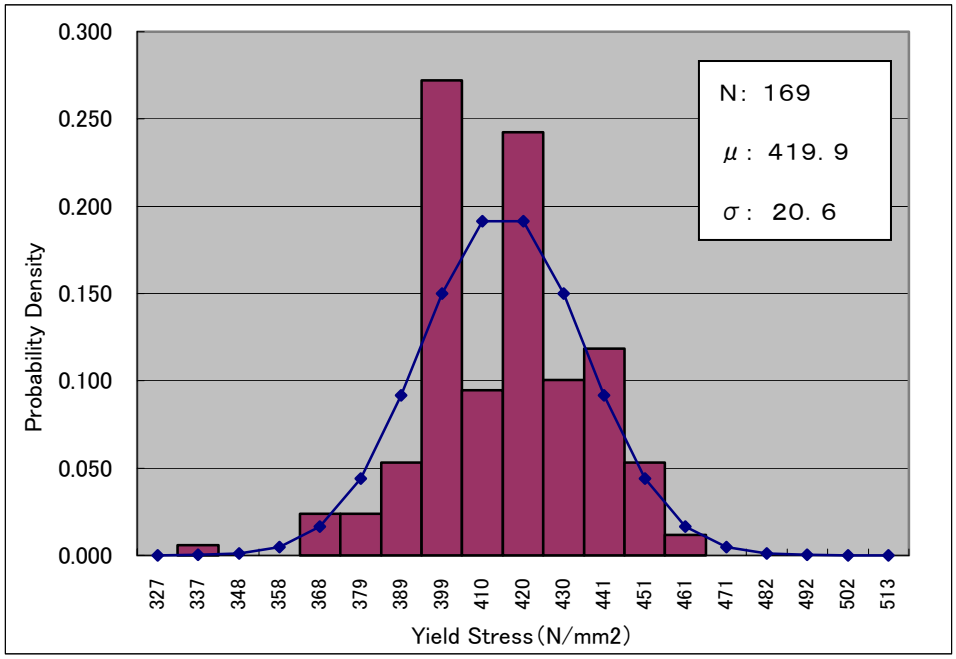

Fig.3.4 Yield stress distribution (SM490)

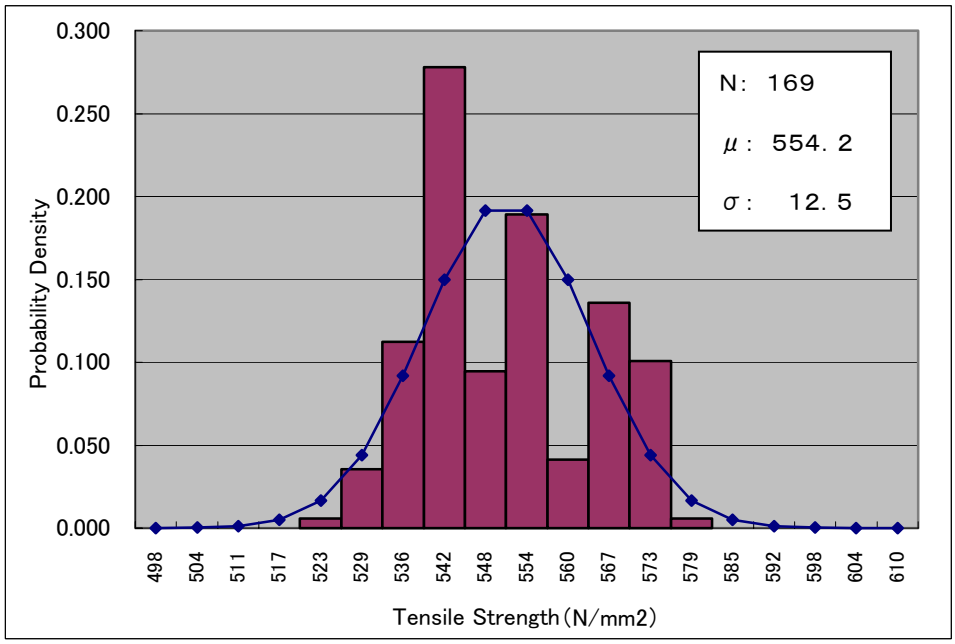

Fig.3.5 Tensile strength distribution (SM490)

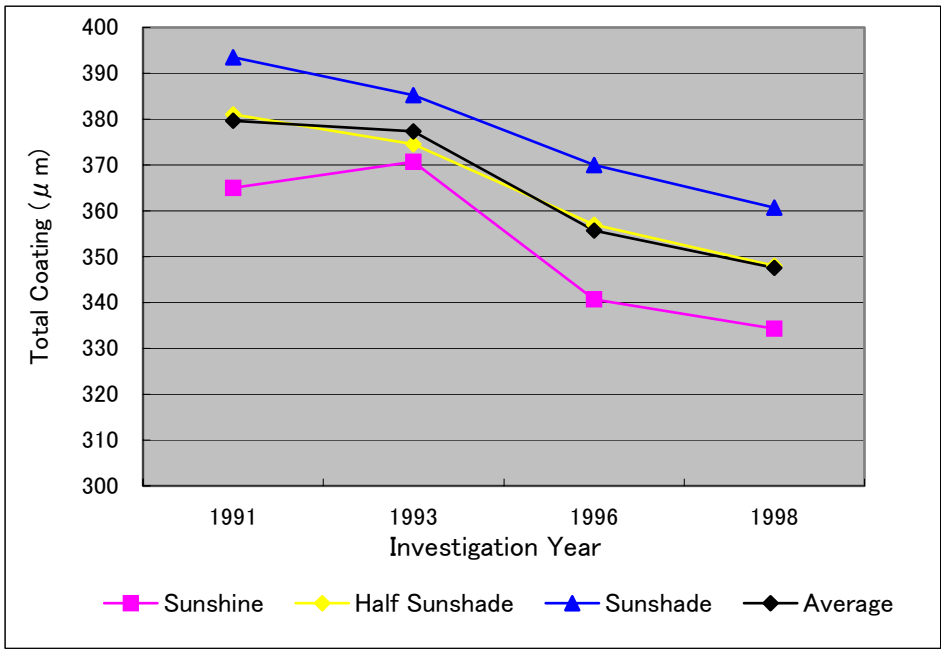

Fig. 3.6 Coating observation at fixed points

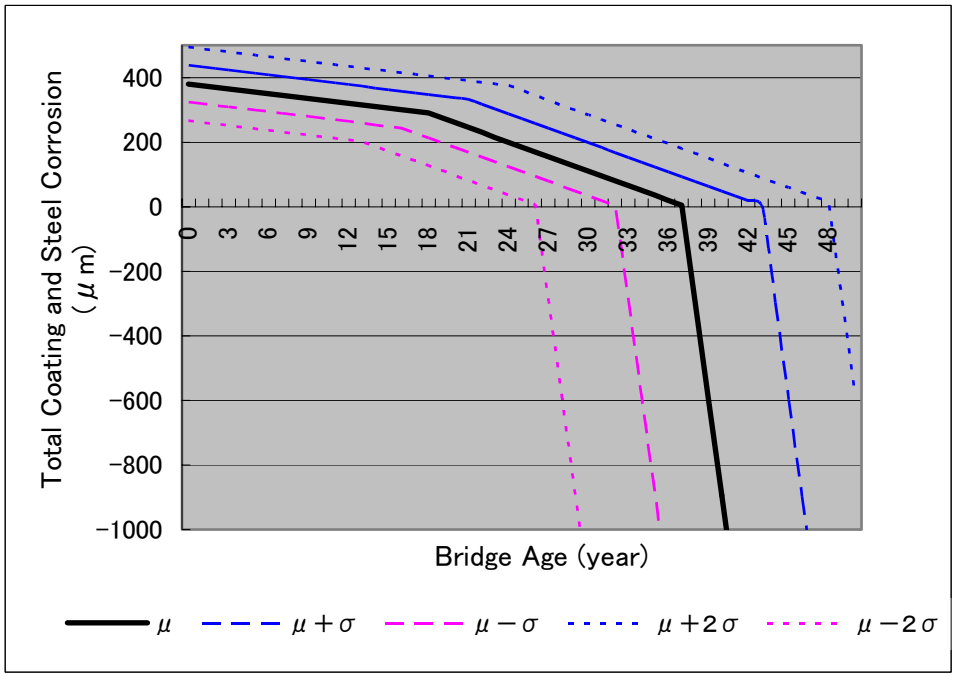

Fig. 3.7 Deteriorating curve for coating and corrosion in a very severe surrounding condition

3.5 Aging Model of Concrete Structures

In general, the aging model for concrete structures is described in Fig.3.8. There are four periods in the concrete deterioration model, e.g., 1) un-progressing period, 2) progressing period, 3) accelerating period, and 4) deteriorating period.

Many scholars and engineers have been studied various damages of concrete structures in various surrounding conditions. Especially, the saline damage and the carbonation of concrete structures have many examples.

For the saline damage, the saline element per unit concrete volume is measured in the concrete structure. For the carbonation of concrete, the carbonated depth is measured in the concrete structure. Since the prediction methods for these damages are also studied, these damages can be easily predicted.

Example of saline damage and carbonation are shown in Fig.3.9 and 3.10, respectively. Based on these data of concrete structures, the aging model for concrete structure can be obtained.

In a severe surrounding condition, including the coastal area, the saline damage and the carbonation of concrete structures are difficult problems in maintenance.

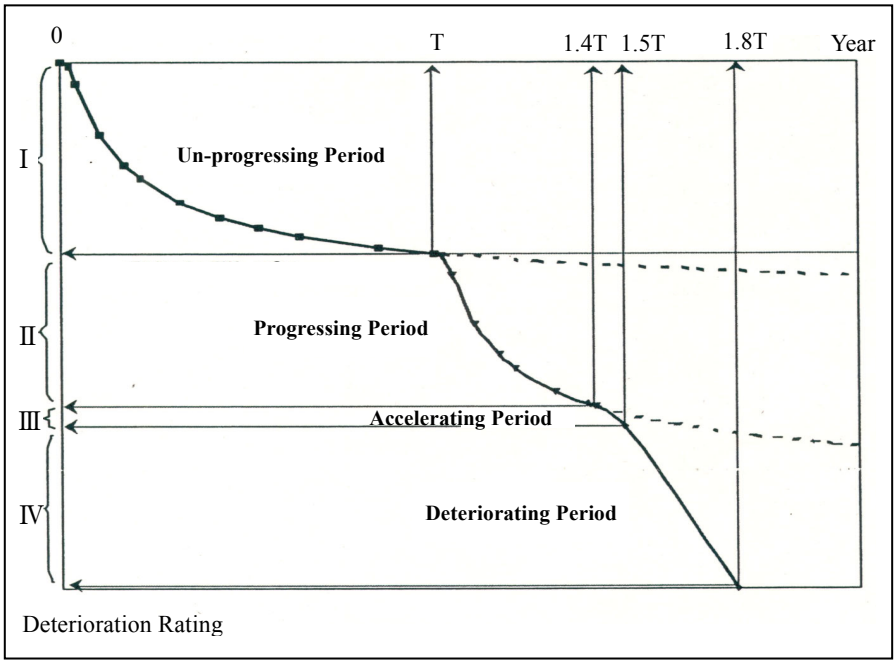

Fig.3.8 Aging model for concrete structures in case of saline damage

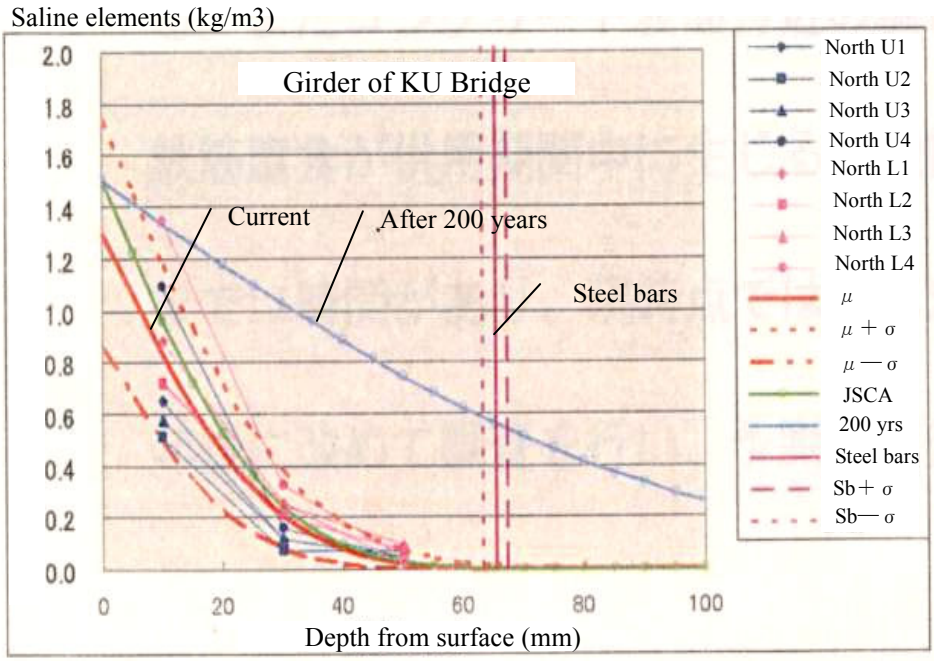

Fig.3.9 Example of saline damage and prediction

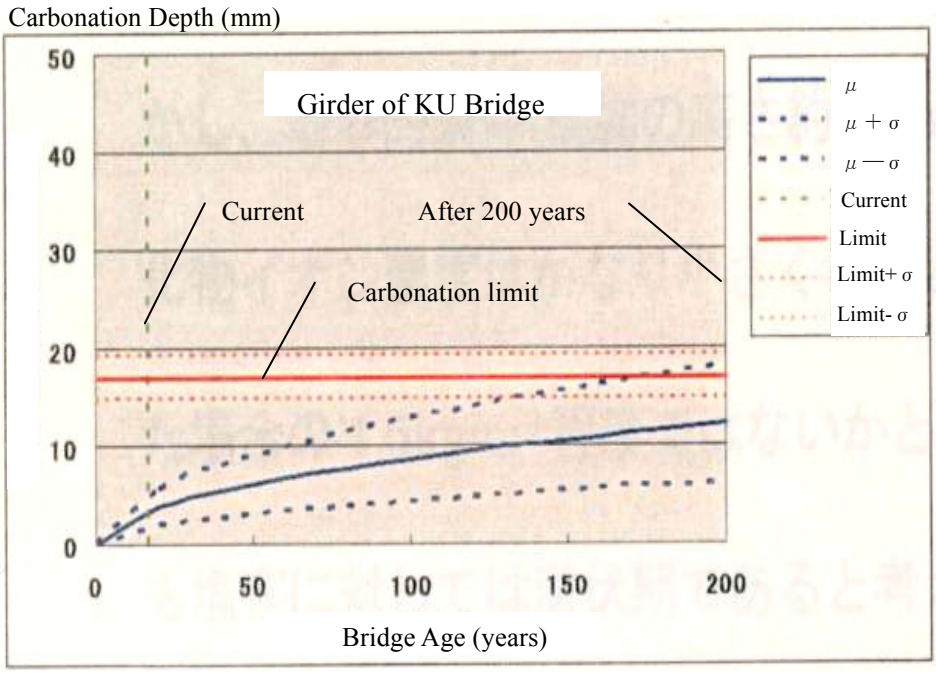

Fig.3.10 Example of carbonation damage and prediction

3.6 Summary

The conclusions in this chapter are summarized as follows.

1) Based on the traffic investigation, the increasing model for live load can be obtained, assuming the variation of live load as well as the increase of the design live load.
2) The maximum model for wind load can be obtained, assuming the variation of design wind velocity as well as the maximum wind velocity, which is determined by the extreme type I distribution.
3) Aging model of steel structures can be obtained, assuming the variation of steel strength, the decrease of coating and the increase of corrosion.
4) Aging model of concrete structures can be obtained from the many accumulated data in maintenance.
5) The above-mentioned model can be used for reliability analysis considering the time-dependent load and strength.

4. Reliability Analysis for Short-span Bridges with Time-dependence

4.1 Introduction

Generally, the coating is applied to steel structures in order to protect the corrosion. In a severe surrounding condition, a high-durability coating is applied to steel structures. However, deterioration of coating is inevitable, which yields to a partial corrosion and a sectional loss, if the repair coating or the overall recoating would not be appropriately carried out.

On the other hand, traffic volumes have increased and traffic vehicles have enlarged according to the economic growth of Japan. In load conditions for steel bridges, the live load has increased and is expected to increase in future.

Therefore, the increasing live load and the decreasing steel strength are considered to have the property of time dependence. The reliability analyses for various types of bridges were carried out by using the Monte Carlo Simulation, considering the various data of loads and strengths, and several comments of reliability for these bridges were made.

The procedure of the reliability analysis, considering the time dependence of load and strength, is shown in Fig. 4.1. In the first stage, data for the time dependence of load and strength are reviewed. In the second stage, the reliability analyses are carried out.

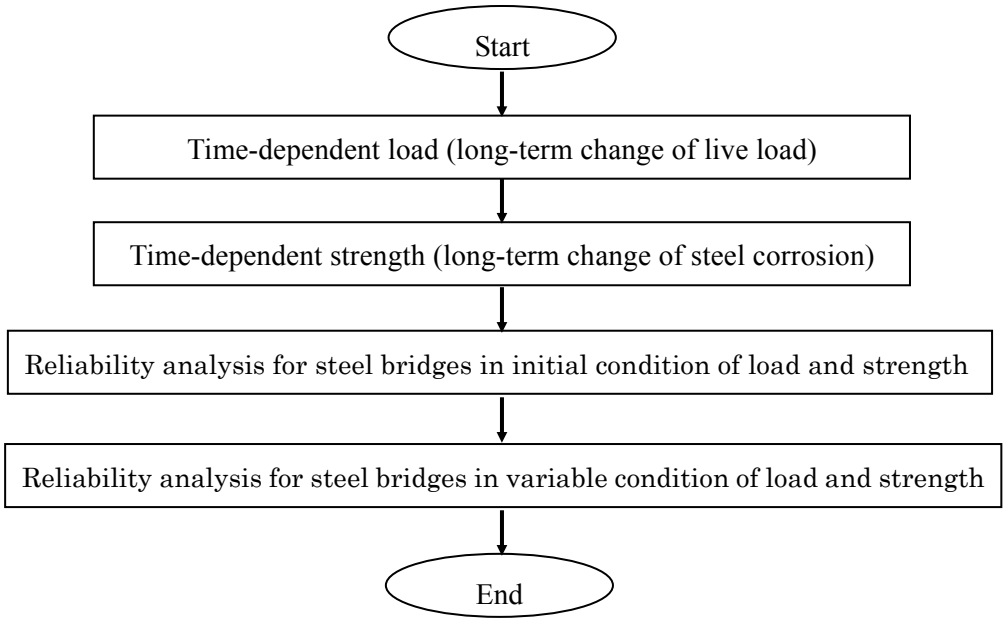

Fig. 4.1 Flowchart of reliability analysis for steel bridges considering time-dependence

4.2 Reliability Analysis for Beam of Steel Deck Plate with Time-dependence on Load and Strength

In order to reduce to the dead load, orthotropic steel decks are selected for of long-span bridges in the Honshu-Shikoku highways. The high durability coating system, in which the total coating is 250 μ m in thickness, is used for these bridges, however, the overall recoating is carried out in some long-span bridges because of severe surrounding conditions on straits.

In this section, the stress check for the lower flange of longitudinal girder of orthotropic steel deck, where much salty splash reaches and does not washed by rain water. And the safety check was carried out by the reliability analysis.

The cross-section of orthotropic steel deck is depicted in Fig. 4.2. The longitudinal girder has a span of 10 meters and is laterally arranged with an interval of 3.5 meters. Actually, the longitudinal girder is a continuous structure in several spans, but is assumed to be simplely supported for a safe assumption.

Firstly, dead load, live load and impact were considered for the allowable stress check. As the live load, a wheel load of 100 kN, which is equal to a half of the load T for design live load B defined in the current DSHB, is applied right on the longitudinal girder. The impact is assumed to be 0.333 for a steel bridge with a span of 10 meters according to the current DSHB. The bending stresses due to these loads were calculated at a quarter and a half of the span.

Considering the reduction of sectional performance, the result of bending stresses is shown in Table 4.1 on the above-mentioned conditions. The five cases are calculated with the variable thickness of lower flange, which are Case1 (design thickness of 13 mm), Case2 (9 mm), Case3 (6 mm), Case4 (3 mm), and Case5 (0 mm), respectively. The bending stresses of almost cases at the quarter and the half of the span are less than 140 MPa for the allowable standard of SS400, excluding the Case 5 at the half of the span. In this calculation, the torsional deformation and the local buckling are negligible, and no fatigue damage assumed to occur.

Secondly, the live load has a large coefficient of variation, and also has a long-term increase. Therefore, the reliability analysis was carried out by the Monte Carlo Simulation, considering the time-dependent load and strength. The dead loads of the orthotropic steel deck as well as

the pavement were considered. Based on the traffic investigation on the Seto-Ohashi Bridges in 1990, the ordinary truck classified in the middle class 3 (total weight of 8-20 tons, with 3 axes) was selected as the representative vehicle. The wheel weight distribution of the middle truck 3 is assumed to be the following normal distribution. One is Live Load 1 (the average of 82kN, the standard deviation of 21kN, and the coefficient of variation of 0.25), based on the traffic investigation, and the other is Live Load 2 (the average of 100kN, the standard deviation of 25kN, and the coefficient of variation of 0.25), based on the current DSHB. The impact is assumed to be 0.333 according to the current DSHB. On the other hand, the yield stress is assumed to have an average of 235 MPa for the yield standard of SS400 and the coefficient of variation of 0.25 according the construction results.

The results of the reliability analyses are shown in Fig. 4.4 and 4.5. The calculation cases are the same as Table 4.1. The trail number is 10,000 for simple calculation. In Fig. 4.4, the reliability index at the quarter of span is always more than 4.2 against the Live Load 1 and the Live Load 2. On the other hand, the reliability index at the half of span is 3.4 in Case 5 against the Live Load 1, and the reliability index is 2.3 in Case 5 against Live Load 2. In Fig. 4.5, the probability of failure at the quarter and the half of span are less than 0.0001 in Case 1 to 4, but the probability of failure at the half of span is 0.0004 against the Live Load 1 in Case 5 and 0.0124 against the Live Load 2 in Case 5.

Consequently, the reliability index is large and the safety was checked in Case 1 to 4. The reliability index is low in Case 5, however, there is no need to consider in a usual maintenance. Based the results of reliability analysis, considering the reducing sectional performance and the increasing live load, the safety of the orthotropic steel deck was checked without a large sectional loss at the lower flange of the longitudinal girder.

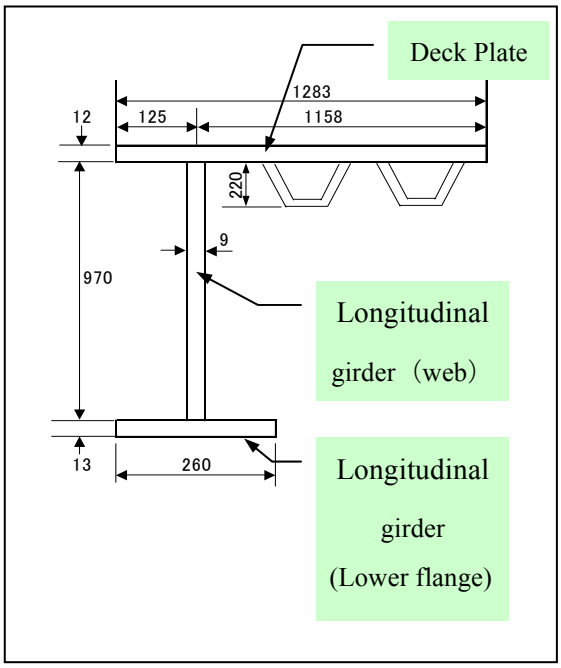

Fig. 4.2 Partial cross-section of orthotropic steel deck

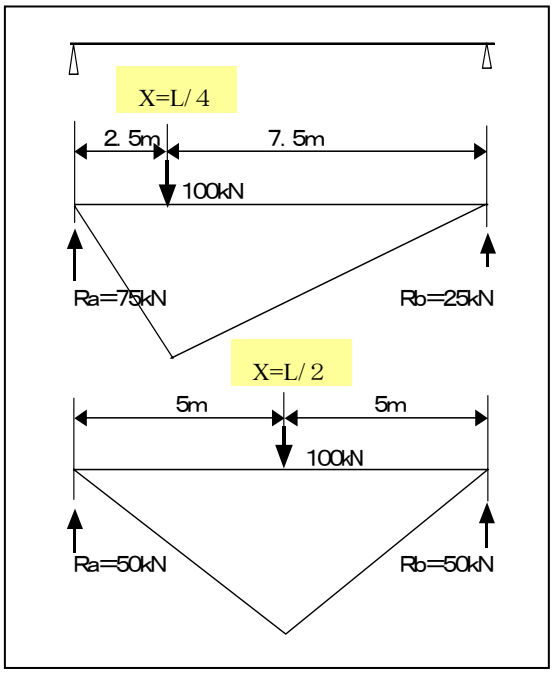

Fig. 4.3 Live load on longitudinal girder of orthotropic steel deck

Table 4.1 Stress Check at lower flange of longitudinal girder

Case	Thichness of lower flange (mm)	Crosssectional area of girder (cm2)	Sectional modulus of girder (cm3)	Bending stress at a quarter (MPa)	Bending stress at a half (MPa)	Allowable stress (MPa)
1	13	353	5464	57	72	140
2	9	343	4540	69	86	140
3	6	335	3858	81	101	140
4	3	327	3175	98	122	140
5	0	320	2486	125	156	140

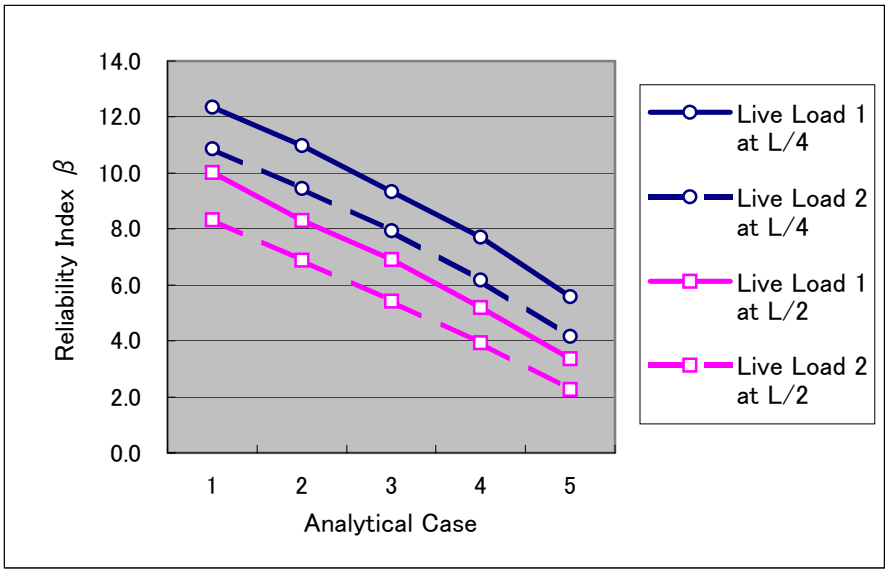

Fig. 4.4 Reliability index in longitudinal girder of orthotropic steel deck

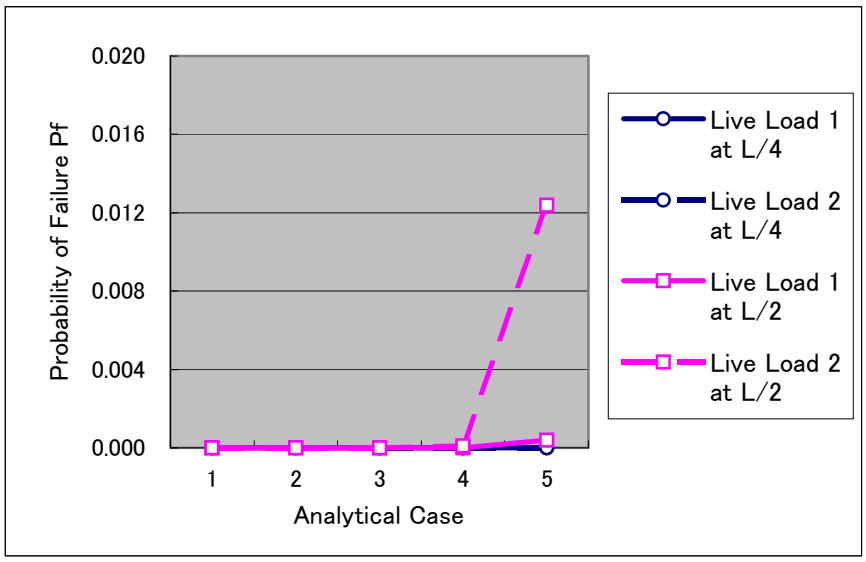

Fig. 4.5 Probability of failure in longitudinal girder of orthotropic steel deck

4.3 Reliability Analysis for Simply Supported Steel Girder with Time-dependence on Load and Strength

The reliability analysis with time-dependent load and strength was carried out for the simple steel bridge with I-shape girders and a reinforced concrete slab. The side view of the simple steel girder is shown in Fig. 4.6. The span length is 40 meters, and the width is 18.25 meters with 6 girders for 4 lanes. The structural model is shown in Fig. 4.7.

The lower flange of the outside I-shape girder is easy to reduce coating and have corrosion due to sunshine. In the reliability analysis with the time-dependent strength, the corrosion and the reduction of thickness were assumed at the lower flange of I-shape girder in the center of the span. Table 4.2 shows the four analytical cases with thickness variation of lower flange, which are Case 1 (design thickness), Case 2 (90% thickness), Case 3 (80% thickness), and Case 4 (70% thickness), respectively.

On the other hand, dead load, live load and impact were considered. In the reliability analysis with the time-dependent load, three analytical cases are calculated with the variation of live load and impact. The three cases of live loads are Live Load 1 (above-mentioned weight distribution with average of 16.4tons), Live Load 2 (current DSHB with average of 20.0tons), and Live Load 3 (25%-increace DSHB with average of 25.0tons), respectively. The coefficient of variation was assumed to 0.25, based on the result of traffic investigation in 1990.

The results of reliability analyses by means of the Monte Carlo Simulation, considering the time-dependent load and strength, are shown in Fig. 4.8. The trial number is 10,000 for simple calculation. In this analysis, the failure is assumed to the yield stress of the lower flange with reduced thickness, which is identified with the limit state of serviceability. The yield stress is assumed to have the normal distribution with the actual average of 420MPa(N/mm^2) for SM490 steels and the coefficient of variation of 0.05.

The results are summarized as follows.

a) In case of Live Load 1, which is equal to the investigated weight distribution, the reliability index is 7.45 in Case 1 (design thickness), and 4.68 in Case 4 (70% thickness).

b) In case of Live Load 2, which is identified with SHD, the reliability index is 6.27 in Case 1, and 3.77 in Case 4.

c) In case of Live Load 3, which is increased by 25% of DSHB, the reliability index is 5.00 in Case 1, and 2.67 in Case 4. The failure probability is 0.0032 in Case 4.

d) On the other hand, when the reliability index equal to 4.0, the thickness is less than 70% in Live Load 1, 77% in Live Load 2, and 84% in Live Load 3.

In addition, Fig. 4.9 and 4.10 show the results of reliability analyses at the center of girder (x=L/2), and at the quarter of the girder (x=L/4), by means of the Monte Carlo Simulation, considering the increasing load and the decreasing strength without repair. In this analysis, the load is assumed to increase as same as the similar curve in Fig. 3.2 from the above-mentioned weight distribution with average of 16.4 tons in 1990. Meanwhile, the strength is assumed to decrease as same as the deteriorating curve for coating and corrosion in Fig. 3.7. The bridge was completed in 1985, and is now 20 years old in 2005. After 40 years old, the reliability index would decrease gradually according to the thickness reduction of lower flange if the appropriate maintenance is not carried out.

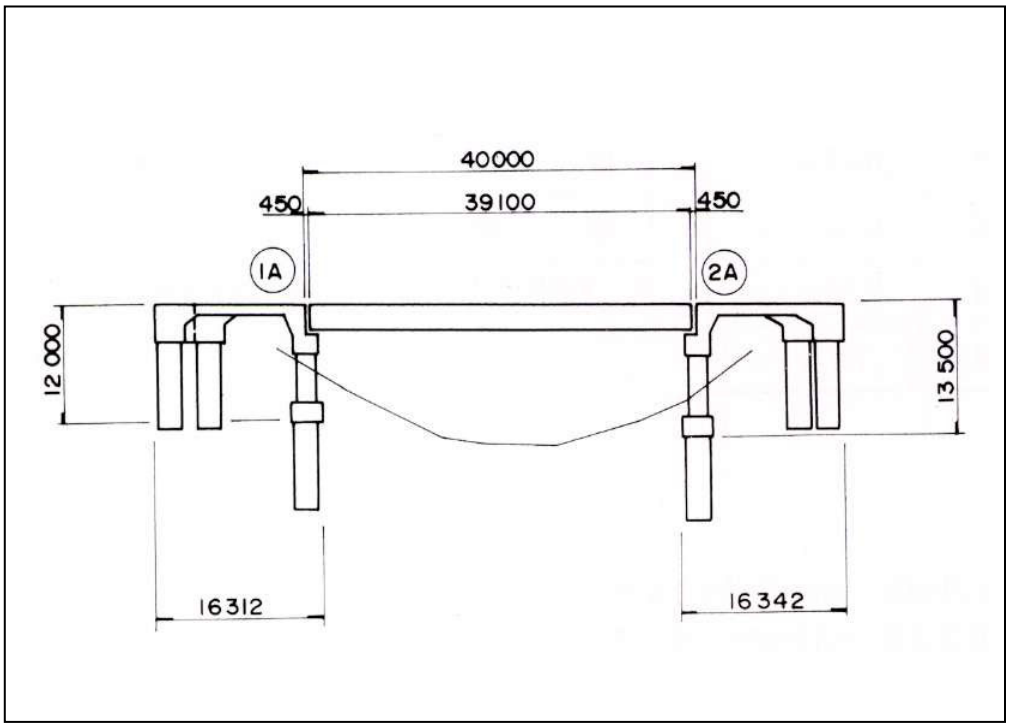

Fig. 4.6 Side view of simple steel girder

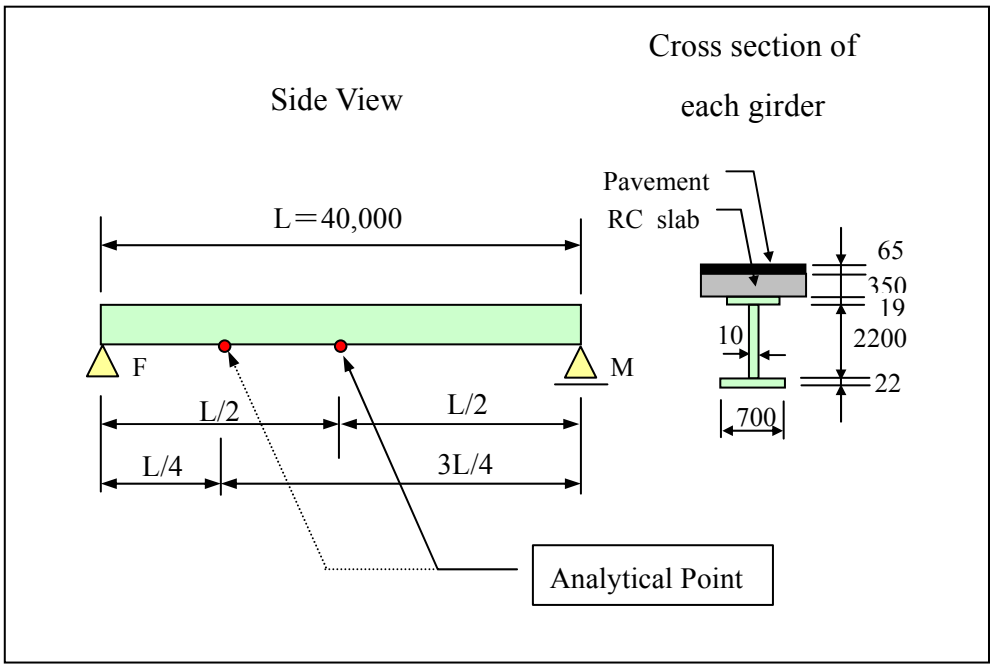

Fig. 4.7 Structural model for simple steel bridge

Table 4.2 Analytical case for simple steel girder

Case	Thickness of lower flange		Sectional area (per girder)		Vertical section modulus (per girder)	
	mm	Ratio	cm2	Ratio	cm3	Ratio
Case 1	22.0	1.000	439	1.000	37,506	1.000
Case 2	19.8	0.900	423	0.964	34,639	0.924
Case 3	17.6	0.800	408	0.929	31,899	0.851
Case 4	15.4	0.700	392	0.893	29,295	0.781

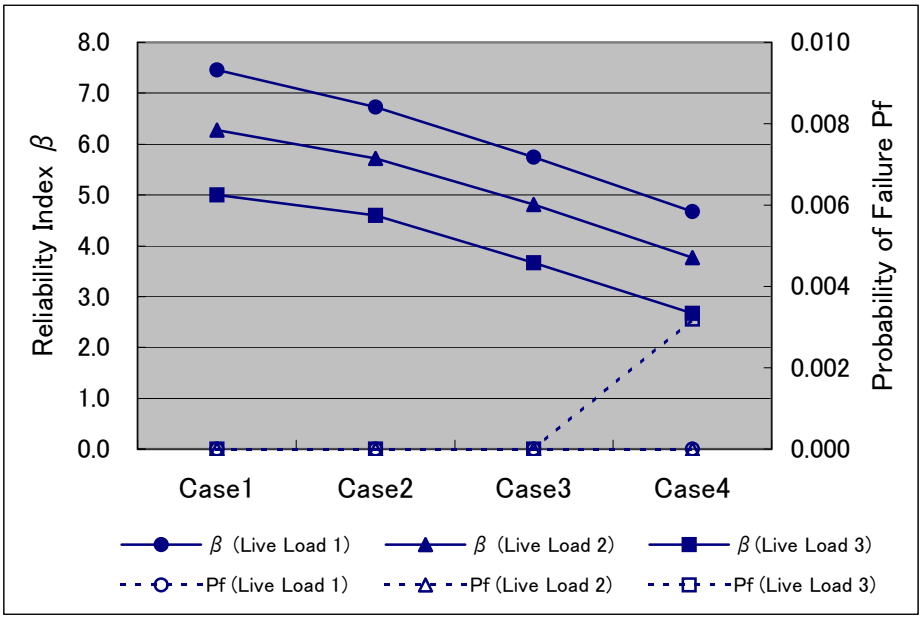

Fig. 4.8 Reliability analysis for simple steel girder at x=L/2 in each case

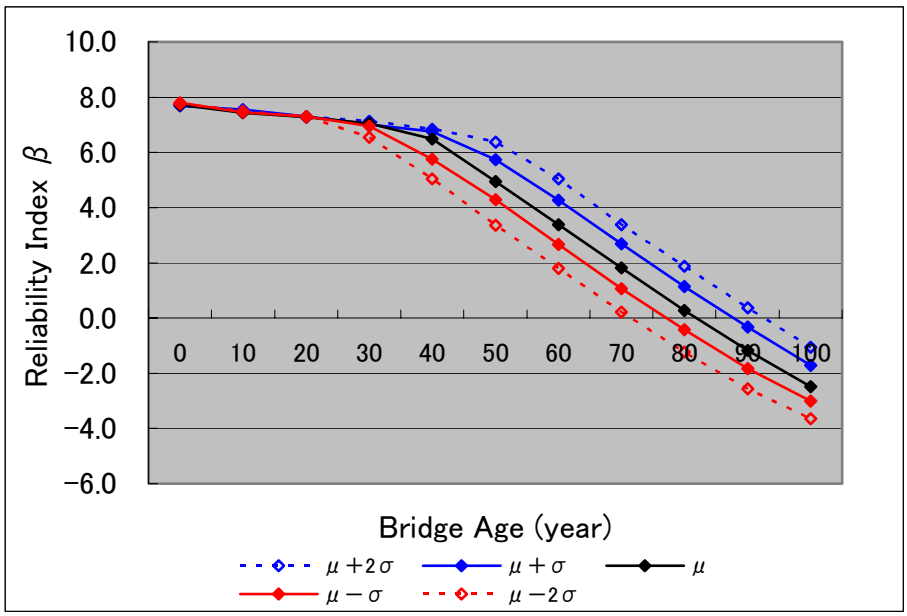

Fig. 4.9 Reliability Analysis for simple steel girder at x=L/2, considering time-dependence

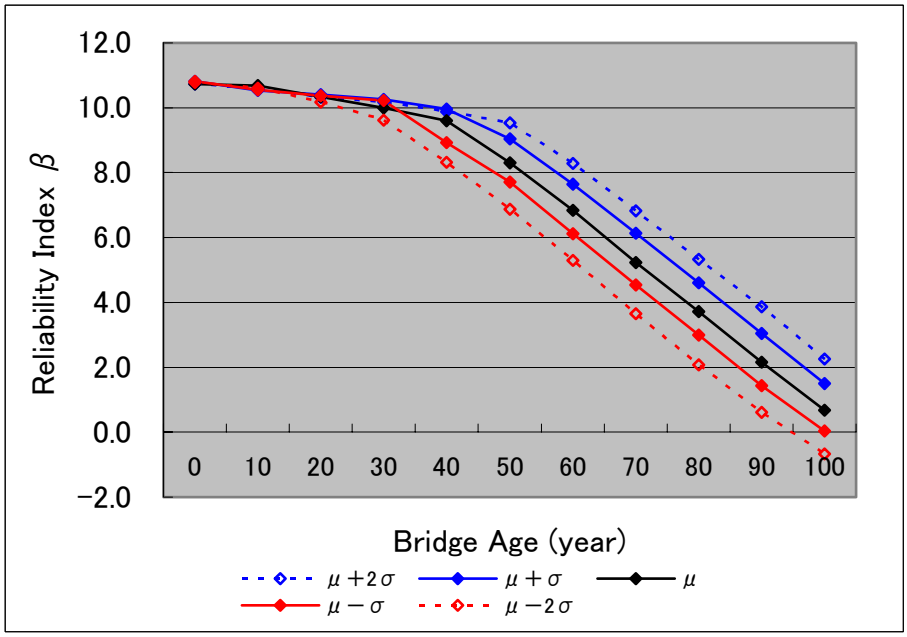

Fig. 4.10 Reliability Analysis for simple steel girder at x=L/4, considering time-dependence

4.4 Reliability Analysis for Continuous Steel Girder with Time-dependence on Load and Strength

The reliability analysis with time-dependent load and strength was carried out for a three-span continuous steel bridge with I-shape girders and a reinforced concrete slab. The side view of the three-span continuous steel girder is shown in Fig. 4.11. The total bridge length is 150 meters. The each span length is 50 meters, and the width is 18.25 meters with 6 girders for 4 lanes. The structural model is shown in Fig. 4.12. The cross section of the girder is assumed to be one of most representatives in the real bridge.

As same as the simple steel bridge, the lower flange of the outside I-shape girder in the three-span continuous steel bridge is easy to reduce coating and have corrosion due to sunshine. In the reliability analysis with the time-dependent strength, the corrosion and the reduction of thickness were assumed at the lower flange of the girder in the center of the side span. Table 4.3 shows the four analytical cases only with thickness variation of lower flange, which are Case 1 (design thickness), Case 2 (90% thickness), Case 3 (80％ thickness), Case 4 (70% thickness), respectively.

As same as the simple steel girder, in the reliability analysis with the time-dependent load, the three analytical cases with the variation of live load and impact. The three kinds of live loads are Live Load 1 (above-mentioned weight distribution with average: 16.4tons), Live Load 2 (current DSHB with average 20.0tons), and Live Load 3 (25%-increace DSHB with average 25.0tons), respectively. Coefficient of variation was assumed to 0.25.

The results of reliability analysis by means of the Monte Carlo Simulation, considering the time-dependent load and strength, are shown in Fig. 4.13. The trial number is 10,000. The failure is assumed to the yield stress of lower flange with reduced thickness. The yield stress is assumed to have the normal distribution with the actual average of 420 MPa(N/mm2) for SM490 steels and the coefficient of variation of 0.05.

The results are summarized as follows.

a) In case of Live Load 1, which is equal to the investigated weight distribution, the reliability index is 7.02 in Case 1 (design thickness), and 5.31 in Case 4 (70% thickness).

b) In case of Live Load 2, which is identified with SHD, the reliability index is 6.10 in Case 1, and 4.35 in Case 4 .

c) In case of Live Load 3, which is increased by 25% of DSHB, the reliability index 4.78 in Case 1, 3.14 in Case 4 . The probability of failure is 0.0010 in Case 4.

d) On the other hand, when the reliability index equal to 4.0, the thickness is less than 70% in Live Load 1 and 2, and 85% in Live Load 3.

In addition, Fig. 4.14 and 4.15 show the results of reliability analyses at the center of side span (x=L/6) and at the center of the center span (x=L/2), respectively, by means of the Monte Carlo Simulation, considering the increasing load and the decreasing strength. The conditions of load and strength are as same as the simple steel bridge. The bridge was also completed in 1985, and is 20 years old in 2005. After 40 years old, the reliability index would decrease gradually according to the thickness reduction of lower flange if the appropriate maintenance is not carried out.

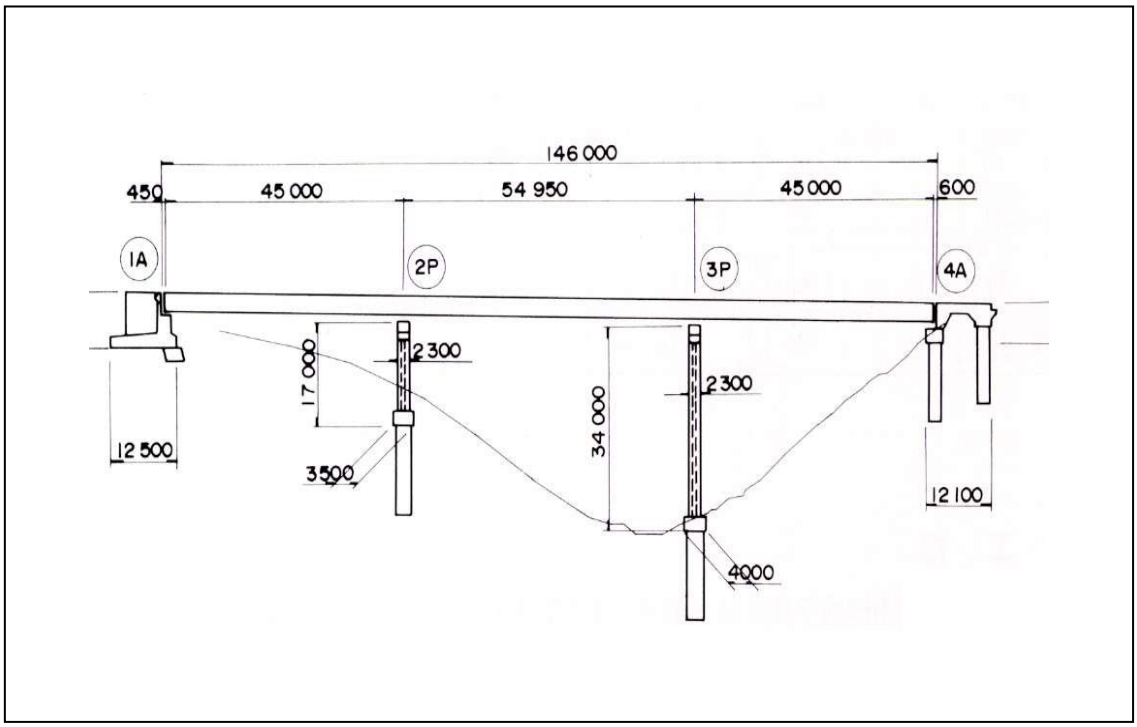

Fig. 4.11 Side view of three-span continuous steel bridge with I-shape girders

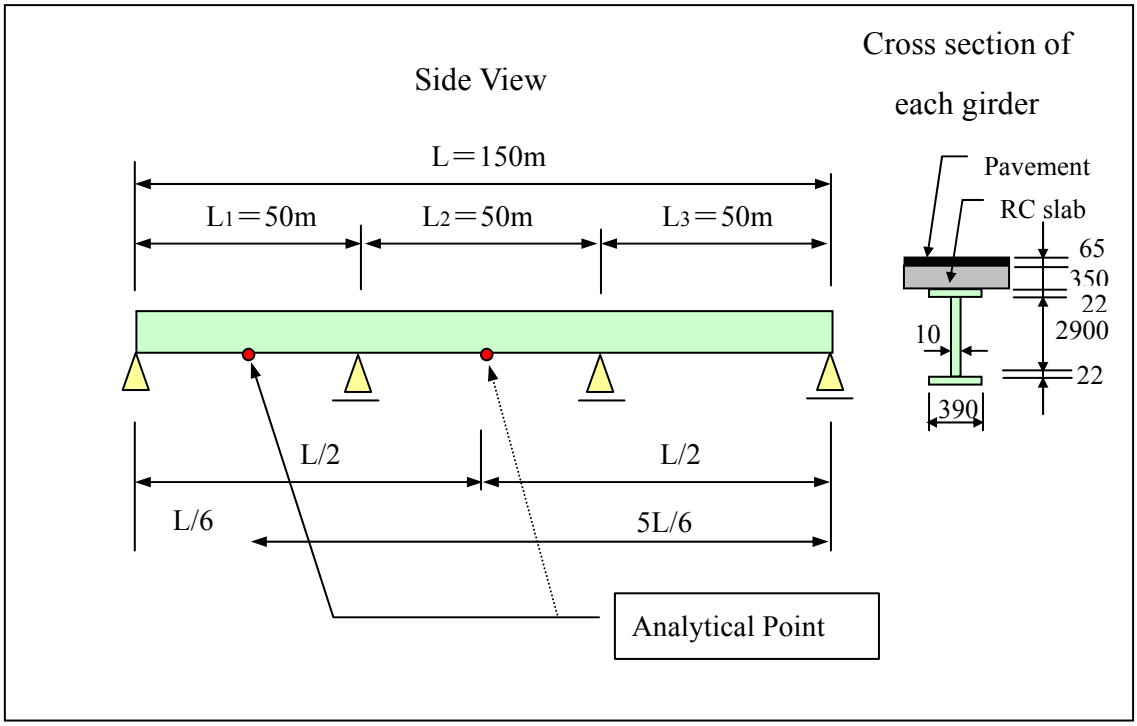

Fig..4.12 Structural model for three-span continuous steel bridge with I-shape girders

Table 4.3 Analytical case for three-span continuous steel bridge with I-shape girders

Case	Thickness of lower flange		Sectional area (per girder)		Vertical section modulus (per girder)	
	mm	Ratio	cm2	Ratio	cm3	Ratio
Case 1	22.0	1.000	453	1.000	37,415	1.000
Case 2	19.8	0.900	445	0.982	35,630	0.952
Case 3	17.6	0.800	437	0.965	33,909	0.906
Case 4	15.4	0.700	428	0.945	32,253	0.862

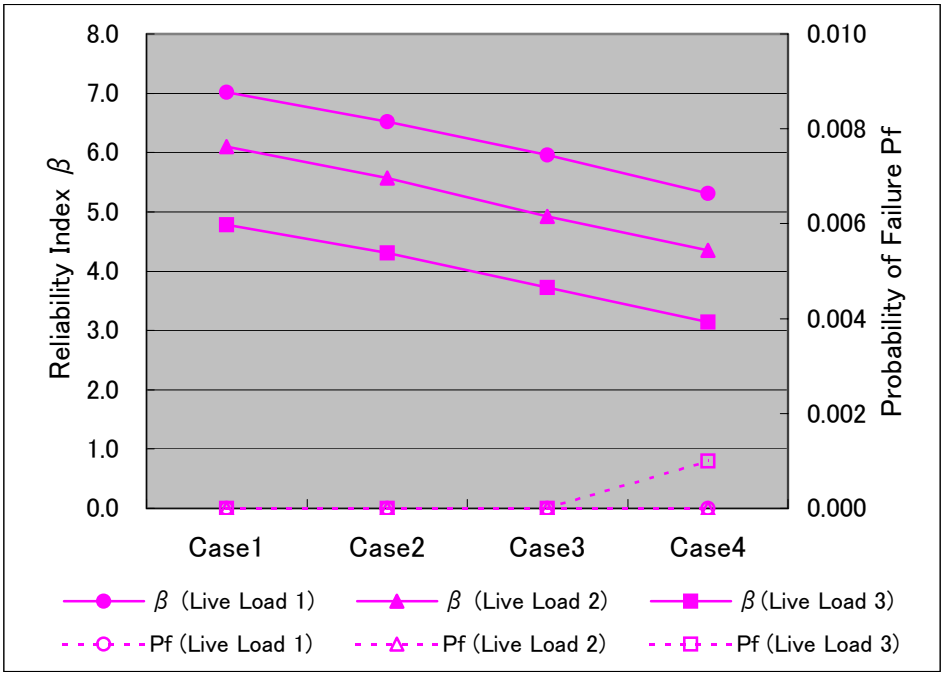

Fig. 4.13 Reliability analysis for three-span continuous steel bridge with I-shape girders at x=L/6 in each case

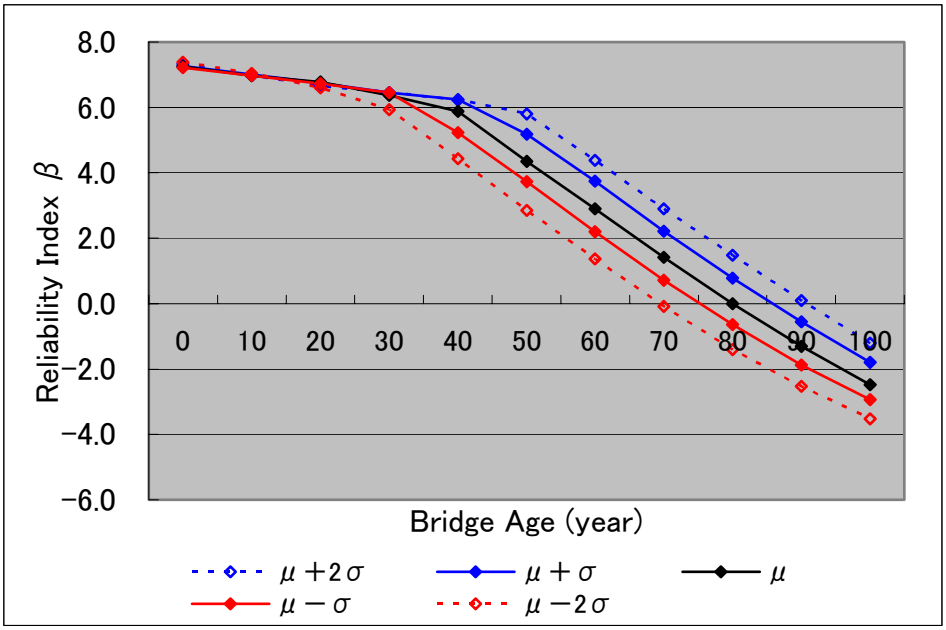

Fig. 4.14 Reliability analysis for three-span continuous steel bridge with I-shape girders at x=L/6, considering time dependence

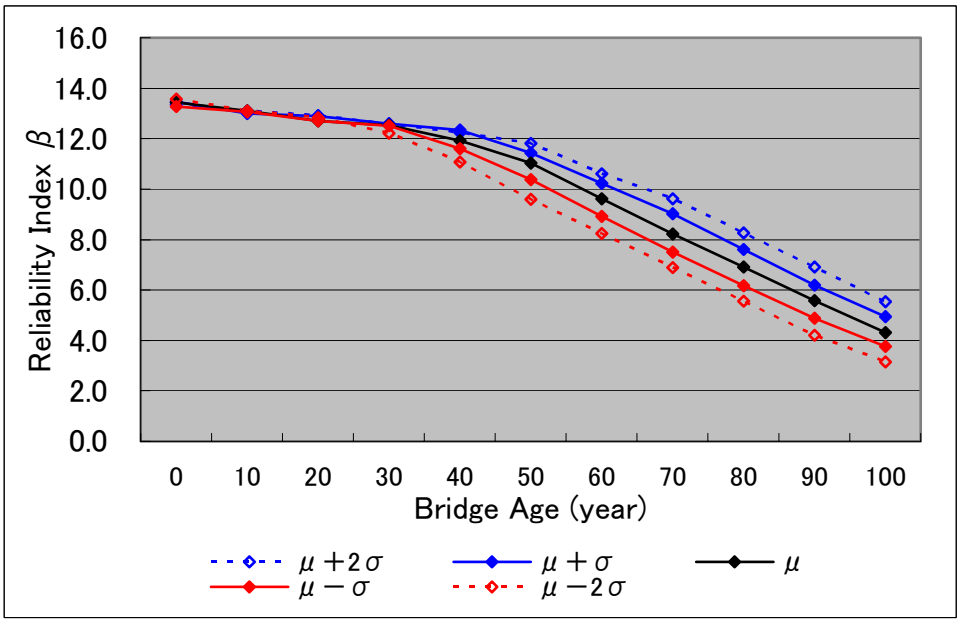

Fig. 4.15 Reliability analysis for three-span continuous steel bridge with I-shape girders at x=L/2, considering time dependence

4.5 Reliability Analysis for Continuous Box Girder with Time-dependence on Load and Strength

The reliability analysis with time-dependent load and strength was carried out for a three-span continuous steel bridge with a box girder and an orthotropic steel deck. The side view of the three-span continuous steel bridge with a box girder is shown in Fig. 4.16. The total bridge length is 300 meters. The each span length is 100 meters, and the width is 18.25 meters with 6 girders for 4 lanes. The structural model is shown in Fig. 4.17. The cross section of the girder is assumed to be one of most representatives in the real bridge.

As same as the simple steel bridge with I-shape girder, the lower flange of the three-span continuous steel bridge with the box girder is influenced by sunshine, coating reduces and corrosion occurs. In the reliability analysis with the time-dependent strength, the corrosion and the reduction of thickness were assumed at the lower flange of the box girder in the center of the side span. Table 4.4 shows the four analytical cases only with thickness variation of lower flange, which are Case1 (design thickness), Case 2 (90% thickness), Case 3 (80% thickness), Case 4 (70% thickness), respectively.

As same as the simple steel girder, in the reliability analysis with the time-dependent load, the three analytical cases with the variation of live load and impact. The three kinds of live loads are Live Load 1 (above-mentioned weight distribution with average: 16.4tons), Live Load 2(current DSHB with average 20.0tons), and Live Load 3 (25%-increace DSHB with average 25.0tons), respectively. Coefficient of variation was assumed to 0.25. However, this bridge has a relatively long span and little influence by live load, and double of the live load was applied as a tandem live load in each case.

The results of reliability analysis by means of the Monte Carlo Simulation, considering the time-dependent load and strength, are shown in Fig. 4.18. The failure is assumed to the yield stress of lower flange with reduced thickness. The yield stress is assumed to have the normal distribution with the actual average of 420 MPa (N/mm2) for SM490 steels and the coefficient of variation of 0.05.

The results are summarized as follows.

a) In case of Live Load 1, which is equal to the investigated weight distribution, the reliability index is 10.7 in Case 1 (design thickness), and 8.3 in Case 4 (70% thickness).

b) In case of Live Load 2, which is identified with SHD, the reliability index is 9.8 in Case 1, and 7.5 in Case 4.

c) In case of Live Load 3, which is increased by 25% of DSHB, the reliability index 8.8 in Case 1, and 6.3 in Case 4.

d) In all cases, the reliability index is more than 6.0 and the probability of failure is less than 0.0001. Because this bridge has a high performance in the sectional modulus, the corrosion proceeding and sectional reduction in the lower flange does not influence the over-stress.

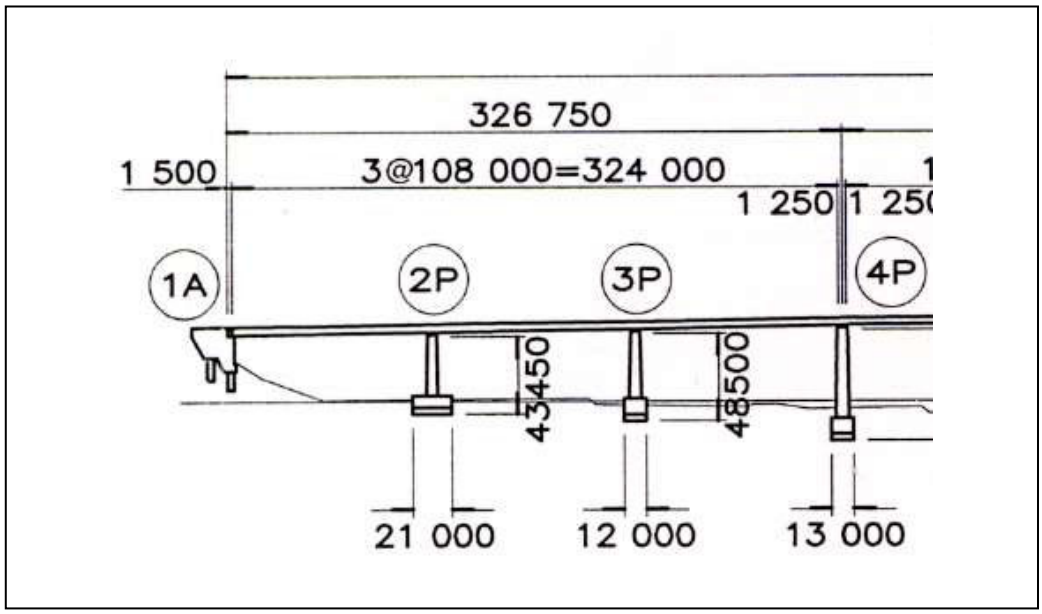

Fig. 4.16 Side view of three-span continuous box girder

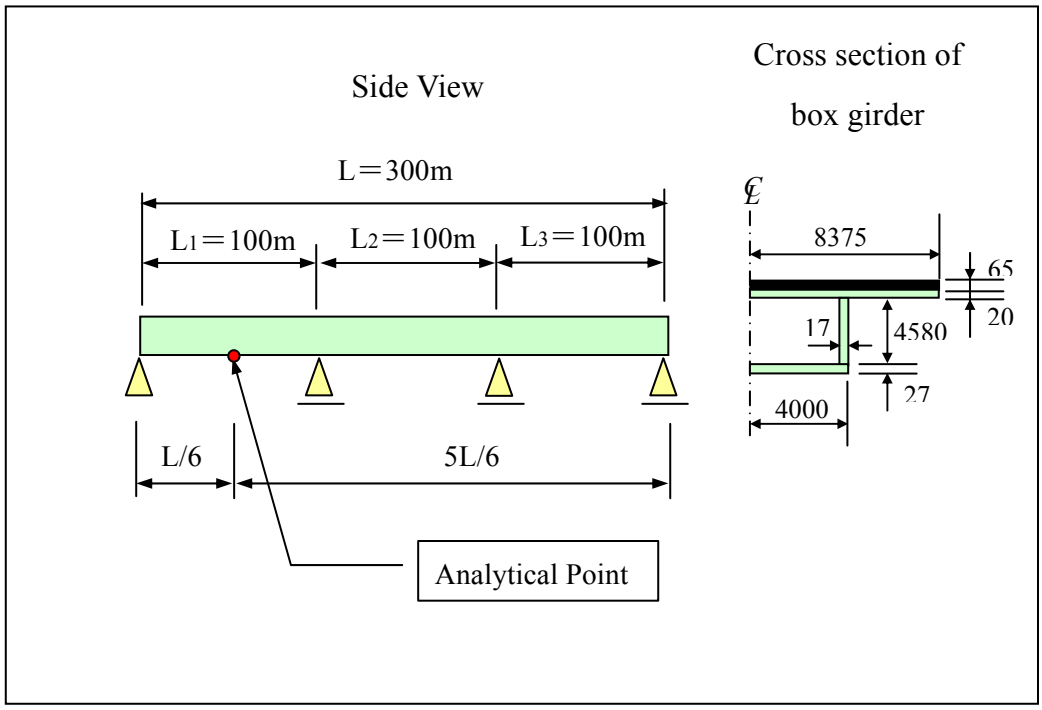

Fig. 4.17 Structural model for three-span continuous box girder

Table 4.4 Analytical cases for three-span continuous box girder

Case	Thickness of lower flange		Sectional area (per 1 box)		Vertical section modulus (per 1 box)	
	mm	Ratio	cm2	Ratio	cm3	Ratio
Case1	18.0	1.000	7,121	1.000	457,242	1.000
Case2	16.2	0.900	6,974	0.979	426,787	0.933
Case3	14.4	0.800	6,826	0.959	396,300	0.867
Case4	12.6	0.700	6,678	0.938	365,782	0.800

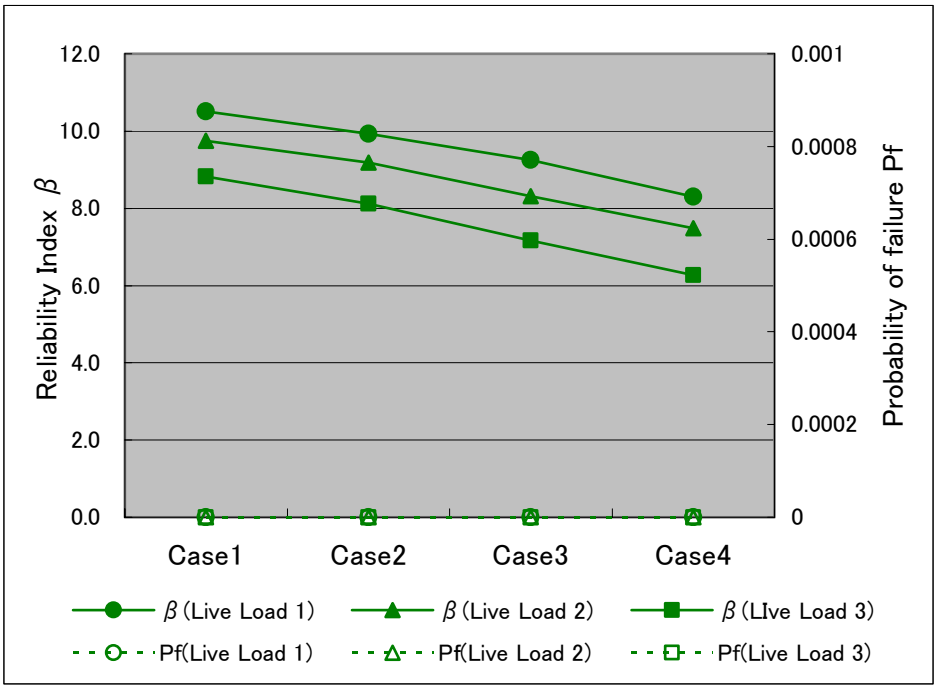

Fig. 4.18 Reliability analysis for three-span continuous box girder

4.6 Reliability Analysis for Reinforced Concrete Girder with Time-dependence on Load and Strength

The reliability analysis with time-dependent load and strength was carried out for the reinforced concrete girder. The side view of the reinforced concrete girder is shown in Fig. 4.19. The span length is 19 meters, and the width is 13.75 meters with reinforced concrete slab for 2 lanes. The structural model is shown in Fig. 4.20.

In general, concrete structures have corrosion in their steel material by the surrounding condition, including the saline attack, carbonation, etc. In the reliability analysis with the time-dependent strength, the steel bars in the lower flange are supposed to have corrosion and reduce their sectional area due to saline attack. Table 4.5 shows the five analytical cases with area variation of steel bar in lower flange, which are Case 1 (design area), Case 2 (75% area), Case 3 (50％ area), Case 4 (25% area) and Case 5 (0% area), respectively.

The dead loads of the reinforced concrete girder as well as the pavement were considered. As same as the section 4.2, the wheel weight distribution of the middle truck 3 is assumed to be the following normal distribution. One is Live Load 1 (the average of 82kN, the standard deviation of 21kN, and the coefficient of variation of 0.25), based on the traffic investigation, and the other is Live Load 2 (the average of 100kN, the standard deviation of 25kN, and the coefficient of variation of 0.25), based on the current DSHB. The impact is assumed to be 0.286 according to the current DSHB. On the other hand, the yield stress of steel bar is assumed to have an average of 345 MPa for the yield standard of SD345 and the coefficient of variation of 0.25 according the construction results.

The calculation cases and the result are tabulated in Table 4.5 and 4.6, respectively. The results of the reliability analyses are also shown in Fig.4.21 and 4.22. In Fig.4.21, the reliability index at the quarter of span is more than 7.5 in Case 1 to 3 against the Live Load 1 and the Live Load 2. The reliability index at the half of span is more than 4.1 in Case 1-3 against the Live Load 1and the Live Load 2. In Fig.4.22, the probability of failure at the quarter span are less than 0.0001 in Case 1 to 3 against the Live Load 1and the Live Load 2, and the probability of failure at the half span is less than 0.0001 in Case 1-3 against the Live Load 1and the Live Load 2.

Consequently, the reliability index is large and the safety was checked in Case 1 to 3. The

reliability index is low in Case 4 and 5, however, there is no need to consider in a usual maintenance. Based the results of reliability analysis, the safety of the reinforced concrete girder was checked without a half sectional loss of steel bars at the lower flange.

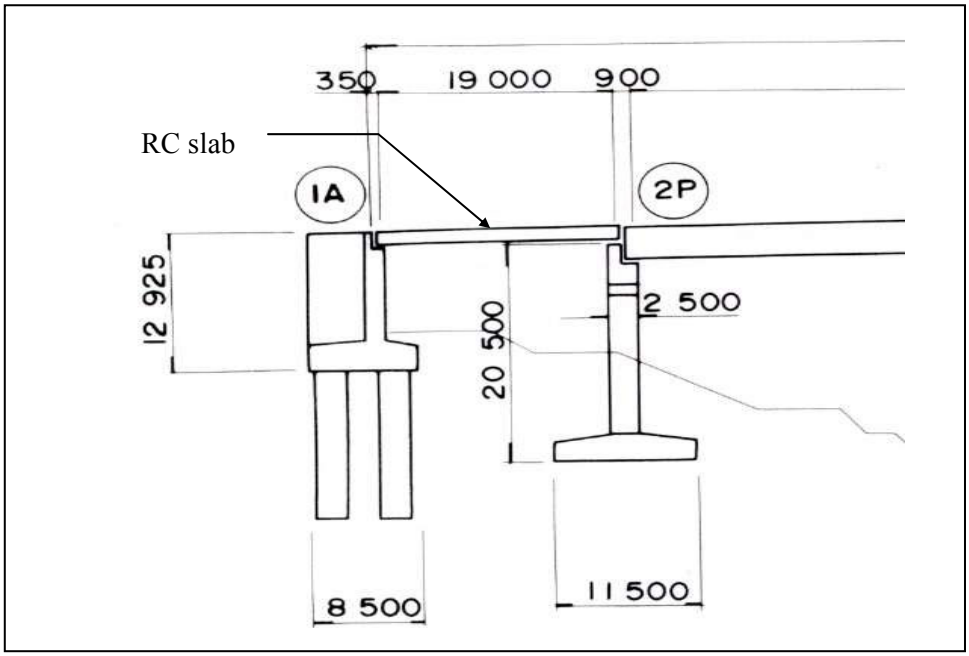

Fig. 4.19 Side view of reinforced concrete girder

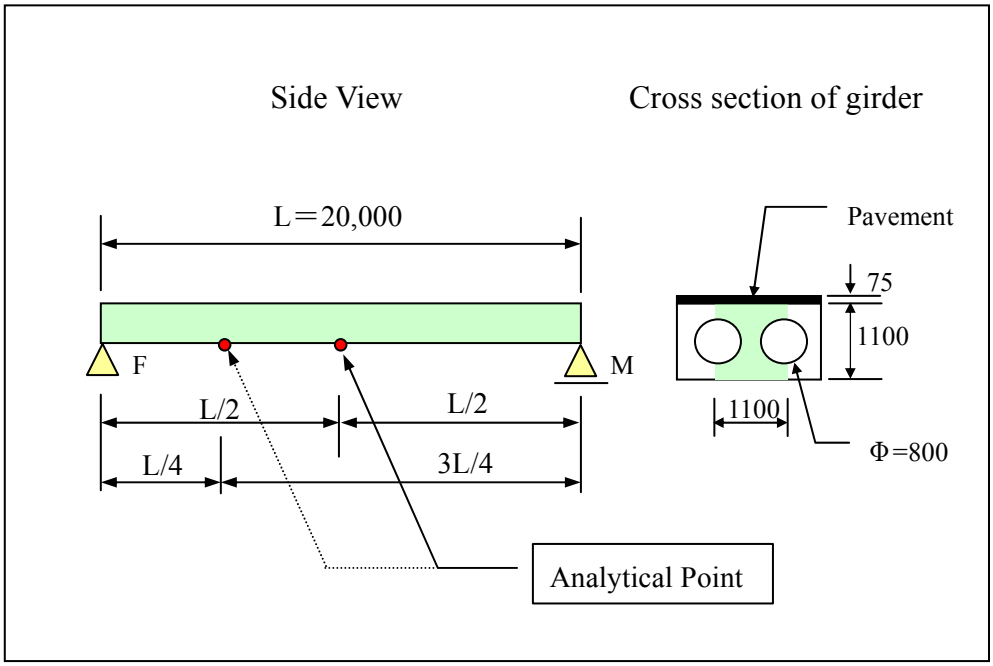

Fig. 4.20 Structural model for reinforced concrete girder

Table 4.5 Analytical case for reinforced concrete girder

Case	Steel bar area in lower flange (per girder)		Sectional area of RC girder (per girder)		Vertical section modulus RC girder (per girder)	
	cm2	Ratio	cm2	Ratio	cm3	Ratio
Case 1	95.28	1.000	7,073	1.000	10,490	1.000
Case 2	71.52	0.750	7,073	1.000	8,514	0.812
Case 3	47.64	0.500	7,073	1.000	6,528	0.622
Case 4	23.82	0.250	7,073	1.000	4,547	0.433
Case 5	0	0.000	7,073	1.000	2,565	0.245

Table 4.6 Reliability Analysis result for reinforced concrete girder (in case of Live Load 2 at x=L/2)

Case	Numbers	Marginal Average Zm	Marginal Standard Deviation σ	Reliability Index β =Zm/ σ	Probability of Safety $\Phi(\beta)$	Probability of Failure Pf= $\Phi(-\beta)$
Case 1	10000	202.0548	20.7238	9.7499	1	0
Case 2	10000	168.8707	23.4059	7.2149	1	0
Case 3	10000	115.3490	27.9272	4.1303	1	0
Case 4	10000	15.8786	37.4613	0.4239	0.6619	0.3381
Case 5	10000	-239.0641	62.8173	-3.8057	0.0001	0.9999

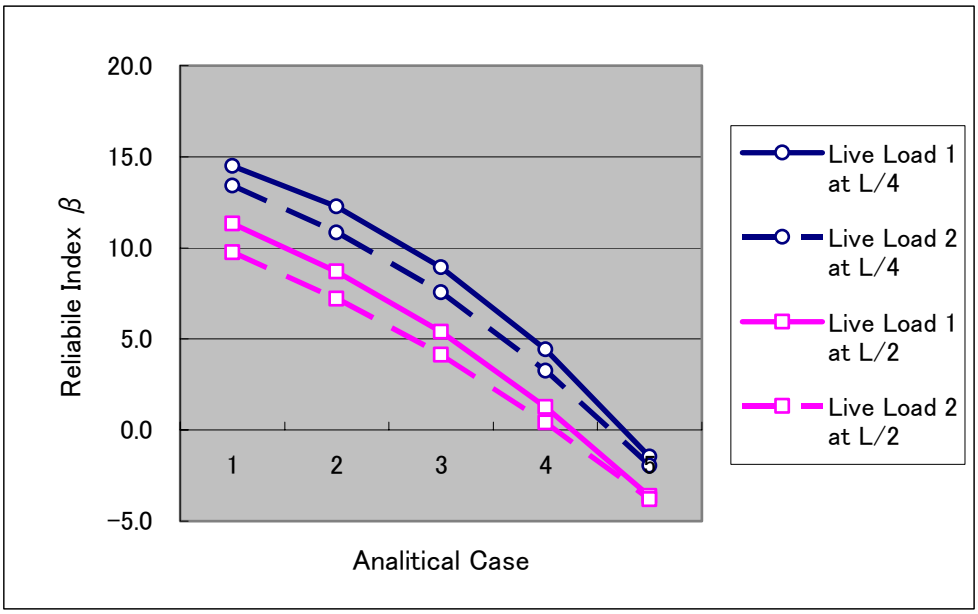

Fig. 4.21 Reliability index of RC girder at x=L/4 and L/2 in each case

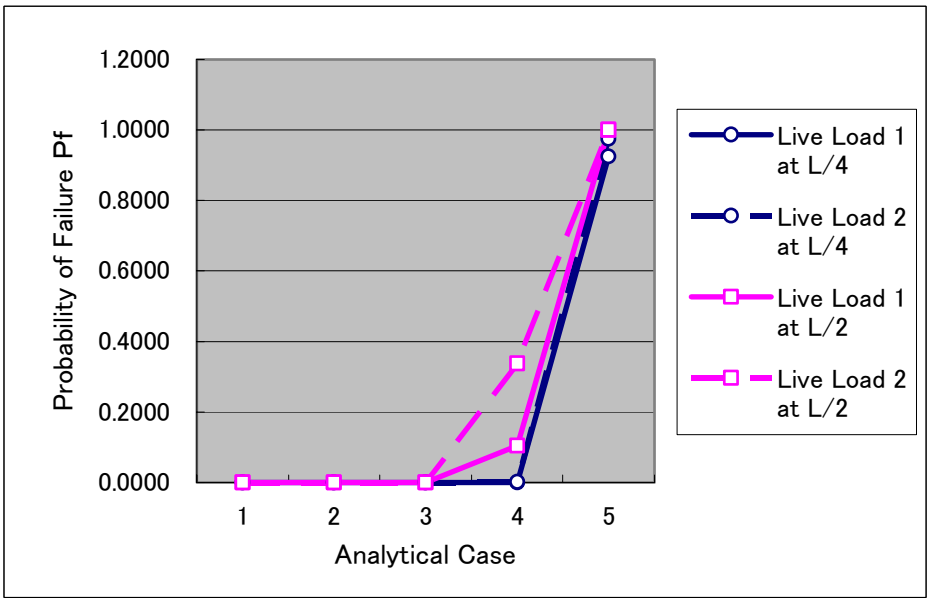

Fig. 4.22 Probability of failure of RC girder at x=L/4 and L/2 in each case

4.7 Summary

The reliability analyses for various bridges were carried out by using the Monte Carlo Simulation, considering the time-dependent load and strength. The conclusions are summarized as follows.

1) The safety of the orthotropic steel deck with the span of 10 meters was checked in case of a three-quarter sectional loss of the lower flange in the longitudinal girder.
2) The safety of the simply supported steel girder with the span of 40 meters was checked in case of a 20-percent sectional loss of the lower flange in the I-shaped girder. Based on the result of long-term prediction, after 40 years old, the reliability index would decrease gradually according to the thickness reduction of lower flange if the appropriate maintenance is not carried out.
3) The safety of the continuous steel girder with the total span of 150 meters was checked in case of a 30-percent sectional loss of the lower flange in the I-shaped girder. Based on the result of long-term prediction, after 40 years old, the reliability index would decrease gradually according to the thickness reduction of lower flange if the appropriate maintenance is not carried out.
4) The safety of the continuous steel box girder with the total span of 300 meters was checked in case of a 30-percent sectional loss of the lower flange in the box girder.
5) The safety of the reinforced concrete girder with the span of 20 meters was checked in case of a half sectional loss of steel bars at the lower flange in the reinforced concrete slab.

5. Reliability Analysis for Long-span Bridges with Time-dependence

5.1 Introduction

Japanese four major islands, i.e., Hokkaido, Honshu, Shikoku and Kyoshu, have been already linked by highways or railways. Especially, Honshu and Shikoku are linked by three routes of Honshu-Shikoku Bridges (Fig.5.1). The Kojima-Sakaide Route, the central route, was completed for highway and railway in 1988, and six long-span bridges are called the Seto-Ohashi Bridges. The Kobe-Naruto Route, the eastern route, was partly opened to traffic in 1985, including the Ohnaruto Bridge (Fig.5.2), and was completed for highway in 1998, including the Akashi Kaikyo Bridge. The Onomichi-Imabari Route, the western route, was almost completed for highway in 1999. Totally, there are eighteen long-span bridges on the three routes.

The Ohnaruto Bridge crosses the Naruto Strait, where is very famous for tidal currents and large whirlpools, and connects the Awaji Island with the Naruto City in Shikoku. The Ohnaruto Bridge is a suspension bridge with the main span of 876 meters, each side span of 330 meters and a backstay span of 93 meters. The total bridge length is 1629 meters. This bridge was constructed by the Honshu-Shikoku Bridge Authority (HSBA) and opened to traffic in 1985 after overcoming the severe natural conditions, including fast tidal currents and strong winds. In order to reduce the tidal force and to minimize the effect on the tidal currents, multi-column type tower foundations are selected for the main tower foundations and the side pier foundation. The maximum tidal current is approximately 10 knots (18.5 km/hr). During substructure construction, special consideration was paid so that no sludgy water leaked out into seawater because the surrounding area is designated to the national park.

The Naruto Strait is also famous for typhoon attacks every year. The basic wind speed is 50 meters per second in 10-minute average at 10-meter high from the sea level, and the design wind speed for the girder is 73 meters per second, which is the highest standard in the Honshu-Shikoku Bridges. Originally, the Ohnaruto Bridge is designed for 6-lane highways and 2-truck railways. Currently, this bridge is opened to traffic for 4-lane highways on the upper deck and an observation pass for public on the lower deck.

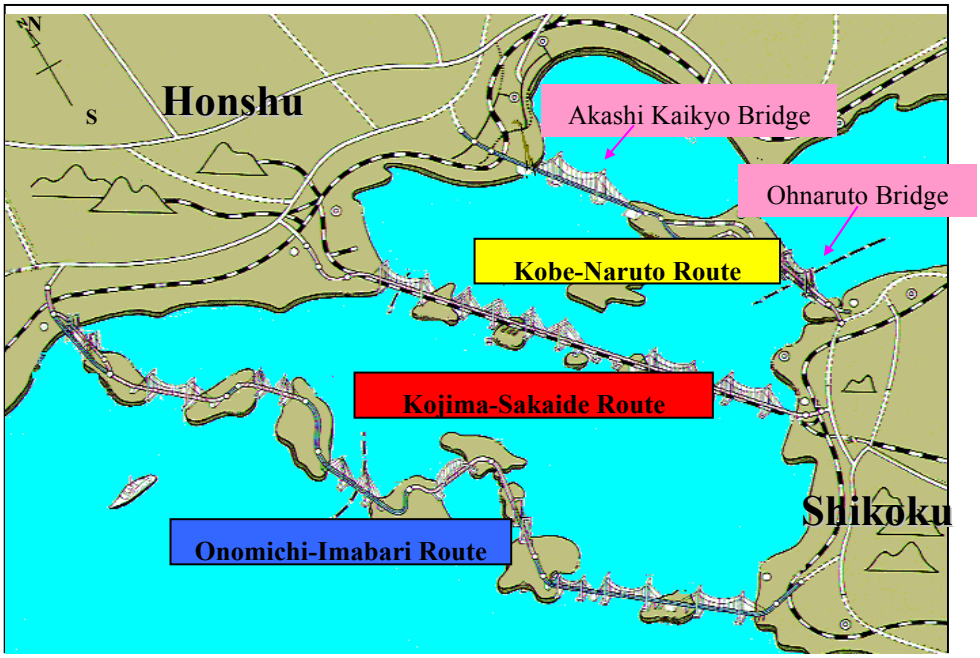

Fig.5.1: The Honshu-Shikoku Bridges

Fig.5.2: The Ohnaruto Bridge, completed in 1985

5.2 Reliability Analysis for Main Cable of Suspension Bridge

5.2.1 Cable Protection System of Suspension Bridge

The main cable of the Ohnaruto Bridge consists of 19,558 galvanized steel wires with each diameter of 5.37 mm. 127 galvanized steel wires were prefabricated for a parallel wire strand (PWS) in shop and 154 strands were erected by the prefabricated strand method in site.

Originally, the protection system for the main cable was composed of galvanized steel wires, paste, wire wrapping and coating, as shown in Fig.5.3. The traditional protection system was also applied to main cables of six suspension bridges in the Honshu-Shikoku Bridges, including the Seto-Ohashi Bridges in 1988.

The investigation into the existing suspension bridges, including the Ohnaruto Bridge, clarified that corrosion occurred in the main cables due to remaining water during construction or operation, as shown in Fig.5.4. A new protection system was required for main cables.

In order to improve the cable protection system, an advanced dehumidification system, which is called “the dry-air injection system,” was developed for the Akashi Kaikyo Bridge during its construction, carrying out various experiments on the galvanized steel wires as well as the cable strands. This system was applied to the existing suspension bridges, including the Ohnaruto Bridge.

As shown in Fig.5.5 and 6.6, the air is dehumidified in the dry-air injection facilities, transported via air injection pipes, injected into the air injection cover, passed through the voids of the galvanized wires, and exhausted out of the air exhaust cover. Totally, four systems are arranged on the Ohnaruto Bridge.

Cable airtight work was carried out from 1999 to 2000 in the Ohnaruto Bridge. In this work, main cables are repainted with soft-type paint, which is composed of soft epoxy resin and soft fluoropolimer paint. Airtight work at cable bands was enhanced by caulking rubbers and sealing compounds. After completion of the airtight work, the dry-air injection system, i.e., the dry-air injection facilities, air injection pipes, and air injection/exhaust covers were installed on the Ohnaruto Bridge.

The fundamental and practical experiments concluded that corrosion does not occur on the galvanized wires in the relative humidity less than 60 percent, if particles are excluded. The target humidity was decided to be 40 percent in the air exhaust cover, which enables that the

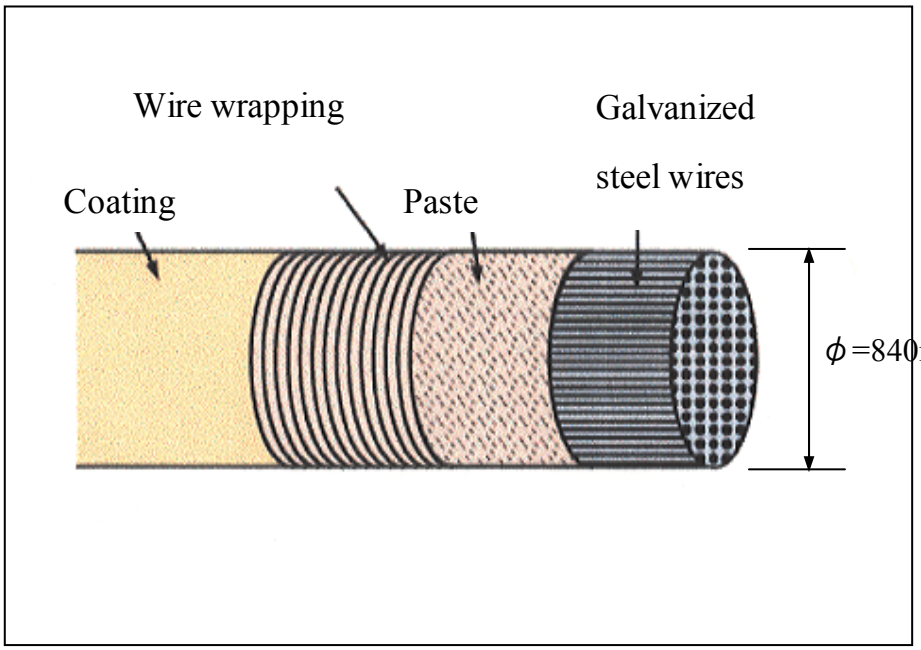

Fig.5.3: Original cable protection system for the Ohnaruto Bridge

Fig.5.4: Corrosion on main cable of the Ohnaruto Bridges

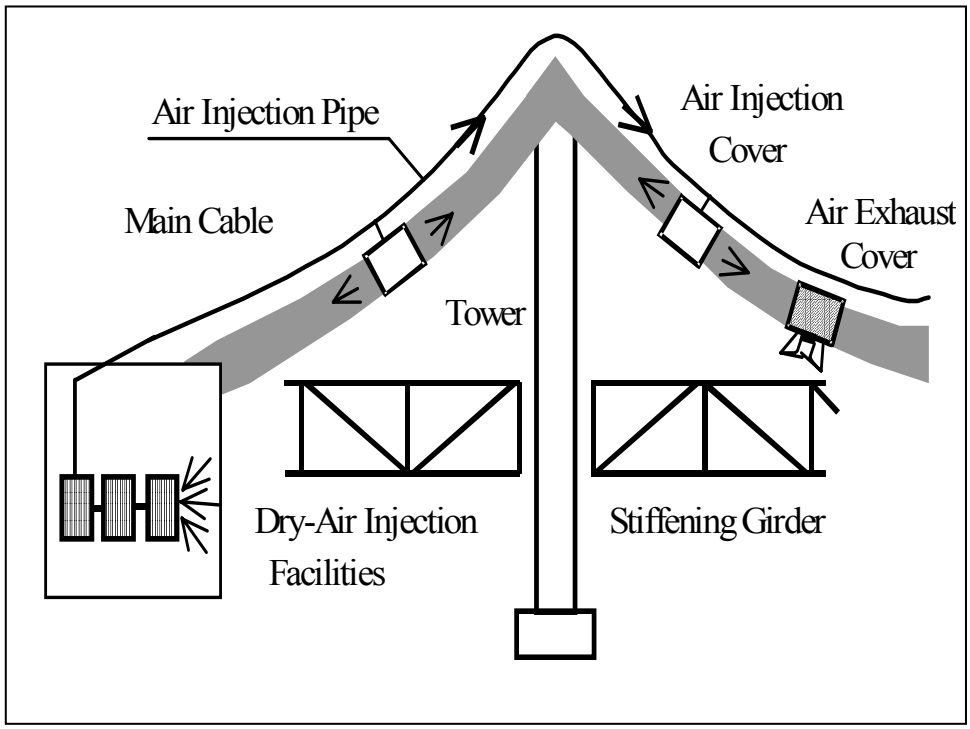

Fig.5.5: Layout of dry-air injection system for the Ohnaruto Bridge

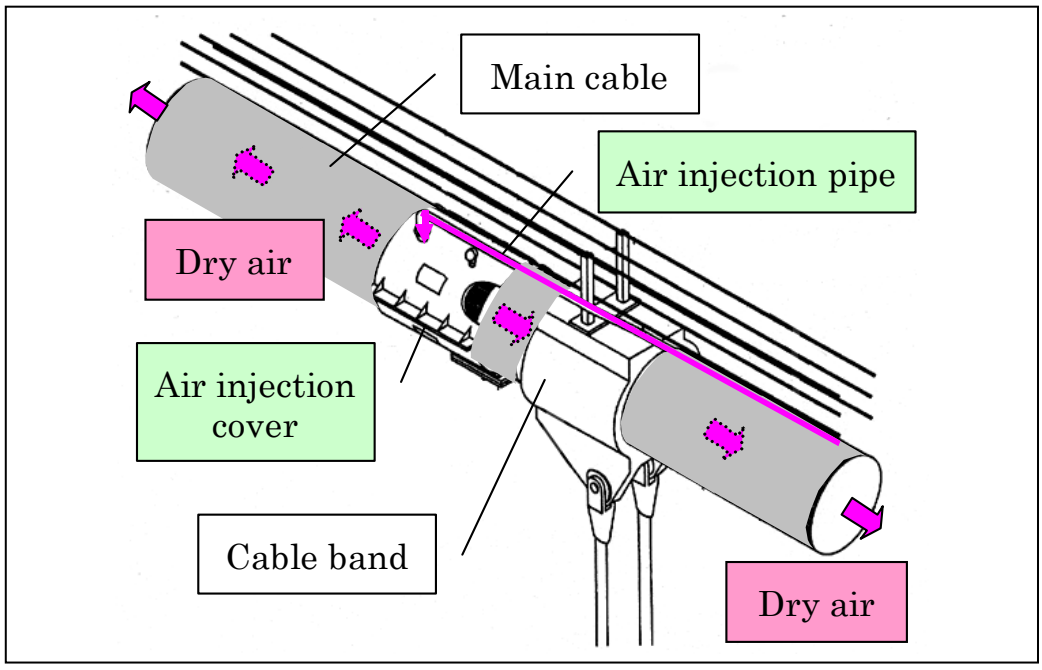

Fig.5.6: Schematic drawing of dry-air injection system

entire main cable is kept in a low humidity throughout the year. The air pressure in the air injection cover is 200-500 mmAq, which is equal to 20-50 hPa. The typical length from the air injection cover to the air exhaust cover is 100-160 meters.

Fig.5.7 shows the relative humidity in the air injection/exhaust cover and the atmospheric humidity and temperature in Naruto from January 2002 through December 2002, which is nearly equal to one year. The relative humidity inside the main cable was almost kept under the target humidity of 40 percent in three systems except one system.

Currently, this system for the Ohnaruto Bridge is not necessarily in a preferable condition, as compared with new suspension bridges, including the Akashi Kaikyo Bridge. No corrosion on the main cables is monitored through the inspection windows on both the air injection covers and the air exhaust covers, while the relative humidity inside the main cable is partially over the target humidity of 40 percent in one of four systems. Investigations are under way, and countermeasures are under consideration.

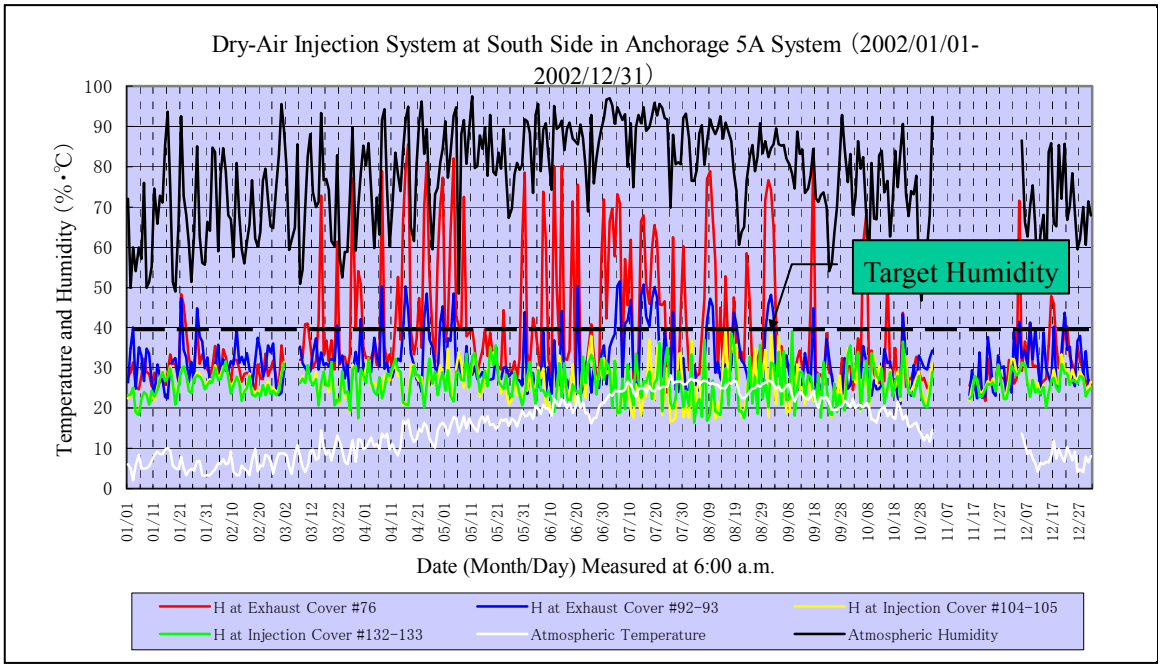

Fig.5.7: Temperature and humidity in main cable of the Ohnaruto Bridge

5.2.2 Reliability Analysis for Main Cables

The main cable consists of approximately twenty thousand galvanized steel wires. Each wire has the 0.7 %-total-elongation yield strength of 1180 MPa (N/mm^2) and the tensile strength of 1600 MPa (N/mm^2). Frequencies of the yield strength and the tensile strength are shown in Fig.5.8, respectively.

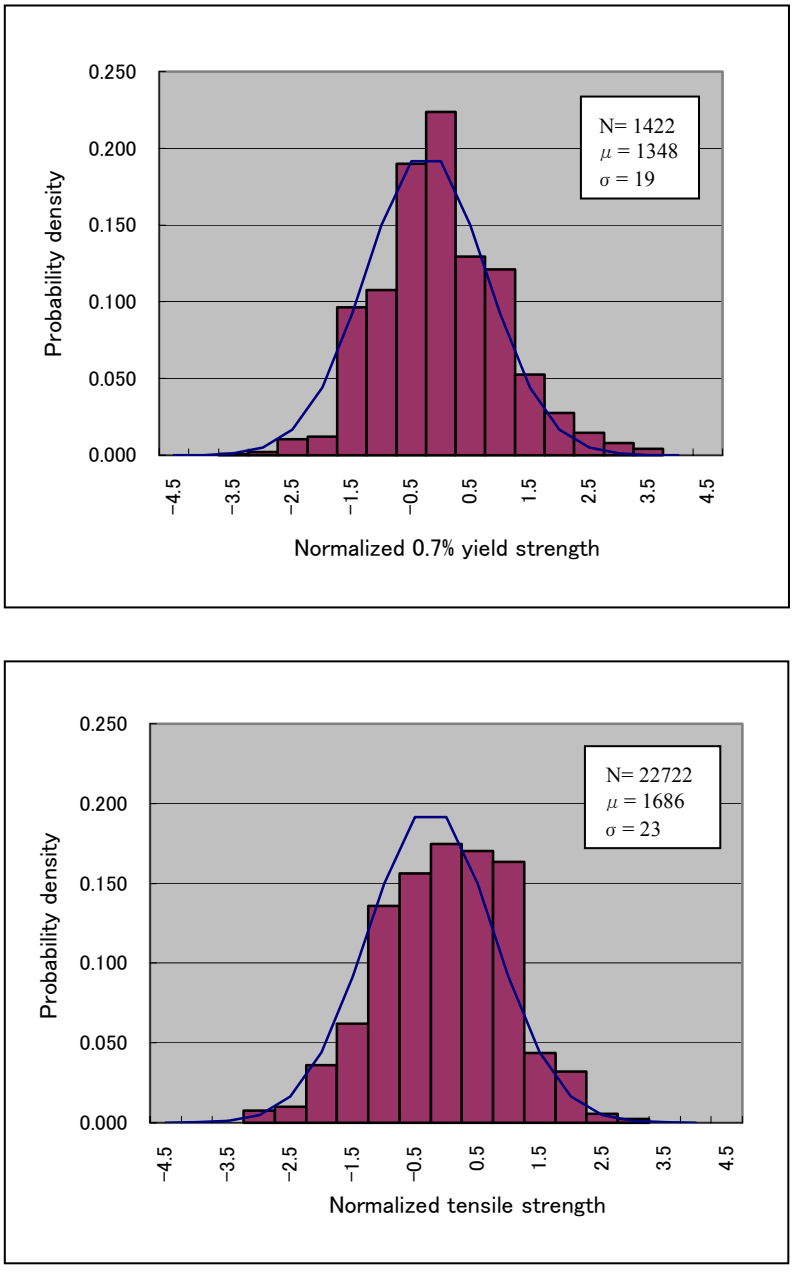

Fig.5.8: Frequency of galvanized steel wires for main cables (yield strength and tensile strength)

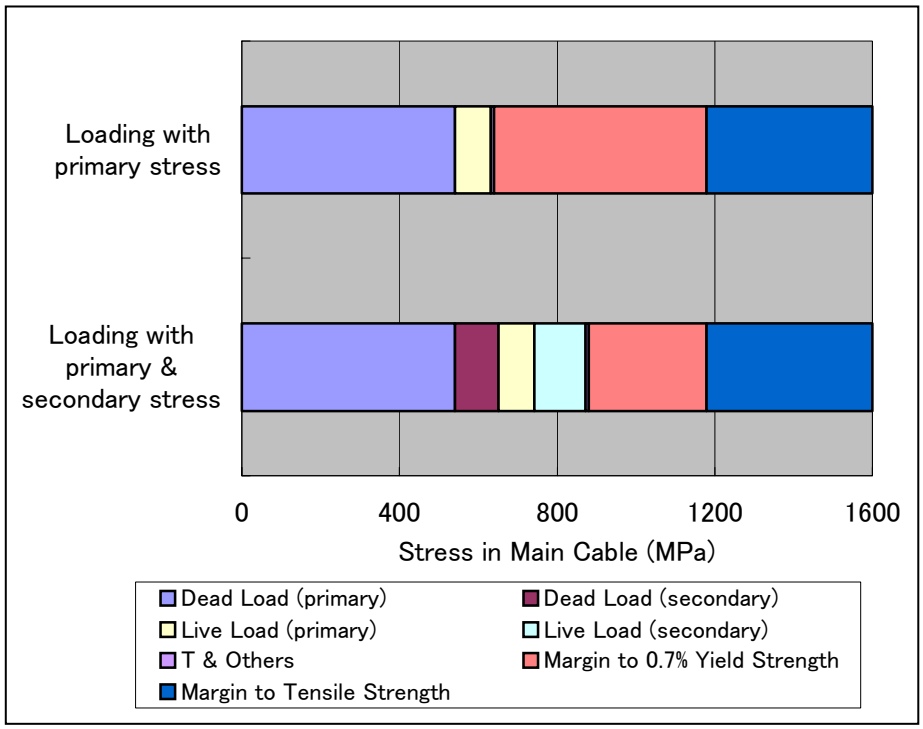

Fig.5.9: Primary stress and secondary stress in main cables

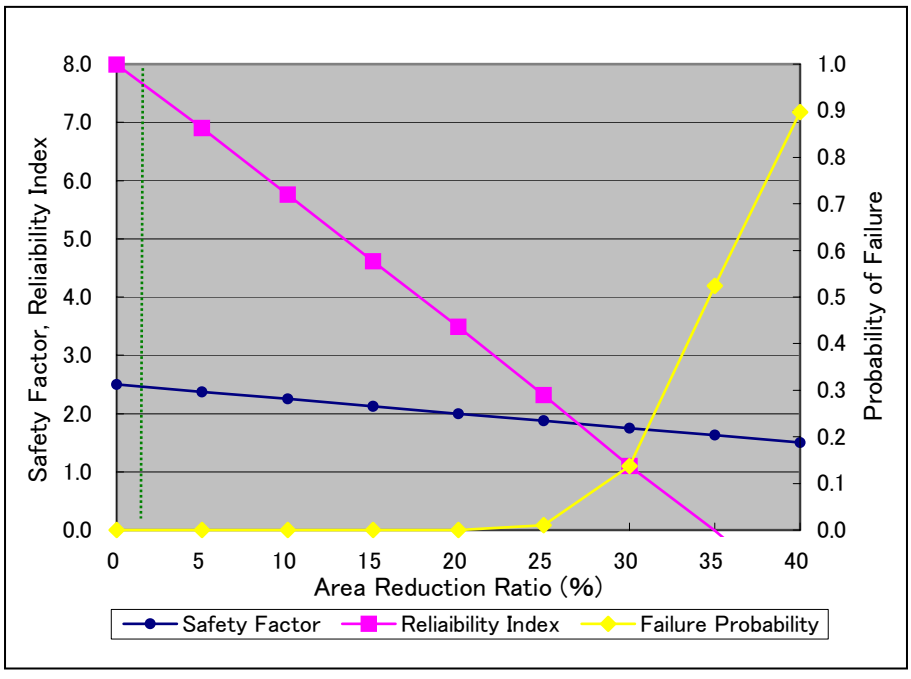

Fig.5.10: Reliability analysis result of main cables

The local bending moment will occur in the main cable due to dead load and the live load, although the main cable is a tensile element. Therefore, the primary stress and the secondary stress are calculated for the dead load and the live load, as shown in Fig.5.9. In the standard loading, the stress ratios in the main cable are 0.845 by dead load, 0.142 by live load and 0.013 by thermal load and others, respectively.

Since the dry-air injection system for the Ohnaruto Bridge is not necessarily in a preferable condition, the reliability analysis for main cables was carried out by the Monte Carlo simulation on the assumption of the cable area reduction. In this analysis, the primary and the secondary stress by the live load only changes in the normal distribution, considering the limit-state loading during operation, and the yield strength for the resistance stress also changes in the normal distribution. The result of reliability analysis is shown in Fig.5.10.

On the other hand, the reduction ratio of corrosion was estimated to be 0.08% per year before introducing of the dry-air injection system. Currently, the total area reduction ratio is less than 1.5% after completion, which means no problem exists in current situation. The system is required to take an early countermeasure.

5.3 Reliability Analysis for Suspender Rope of Suspension Bridge

5.3.1 Suspender Ropes of Suspension Bridge

Suspender ropes of the Ohnaruto Bridge are “center-fit rope cores (CFRC)” with the diameter of 60 and 70 mm, which are twisted with many galvanized wires, are hung on cable bands and are anchored to girders, as shown in Fig.5.11. Coating was carried out on each suspender rope by the dipping method at the site except the anchoring ends in the shop. Under the severe natural condition, corrosions were recognized in suspender ropes not only at general portion but also at anchoring ends, as shown in Fig.5.12. The investigation and the rehabilitation have been under way since 2002.

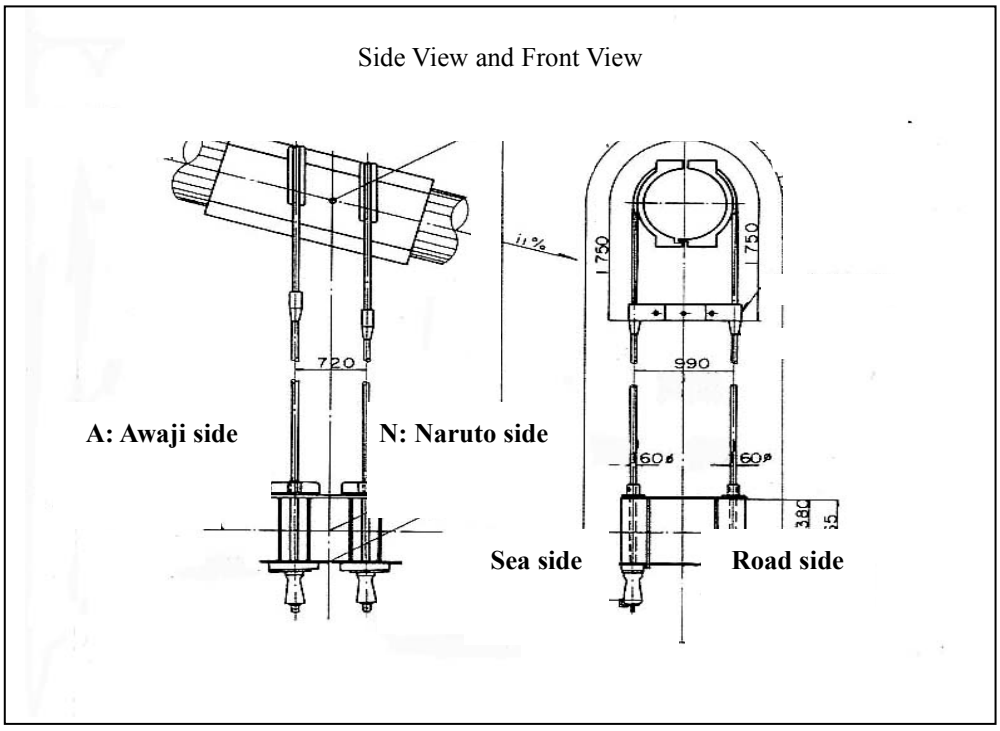

Fig.5.11: Suspender ropes of the Ohnaruto Bridge

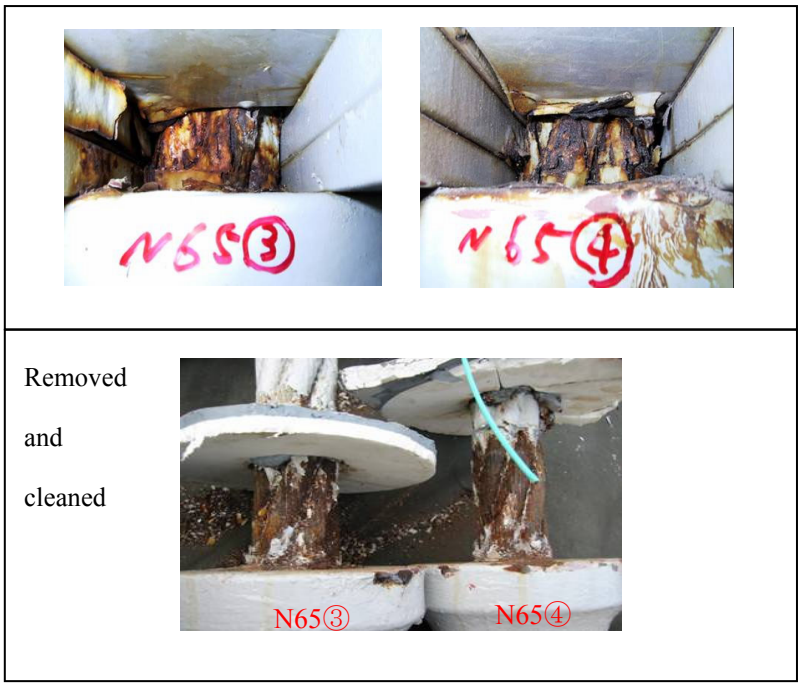

Fig.5.12: Corroded anchoring ends

The general portions of suspender ropes were checked by a non-destructive inspection method, called “the electromagnetic flux method.” In this method, the cross section of suspender rope is supposed to be proportional to the magnetic flux induced by electromagnets. The inspection results for eight general portions of suspender ropes are shown in Fig.5.13. The maximum loss in cross section is not more than 1 percent in the general portions of suspender ropes.

In addition, corrosions were observed in anchoring ends, and another non-destructive inspection method, called “the electromagnetic wave method” was tested, as shown as Fig.5.14. In this method, an electromagnetic wave from a transmitter goes down to the anchoring end, reflects at the anchoring end, and comes back to a receiver. If a sectional loss occurs in the anchoring end, the reflected electromagnetic waves will be reduced more than the distance reduction. The reduction ratio depends on the frequency of electromagnetic wave. The inspection results for eight anchoring ends of suspender ropes yielded that more measured data are required in order to evaluate more precisely the sectional loss at the anchoring ends.

Since corrosions were observed in anchoring ends, two suspender ropes were replaced by new suspender ropes. The removed suspender ropes were inspected by the improved electromagnetic method for the anchoring ends. The electromagnetic method revealed that anchoring ends have the maximum loss of 9 percent in cross section.

The removed suspender ropes were also reassembled in order to check corrosions inside the ropes and were tested in order to measure the remaining tensile strength. The maximum reduction ratio of the tensile strength is 22 percent, as shown in Fig.5.15. By interpolating the relationship of sectional reduction ratio and the tensile strength reduction ratio, the safety factor of the suspender rope is checked, as shown in Fig.5.16. The corrosion in the anchoring end is assumed to progress in proportional to the bridge age. In the anchoring end, the safety factor will reduce to be less than 3.0 at the bridge age of approximately 40 years old. Anti-corrosion measures are required for the anchoring ends.

Fig.5.13(a): Inspection method for general portions of suspender ropes

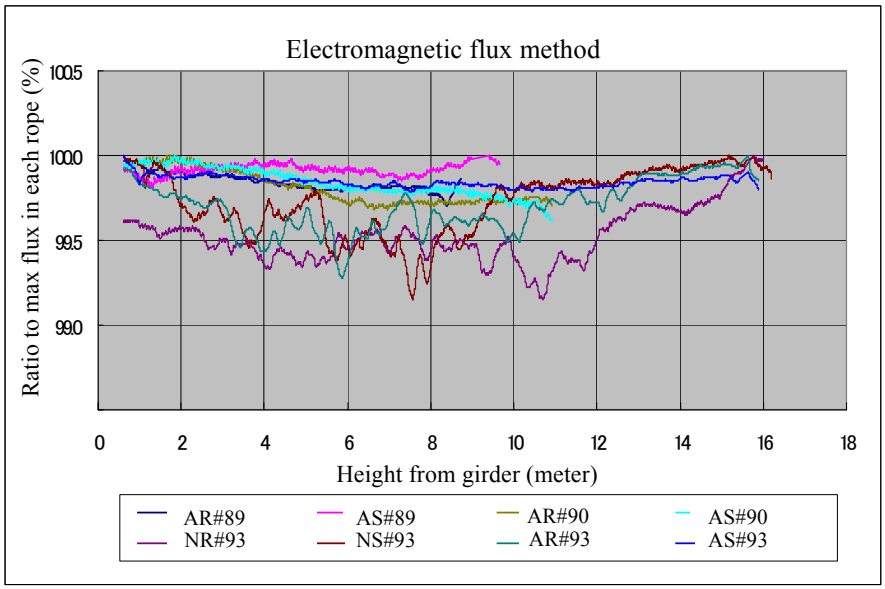

Fig.5.13(b): Inspection result in general portions of suspender ropes

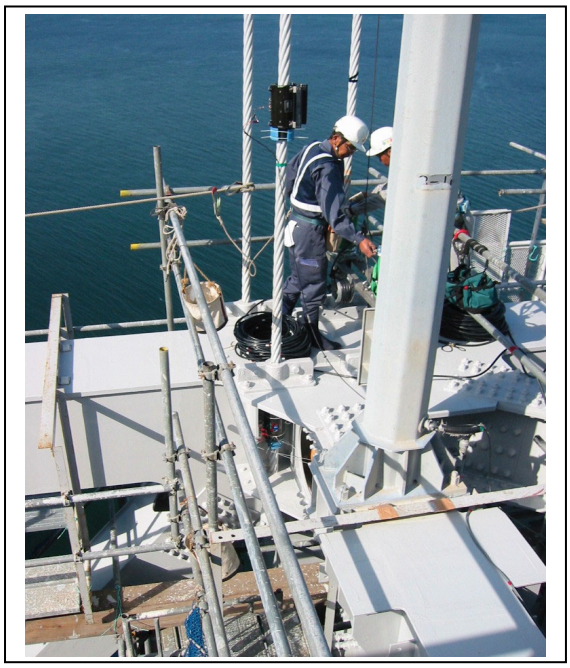

Fig.5.14(a): Inspection method at anchoring ends of suspender ropes

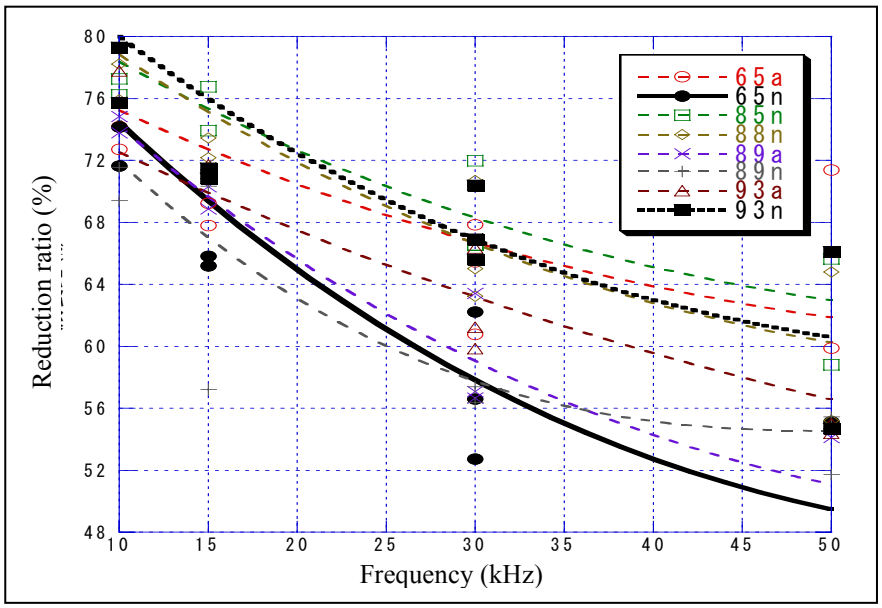

Fig.5.14(b): Inspection result at anchoring ends of suspender ropes

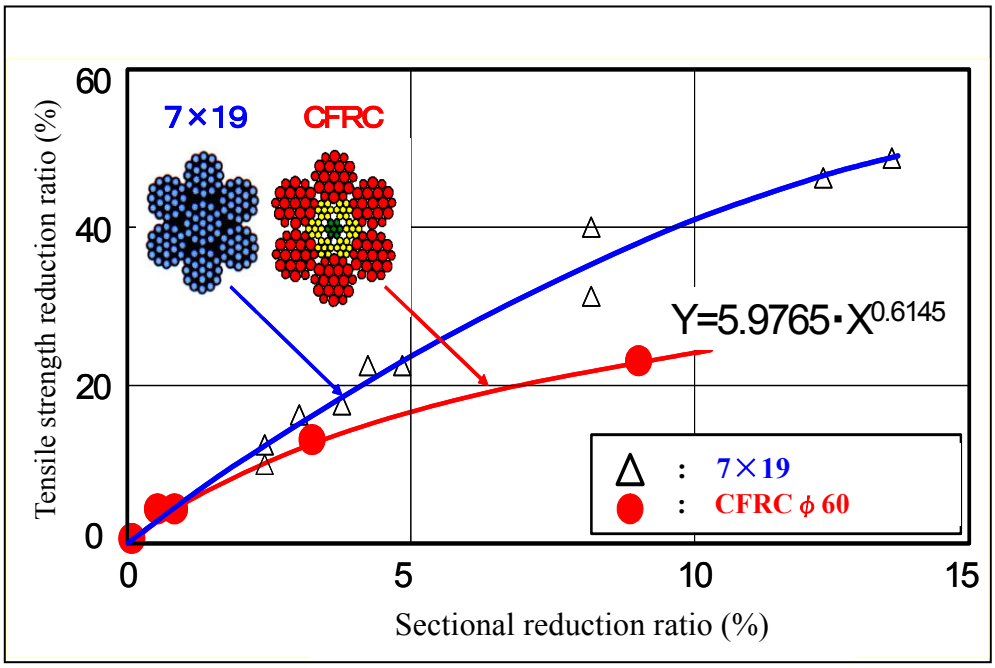

Fig.5.15: Relation between sectional reduction and tensile strength reduction

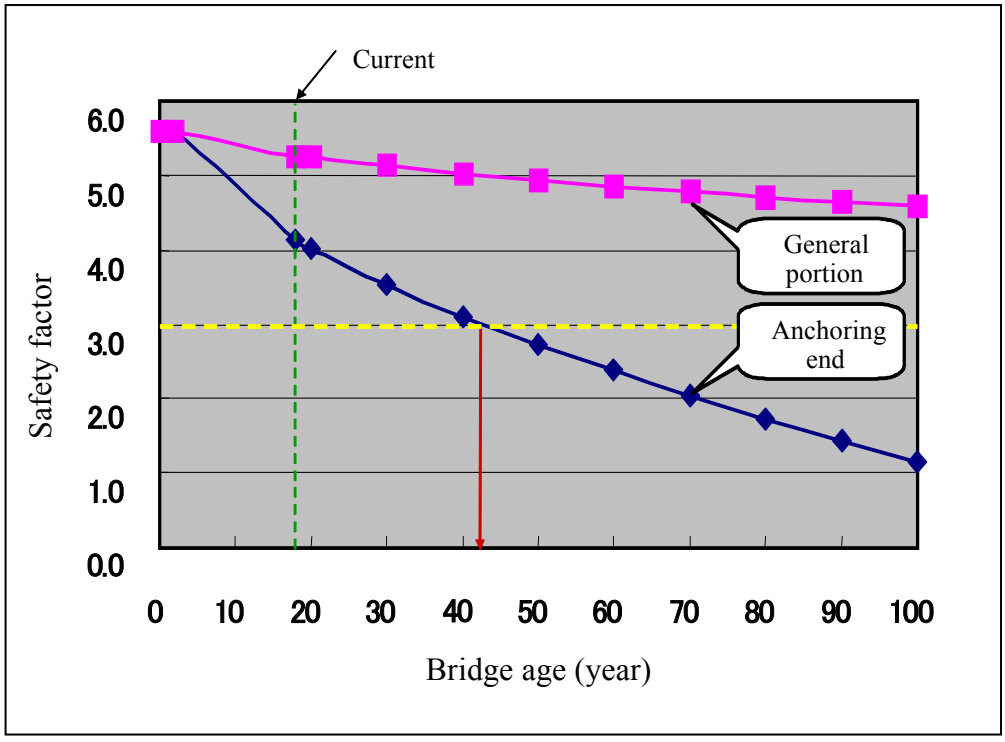

Fig.5.16: Long-term safety check for suspender ropes

5.3.2 Reliability Analysis for Suspender Ropes

Each suspender rope with the diameter of 60 mm has the design tensile strength of 260 ton. The frequency of the tensile strength is shown in Fig.5.17. And the frequency of the live load, which is most influential in suspender ropes, is shown in Fig.5.18.

After the safety check for the suspender ropes, the reliability analysis was carried out by the Monte Carlo simulation, considering the time history due to the corrosion as same as the safety check. In this analysis, the force by the live load, including the impact, only changes in the normal distribution, and the tensile strength for the resistance force also changes in the normal distribution, as shown in Fig.5.19.

The reliability analysis result of suspender ropes is shown in Fig.5.20. The corrosion in the anchoring end is assumed to progress in proportional to the bridge age, which is underestimated in general. The relationship between the sectional ratio and the tensile strength ratio is assumed to be the same as in Fig.5.16. The result yields that the reliability index is more than 5.0 at the bridge age of 70 years old. Anti-corrosion measures are required for the anchoring ends for the preventive maintenance.

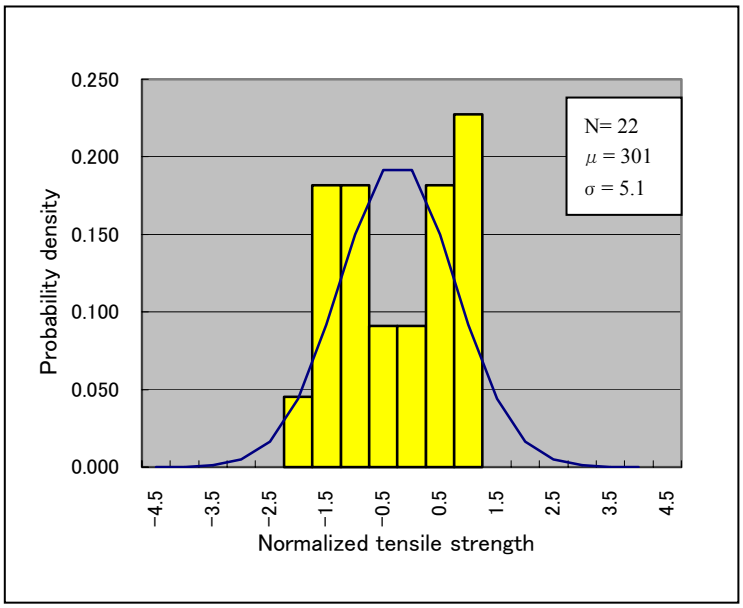

Fig.5.17: Frequency of suspender ropes

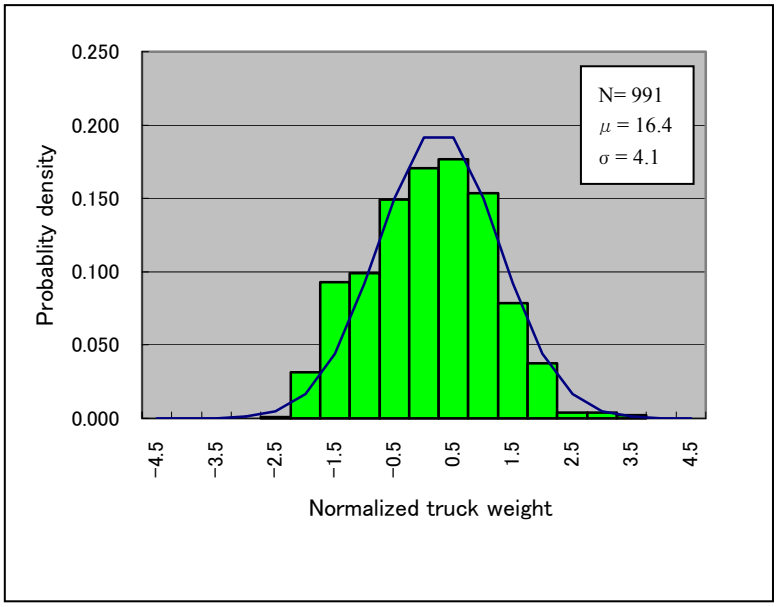

Fig.5.18: Frequency of live load

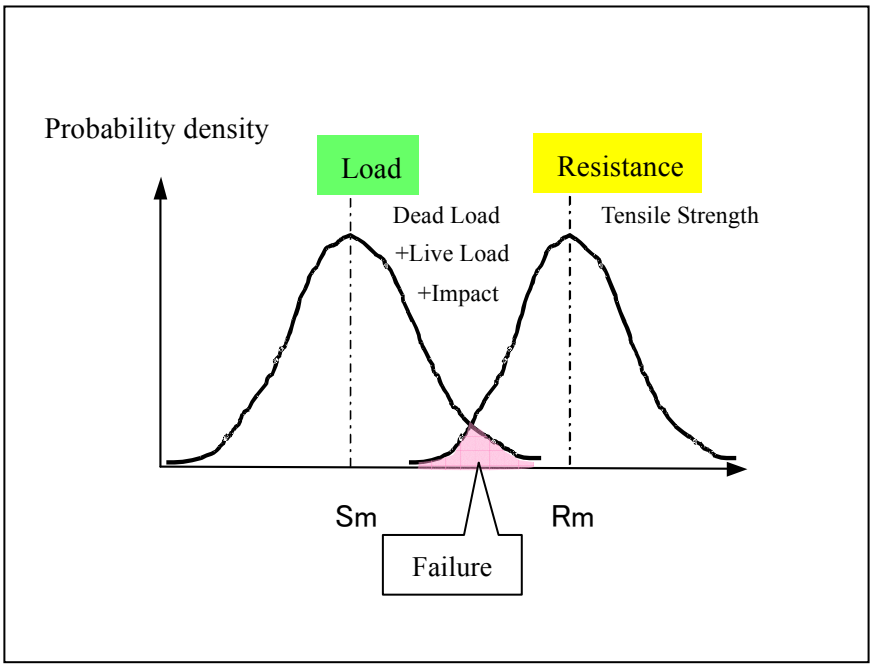

Fig.5.19: Reliability analysis method for suspender ropes

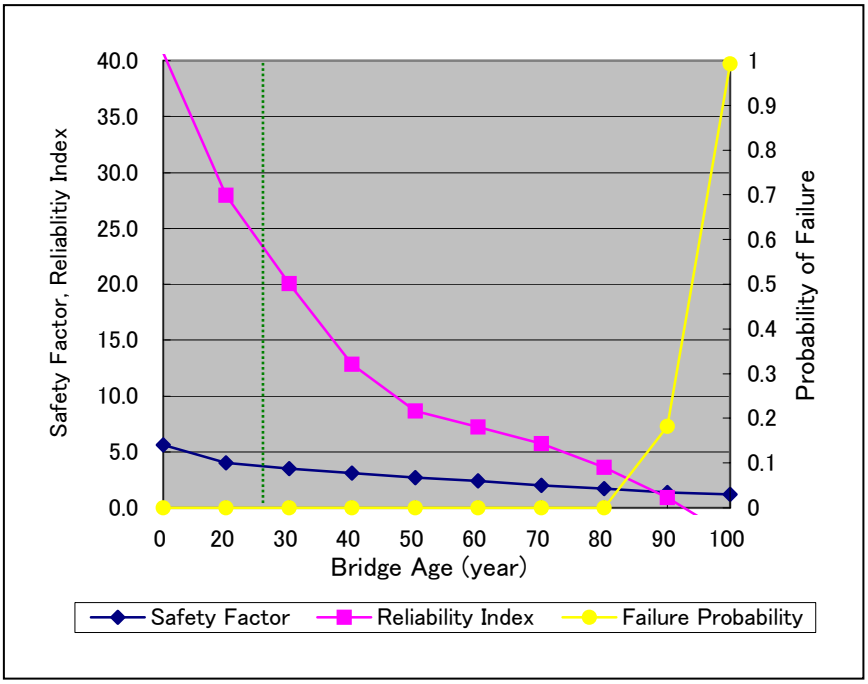

Fig.5.20: Reliability analysis result of suspender ropes

5.4 Reliability Analysis for Entire System of Suspension Bridge

5.4.1 Structural Modeling of Suspension Bridge

In order to evaluate the reliability index and the probability of failure in the entire system of suspension bridge, a two-dimensional full model was made in the bridge-axis direction as shown in Fig. 5.21. The finite element analysis by the linear theory was applied to this modeling for a simple calculation.

The coordinates and restrains of structural model are shown in Table 5.1. And sectional performances, dead loads, live loads and wind loads of structural model are shown in Table 5.2, Table 5.3 and Table 5.4, respectively. These design dimensions were determined in consideration of real suspension bridges. 8 to 10 suspender ropes were assumed to be a bar model for the simplicity.

Analytical results due to dead loads in the vertical direction are shown in Fig. 5.22-5.24, respectively. Analytical results due to live loads in the vertical direction are shown in Fig. 5.25-5.27, respectively. In addition, the analytical results due to wind loads in the lateral direction, using this model with little modification, are shown in Fig. 5.28-5.30, respectively.

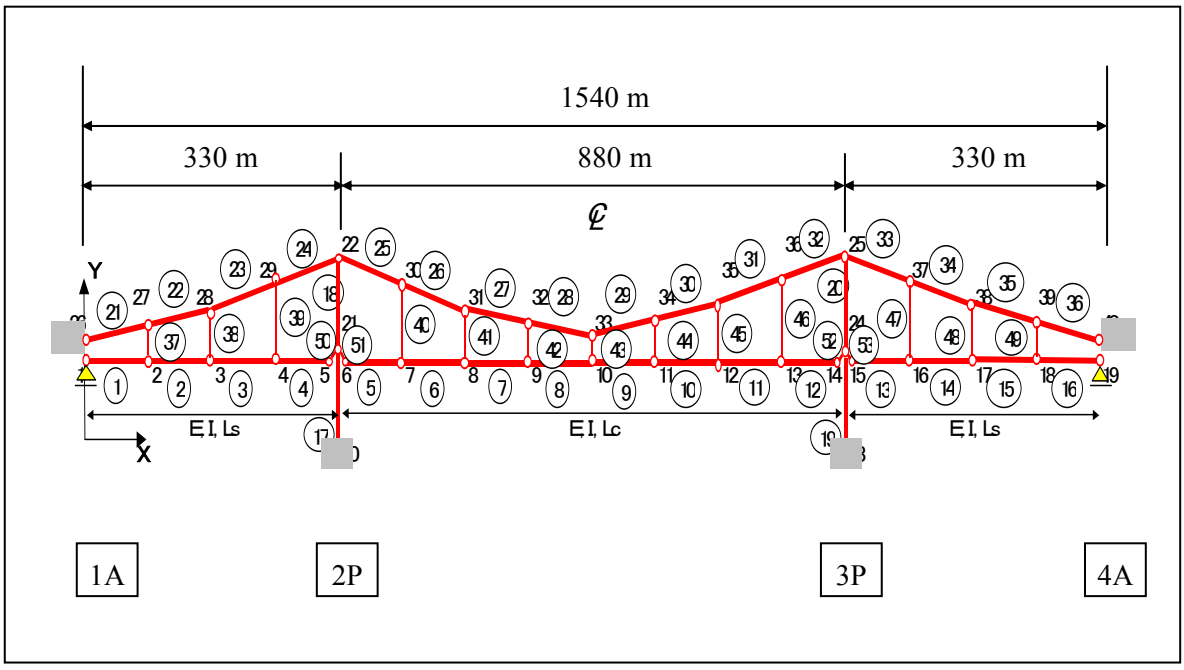

Fig. 5.21 Structural model for a suspension bridge with the main span of 880 m

Table 5. 1 Coordinates and restrains of structural model

Node #	x coordinate	y coordinate	x restrain	y restrain	Rotation	Location
1	10	50	1	1	0	Bearing 1A
2	88.75	50	0	0	0	
3	167.5	50	0	0	0	
4	246.25	50	0	0	0	
5	325	50	1	1	0	Link 2P
6	335	50	1	1	0	Link 2P
7	443.75	50	0	0	0	
8	552.5	50	0	0	0	
9	661.25	50	0	0	0	
10	770	50	0	0	0	CL of Girder
11	878.75	50	0	0	0	
12	987.5	50	0	0	0	
13	1096.25	50	0	0	0	
14	1205	50	1	1	0	Link 3P
15	1215	50	1	1	0	Link 3P
16	1293.75	50	0	0	0	
17	1372.5	50	0	0	0	
18	1451.25	50	0	0	0	
19	1530	50	1	1	0	Bearing 4A
20	330	0	1	1	0	Foundation 2P
21	330	55	0	1	0	
22	330	150	0	1	0	Tower Top 2P
23	1210	0	1	1	0	Foundation 3P
24	1210	55	0	1	0	
25	1210	150	0	1	0	Tower Top 3P
26	0	55	1	1	1	Anchorage 1A
27	88.75	61.871	0	0	1	
28	167.5	79.475	0	0	1	
29	246.25	107.899	0	0	1	
30	443.75	107.23	0	0	1	
31	552.5	78.213	0	0	1	
32	661.25	60.803	0	0	1	
33	770	55	0	0	1	CL of Cable
34	878.75	60.803	0	0	1	
35	987.5	78.213	0	0	1	
36	1096.25	107.23	0	0	1	
37	1293.75	107.899	0	0	1	
38	1372.5	79.475	0	0	1	
39	1451.25	61.871	0	0	1	
40	1540	55	1	1	1	Anchorage 4A

Note 1) Unit of x or y coordinate is meter 2) Restarin 0: free, 1: fixed

Table 5.2 Sectional performances and dead loads of structural model in vertical direction

Element #	Node i	Node j	E (kN/m2)	A (m2)	I (m4)	wxi	wxj	wyi	wyj
1	1	2	2.00E+08	2	70	0	0	−300	−300
2	2	3	2.00E+08	2	70	0	0	−300	−300
3	3	4	2.00E+08	2	70	0	0	−300	−300
4	4	5	2.00E+08	2	70	0	0	−300	−300
5	6	7	2.00E+08	2	70	0	0	−300	−300
6	7	8	2.00E+08	2	70	0	0	−300	−300
7	8	9	2.00E+08	2	70	0	0	−300	−300
8	9	10	2.00E+08	2	70	0	0	−300	−300
9	10	11	2.00E+08	2	70	0	0	−300	−300
10	11	12	2.00E+08	2	70	0	0	−300	−300
11	12	13	2.00E+08	2	70	0	0	−300	−300
12	13	14	2.00E+08	2	70	0	0	−300	−300
13	15	16	2.00E+08	2	70	0	0	−300	−300
14	16	17	2.00E+08	2	70	0	0	−300	−300
15	17	18	2.00E+08	2	70	0	0	−300	−300
16	18	19	2.00E+08	2	70	0	0	−300	−300
17	20	21	2.00E+08	4	30	0	0	−600	−600
18	21	22	2.00E+08	4	30	0	0	−600	−600
19	23	24	2.00E+08	4	30	0	0	−600	−600
20	24	25	2.00E+08	4	30	0	0	−600	−600
21	26	27	2.00E+08	1	0	0	0	−80	−80
22	27	28	2.00E+08	1	0	0	0	−80	−80
23	28	29	2.00E+08	1	0	0	0	−80	−80
24	29	22	2.00E+08	1	0	0	0	−80	−80
25	22	30	2.00E+08	1	0	0	0	−80	−80
26	30	31	2.00E+08	1	0	0	0	−80	−80
27	31	32	2.00E+08	1	0	0	0	−80	−80
28	32	33	2.00E+08	1	0	0	0	−80	−80
29	33	34	2.00E+08	1	0	0	0	−80	−80
30	34	35	2.00E+08	1	0	0	0	−80	−80
31	35	36	2.00E+08	1	0	0	0	−80	−80
32	36	25	2.00E+08	1	0	0	0	−80	−80
33	25	37	2.00E+08	1	0	0	0	−80	−80
34	37	38	2.00E+08	1	0	0	0	−80	−80
35	38	39	2.00E+08	1	0	0	0	−80	−80
36	39	40	2.00E+08	1	0	0	0	−80	−80
37	2	27	2.00E+08	0.2	0	0	0	−10	−10
38	3	28	2.00E+08	0.2	0	0	0	−10	−10
39	4	29	2.00E+08	0.2	0	0	0	−10	−10
40	7	30	2.00E+08	0.2	0	0	0	−10	−10
41	8	31	2.00E+08	0.2	0	0	0	−10	−10
42	9	32	2.00E+08	0.2	0	0	0	−10	−10
43	10	33	2.00E+08	0.2	0	0	0	−10	−10
44	11	34	2.00E+08	0.2	0	0	0	−10	−10
45	12	35	2.00E+08	0.2	0	0	0	−10	−10
46	13	36	2.00E+08	0.2	0	0	0	−10	−10
47	16	37	2.00E+08	0.2	0	0	0	−10	−10
48	17	38	2.00E+08	0.2	0	0	0	−10	−10
49	18	39	2.00E+08	0.2	0	0	0	−10	−10
50	5	21	2.00E+08	1	0	0	0	−100	−100
51	6	21	2.00E+08	1	0	0	0	−100	−100
52	14	24	2.00E+08	1	0	0	0	−100	−100
53	15	24	2.00E+08	1	0	0	0	−100	−100

Table 5.3 Sectional performances and live loads of structural model in vertical direction

Element #	Node i	Node j	E (kN/m2)	A (m2)	I (m4)	wxi	wxj	wyi	wyj
1	1	2	2.00E+08	2	70	0	0	0	0
2	2	3	2.00E+08	2	70	0	0	0	0
3	3	4	2.00E+08	2	70	0	0	0	0
4	4	5	2.00E+08	2	70	0	0	0	0
5	6	7	2.00E+08	2	70	0	0	−50	−50
6	7	8	2.00E+08	2	70	0	0	−50	−50
7	8	9	2.00E+08	2	70	0	0	−50	−50
8	9	10	2.00E+08	2	70	0	0	−50	−50
9	10	11	2.00E+08	2	70	0	0	−50	−50
10	11	12	2.00E+08	2	70	0	0	−50	−50
11	12	13	2.00E+08	2	70	0	0	−50	−50
12	13	14	2.00E+08	2	70	0	0	−50	−50
13	15	16	2.00E+08	2	70	0	0	0	0
14	16	17	2.00E+08	2	70	0	0	0	0
15	17	18	2.00E+08	2	70	0	0	0	0
16	18	19	2.00E+08	2	70	0	0	0	0
17	20	21	2.00E+08	4	30	0	0	0	0
18	21	22	2.00E+08	4	30	0	0	0	0
19	23	24	2.00E+08	4	30	0	0	0	0
20	24	25	2.00E+08	4	30	0	0	0	0
21	26	27	2.00E+08	1	0	0	0	0	0
22	27	28	2.00E+08	1	0	0	0	0	0
23	28	29	2.00E+08	1	0	0	0	0	0
24	29	22	2.00E+08	1	0	0	0	0	0
25	22	30	2.00E+08	1	0	0	0	0	0
26	30	31	2.00E+08	1	0	0	0	0	0
27	31	32	2.00E+08	1	0	0	0	0	0
28	32	33	2.00E+08	1	0	0	0	0	0
29	33	34	2.00E+08	1	0	0	0	0	0
30	34	35	2.00E+08	1	0	0	0	0	0
31	35	36	2.00E+08	1	0	0	0	0	0
32	36	25	2.00E+08	1	0	0	0	0	0
33	25	37	2.00E+08	1	0	0	0	0	0
34	37	38	2.00E+08	1	0	0	0	0	0
35	38	39	2.00E+08	1	0	0	0	0	0
36	39	40	2.00E+08	1	0	0	0	0	0
37	2	27	2.00E+08	0.2	0	0	0	0	0
38	3	28	2.00E+08	0.2	0	0	0	0	0
39	4	29	2.00E+08	0.2	0	0	0	0	0
40	7	30	2.00E+08	0.2	0	0	0	0	0
41	8	31	2.00E+08	0.2	0	0	0	0	0
42	9	32	2.00E+08	0.2	0	0	0	0	0
43	10	33	2.00E+08	0.2	0	0	0	0	0
44	11	34	2.00E+08	0.2	0	0	0	0	0
45	12	35	2.00E+08	0.2	0	0	0	0	0
46	13	36	2.00E+08	0.2	0	0	0	0	0
47	16	37	2.00E+08	0.2	0	0	0	0	0
48	17	38	2.00E+08	0.2	0	0	0	0	0
49	18	39	2.00E+08	0.2	0	0	0	0	0
50	5	21	2.00E+08	1	0	0	0	0	0
51	6	21	2.00E+08	1	0	0	0	0	0
52	14	24	2.00E+08	1	0	0	0	0	0
53	15	24	2.00E+08	1	0	0	0	0	0

Note 1) a concentrated live load (-800kN) is applied at the center of main span (node 10).

Table 5.4 Sectional performances and wind loads of structural model in lateral direction

Element #	Node i	Node j	E (kN/m2)	A (m2)	I (m4)	wxi	wxj	wzi	wzj
1	1	2	2.00E+08	2	420	0	0	−60	−60
2	2	3	2.00E+08	2	420	0	0	−60	−60
3	3	4	2.00E+08	2	420	0	0	−60	−60
4	4	5	2.00E+08	2	420	0	0	−60	−60
5	6	7	2.00E+08	2	420	0	0	−60	−60
6	7	8	2.00E+08	2	420	0	0	−60	−60
7	8	9	2.00E+08	2	420	0	0	−60	−60
8	9	10	2.00E+08	2	420	0	0	−60	−60
9	10	11	2.00E+08	2	420	0	0	−60	−60
10	11	12	2.00E+08	2	420	0	0	−60	−60
11	12	13	2.00E+08	2	420	0	0	−60	−60
12	13	14	2.00E+08	2	420	0	0	−60	−60
13	15	16	2.00E+08	2	420	0	0	−60	−60
14	16	17	2.00E+08	2	420	0	0	−60	−60
15	17	18	2.00E+08	2	420	0	0	−60	−60
16	18	19	2.00E+08	2	420	0	0	−60	−60
17	20	21	2.00E+08	4	1240	120	120	0	0
18	21	22	2.00E+08	4	1240	120	120	0	0
19	23	24	2.00E+08	4	1240	−120	−120	0	0
20	24	25	2.00E+08	4	1240	−120	−120	0	0
21	26	27	2.00E+08	1	0	0	0	−10	−10
22	27	28	2.00E+08	1	0	0	0	−10	−10
23	28	29	2.00E+08	1	0	0	0	−10	−10
24	29	22	2.00E+08	1	0	0	0	−10	−10
25	22	30	2.00E+08	1	0	0	0	−10	−10
26	30	31	2.00E+08	1	0	0	0	−10	−10
27	31	32	2.00E+08	1	0	0	0	−10	−10
28	32	33	2.00E+08	1	0	0	0	−10	−10
29	33	34	2.00E+08	1	0	0	0	−10	−10
30	34	35	2.00E+08	1	0	0	0	−10	−10
31	35	36	2.00E+08	1	0	0	0	−10	−10
32	36	25	2.00E+08	1	0	0	0	−10	−10
33	25	37	2.00E+08	1	0	0	0	−10	−10
34	37	38	2.00E+08	1	0	0	0	−10	−10
35	38	39	2.00E+08	1	0	0	0	−10	−10
36	39	40	2.00E+08	1	0	0	0	−10	−10
37	2	27	2.00E+08	0.2	0	3	3	0	0
38	3	28	2.00E+08	0.2	0	3	3	0	0
39	4	29	2.00E+08	0.2	0	3	3	0	0
40	7	30	2.00E+08	0.2	0	3	3	0	0
41	8	31	2.00E+08	0.2	0	3	3	0	0
42	9	32	2.00E+08	0.2	0	3	3	0	0
43	10	33	2.00E+08	0.2	0	3	3	0	0
44	11	34	2.00E+08	0.2	0	3	3	0	0
45	12	35	2.00E+08	0.2	0	3	3	0	0
46	13	36	2.00E+08	0.2	0	3	3	0	0
47	16	37	2.00E+08	0.2	0	3	3	0	0
48	17	38	2.00E+08	0.2	0	3	3	0	0
49	18	39	2.00E+08	0.2	0	3	3	0	0
50	5	21	2.00E+08	1	0	0	0	0	0
51	6	21	2.00E+08	1	0	0	0	0	0
52	14	24	2.00E+08	1	0	0	0	0	0
53	15	24	2.00E+08	1	0	0	0	0	0

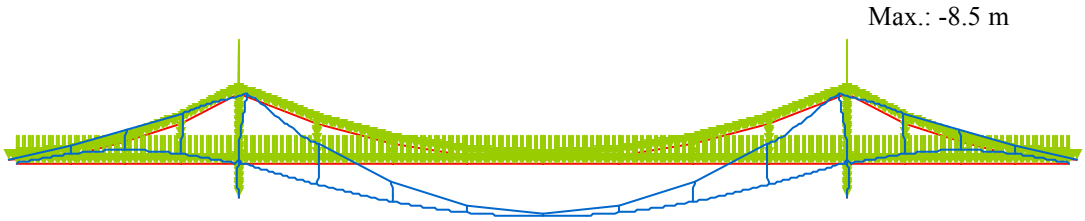

Fig. 5.22 Displacements of suspension bridge due to dead load

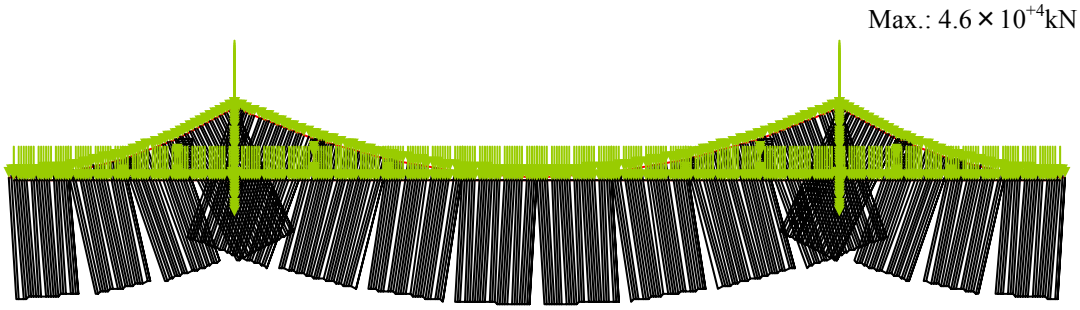

Fig. 5.23 Axial forces of suspension bridge due to dead load

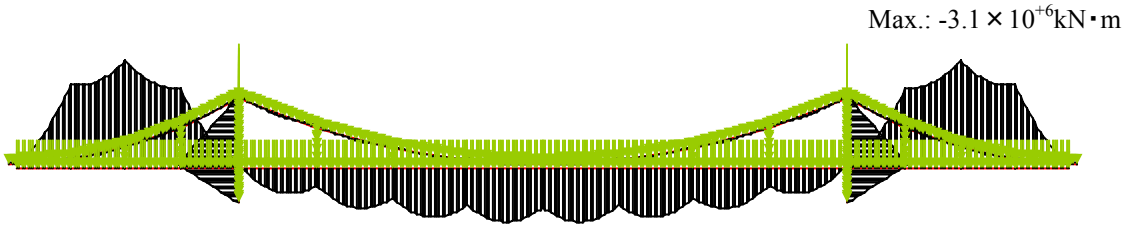

Fig. 5.24 Bending moments of suspension bridge due to dead load

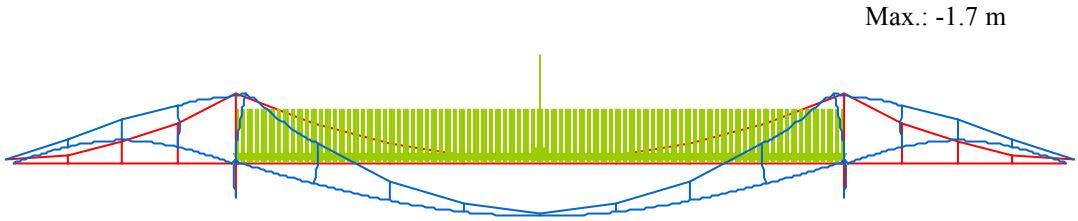

Fig. 5.25 Displacements of suspension bridge due to live load

Fig. 5.26 Axial forces of suspension bridge due to live load

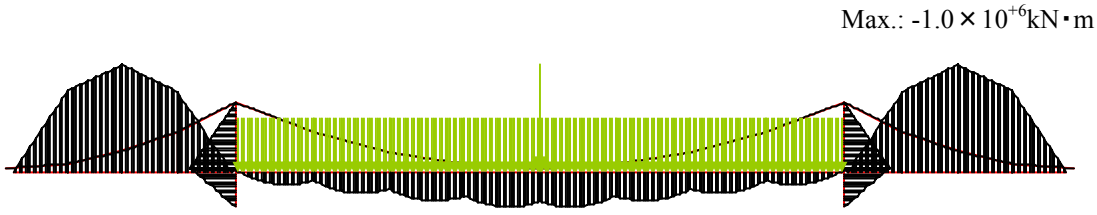

Fig. 5.27 Bending moments of suspension bridge due to live load

Max.: -6.2 m

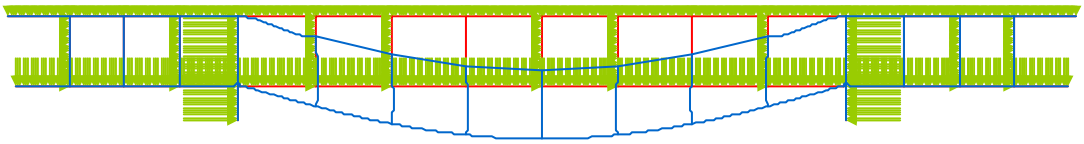

Fig. 5.28 Lateral displacements of suspension bridge due to wind load

Max.: $2.7 \times 10^{+3}$kN

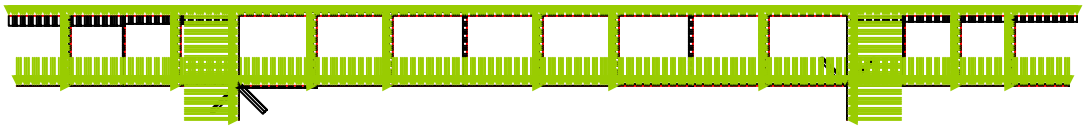

Fig. 5.29 Axial forces of suspension bridge due to wind load

Max.: $6.6 \times 10^{+6}$kN·m

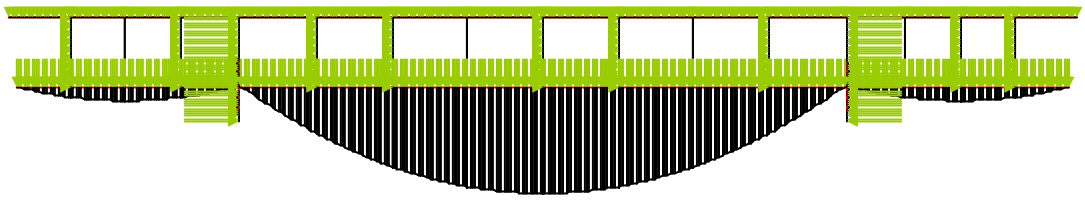

Fig. 5.30 Bending moments of suspension bridge due to wind load

5.4.2 Reliability Analysis of Suspension Bridge

By using the full model of suspension bridge, the reliability analysis carried out by the Monte Carlo simulation on the assumption of increasing the live load or the wind load.

In the first analysis, the stress due to the live load only changes in the normal distribution. Considering the long-term change of the live load, the reliability analysis are carried out in the following three cases, 1) design live load for the suspension bridge, 2) 10-percent increase of design live load, and 3) 20-percent increase of design live load. Each live load is assumed to have the coefficient of variation of 0.05. The yield stress of the cable is 1180 MPa. The buckling stress of girders are 490 MPa for HT780 at the center of main span, and 360 MPa for SM570 at the center of side span, respectively. Each yield stress or buckling stress assumed to have the coefficient of variation of 0.05. The result of reliability analysis of suspension bridge due to dead load and live load is shown in Table 5.5 and Fig.5.31 for representative members. Against the design live load, element 3 (center of side span) has the lowest reliability index of 3.6, element 9 (center of the main span) has a high reliability index of 15.9. Element 29 (cable at center) and 25 (cable at tower) have high reliability indices of more than 12.0.

In the second analysis, the stress due to the wind load only changes in the normal distribution. Considering the return period of the wind load, the reliability analysis are carried out in the following three cases, 1) design wind load for the suspension bridge, 2) 5-percent increase of design wind load, and 3) 10-percent increase of design wind load. Each wind load is assumed to have the coefficient of variation of 0.10. The yield stress of main cable and the buckling stress of girder are assumed to be the same as in the above-mentioned cases. The result of reliability analysis of suspension bridge due to dead load and wind load is shown in Table 5.6 and Fig.5.32 for representative members. Against the design wind load, element 9 (center of the main span) has the lowest reliability index of 3.9, element 3 (center of side span) has the second lowest reliability index of 5.9. Element 29 (cable at center) and element 25 (cable at tower) have the reliability indices of 8.5 and 12.9, respectively.

Table 5.5 Results of reliability analysis of suspension bridge due to dead load and live load

	Design live load	10% increase	20% increase
Reliability Index			
Element 9 (center of main span)	15.855	15.743	15.656
Element 3 (center of side span)	3.629	3.218	2.826
Element 29 (cable at center)	12.887	12.793	12.624
Element 25 (cable at tower)	12.327	12.306	12.055
Probability of Failure			
Element 9 (center of main span)	0.0000	0.0000	0.0000
Element 3 (center of side span)	0.0002	0.0007	0.0021
Element 29 (cable at center)	0.0000	0.0000	0.0000
Element 25 (cable at tower)	0.0000	0.0000	0.0000

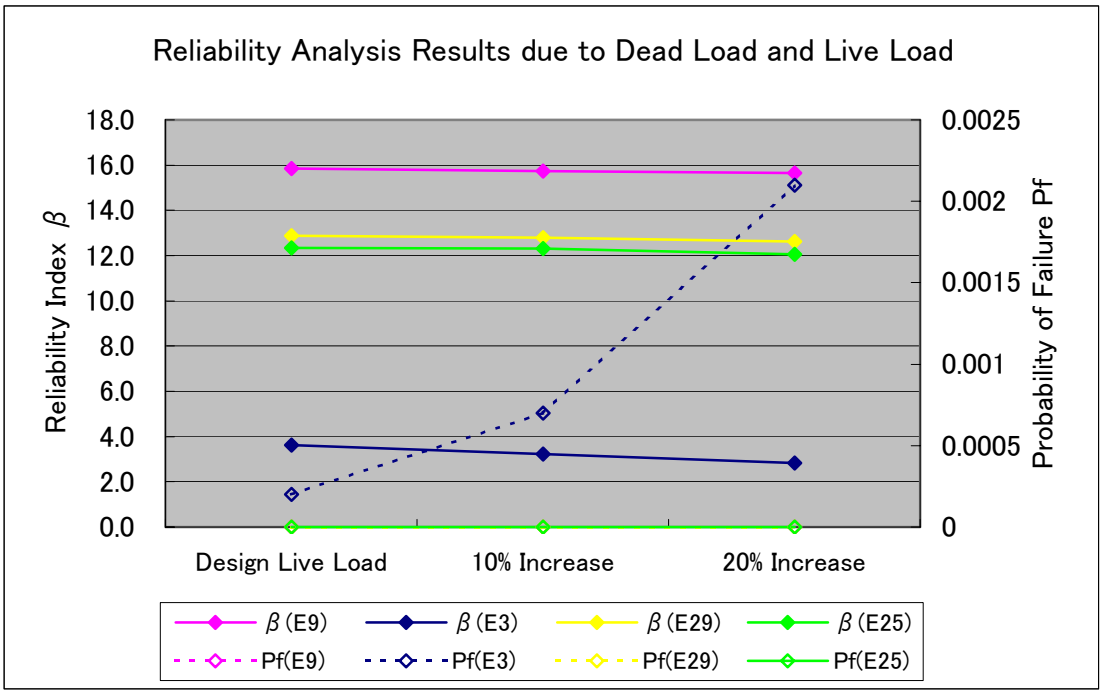

Fig. 5.31 Result of reliability analysis of suspension bridge due to dead load and live load

Table 5.6 Results of reliability analysis of suspension bridge due to dead load and wind load

	Design wind load	5% increase	10% increase
Reliability Index			
Element 9 (center of main span)	3.898	3.504	2.995
Element 3 (center of side span)	5.874	5.793	5.681
Element 29 (cable at center)	8.459	8.060	7.811
Element 25 (cable at tower)	12.846	12.601	12.565
Probability of Failure			
Element 9 (center of main span)	0.0001	0.0003	0.0015
Element 3 (center of side span)	0.0000	0.0000	0.0000
Element 29 (cable at center)	0.0000	0.0000	0.0000
Element 25 (cable at tower)	0.0000	0.0000	0.0000

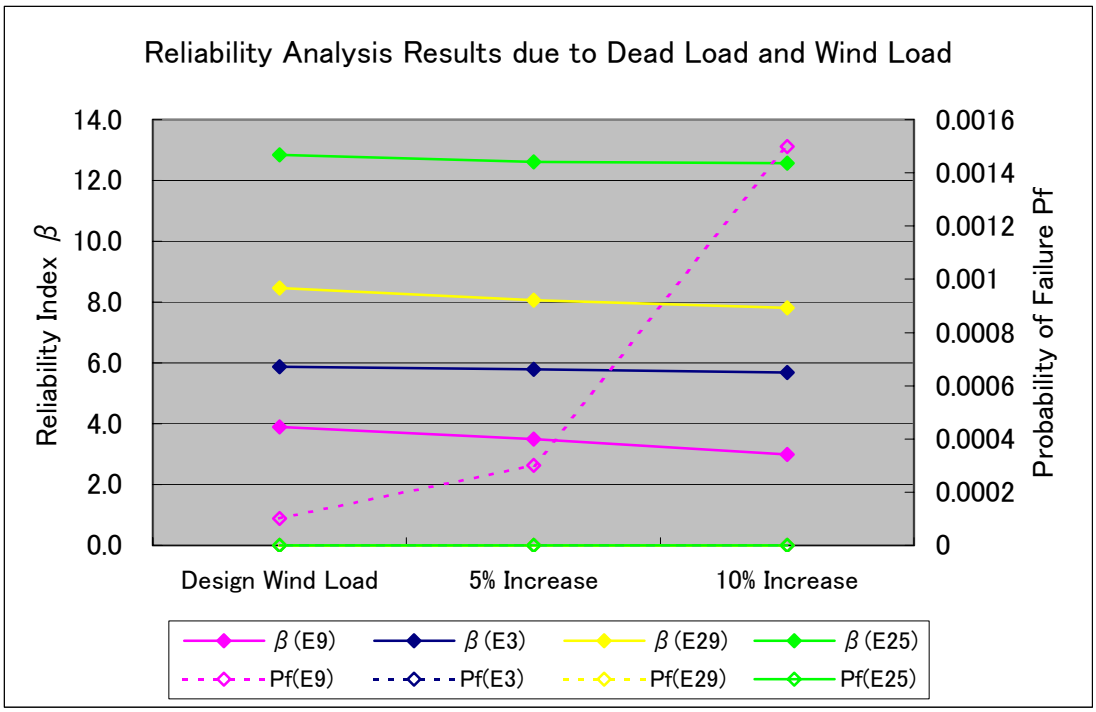

Fig. 5.32 Result of reliability analysis of suspension bridge due to dead load and wind load

5.5 Summary

The conclusions are summarized as follows.

1) The dry-air injection system was introduced to the Ohnaruto Bridge in order to protect the main cable against corrosion, and the four systems are in almost permissible conditions.

2) The suspender ropes have corrosions especially in the anchoring ends, and the safety factor of the suspender rope is verified. Anti-corrosion measures are required for the anchoring ends.

3) The reliability analysis for the main cable as well as the suspender ropes were carried out, and the reliability index and the probability of failure are checked.

4) The reliability analysis for the entire system of the suspension bridge carried out, and the reliability index and the probability of failure in girders and cables are checked.

6. Structural Analysis for Long-span Bridges with Time-dependence

6.1 Introduction

In recent years cable-stayed bridge bridges seem to have been preferably constructed throughout the world. A cable-stayed bridge consists of three major elements: that is, girder, towers and cables. It is advantageous because of 1) economical design through the pre-tensioning of cables, 2) easier erection using cables and 3) relatively simple and elegant alignment.

However, the Locked Coil Rope (hereafter referred to as LCR) cables have been reported to have undergone significant creep or relaxation. For this reason, DIN 1073 of West Germany requires that the creep strain from 0.010% to 0.015% must be taken into account in the design unless appropriate creep tests are conducted. In Onomichi Bridge (hereafter referred to as O Bridge) it was reported from a series of field measurement that creep strain of 0.018% has occurred. On the other hand, in Kawasaki Bridge (hereafter referred to as K Bridge), the maximum relaxation of the cables has been reported to have amounted to 11.8% at 3.5 years after construction.

According to the study by Nakai et al., the total creep elongation is the sum of the elongation of each component wire and the structural elongation caused by the relative movements between the interfaces of the wires; furthermore, they demonstrated that the creep elongation of the spiral ropes is several times larger than that of the wires themselves.

An attempt is made in this study to evaluate the creep and relaxation of cable-stayed bridges assuming that the cables follow the linear visco-elastic law based on the field measurements on the existing bridges conducted by two different organizations.

6.2 Cable-stayed Bridges in Japan

6.2.1 Cables of Cable-stayed Bridges

The types of cables can be classified into: LCR and Parallel Wire Strand (hereafter referred to as PWS). In case of the former in particular, a special attention is called for the creep phenomenon. Several characteristics of cables are investigated on 14 typical cable-stayed bridges in Japan and are listed in Table 6.1, together with KS Bridge, that is subjected to rather

Table 6.1(a) Cable dimensions of cable-stayed bridges in Japan

No.	Initial	Name	Arrangement	Plane	Rope	Area (cm^2)	Breaking Strength σ_b (t/cm^2)	Maximum Force T_{max} (t)	Prestress T_p (t)	$\frac{T_{max}}{T_b}$	$\frac{T_p}{T_b}$	Y ($\times 10^4$)
1	Y	YAMATOGAWA BRIDGE	HARP (2)	1	PWS217 x 19 PWS169 x 19 PWS217 x 13 PWS217 x 13	809.6 630.5 553.9 553.9	16.0 16.0 16.0 16.0	4408 3203 3347 3052	201 148 212 222	0.340 0.318 0.378 0.344	0.016 0.015 0.024 0.025	17.44
2	SH	SUEHIRO BRIDGE	FAN (2)	1	PWS169 x 7 + PWS127 x 6	381.9 381.9	16.5 16.5	901 801 784 636		0.143 0.127 0.124 0.101		8.85
3	K	KAMOME BRIDGE	FAN MULTI-CABLE	1	PWS271 x 2 PWS184 x 2 PWS114 x 2	106.4 72.3 44.3	15.7 15.7 15.7	539 366 227	40 79 33	0.323 0.323 0.323	0.024 0.069 0.049	7.92
4	R	ROKKOH BRIDGE	FAN (6)	2	PWS217 x 2	85.2	15.2	430	130	0.331	0.100	0.25
5	T	TOYOSATO BRIDGE	FAN (2)	1	PWS154 x 16 PWS127 x 12	483.7 299.2	15.7 15.7	2548 1167	556 549	0.335 0.248	0.073 0.117	5.21
6	O	ONOMICHI BRIDGE	RADIAL (2)	2	LCR-D70 x 4 LCR-D66 x 4 LCR-D56 x 4 LCR-D54 x 4	138.8 122.4 89.6 83.2	11.8 12.1 11.8 12.0	330 327 218 222	13 137 113 48	0.202 0.221 0.206 0.222	0.008 0.007 0.129 0.048	16.13
7	SG	SUIGOH BRIDGE	HARP (3)	1	PWS169 x 19 PWS169 x 13 PWS169 x 7 +PWS127 x 6	630.5 431.4 381.9	16.5 16.5 16.5	3137 1967 1736	453 58 362	0.302 0.276 0.276	0.044 0.008 0.057	1.09
8	D	DAIKOKU BRIDGE	FAN (2)	2	PWS127 x 12 PWS127 x 9 PWS127 x 12 PWS127 x 9	299.2 224.4 299.2 224.4	16.0 16.0 16.0 16.0	919 622 1044 513		0.192 0.173 0.218 0.143		1.15

Table 6.1(b) Cable dimensions of cable-stayed bridges in Japan

No.	Initial	Name	Arrangement	Plane	Rope	Area (cm^2)	Breaking Strength σ_b (t/cm^2)	Maximum Force T_{max} (t)	Prestress T_p (t)	$\frac{T_{max}}{T_b}$	$\frac{T_p}{T_b}$	Y ($\times 10^4$)
9	A	ARAKAWA BRIDGE	HARP (2)	1	PWS127 X 7 +PWS91 X 6	281.8 281.8	16.0 16.0	1350 962	100 500	0.299 0.213	0.022 0.111	1.84
10	I	ISIKARI BRIDGE	FAN (2)	2	PWS127 X 4	99.7	16.0	174	93	0.111	0.059	7.05
11	E	EISAI BRIDGE	RADIAL (6)	2	LCR-F100φ LCR-E92φ LCR-E80φ LCR-D70φ	70.4 58.4 44.8 34.7	12.0 11.8 11.9 11.7	268 224 170 119		0.317 0.324 0.320 0.293		2.06
12	G	GASSHOH BRIDGE	FAN (3)	2	LCR-E80φ x 4 LCR-D70φ x 4 LCR-D60φ x 4	179.2 138.8 102.0	13.0 13.0 13.0	992 589 440	408	0.426 0.326 0.332	0.175	4.80
13	M	MAYA BRIDGE	FAN (2)	1	LCR-D58φ x 12	280.8	15.0	1685	400	0.400	0.095	0.32
14	SI	SHINOH BRIDGE	HARP (2)	2	LCR-H100φ x 4 LCR-E90φ x 4	290.4 228.8	16.1 13.4	600 270	600 350	0.128 0.088	0.128 0.114	1.12
15	KS	KAWASAKI BRIDGE	FAN	2	LCR-D50φ LCR-D70φ	18.2 33.8	11.4 12.0	33 94	26 35	0.158 0.233	0.127 0.086	0.17

extensive study. Among those 15 bridges, PWS are used in 9 bridges and LCR in other 6 bridges. In Japan, LCR was used earlier, and then PWS has become more popular. Recently, however, LCR tends to be in use again because of easiness to use and of the resistance against the corrosion. The maximum cable force, resulting from the combination of the live loads, amounts approximately from 10 % to 40 % of the breaking strength, and the prestress forces amounts from 1% to 10%.

6.2.2 Relative Stiffness Ratio of Cables

The design of cable-stayed bridges may be significantly controlled by the stiffness of cable. For simple representation of the load distribution to the main girder, tower and cables, the following ratio will be defined as the relative stiffness ratio of the cable:

$$\gamma = \frac{Ec \sum_{i} (Aci / li) \sin^2 \theta i}{EgIg / Lt^3} \quad \cdots\cdots (6.1)$$

where li is length of each cable, Aci is area of each cable, θi is slope of each cable, Ec is Young's modulus of cables, Eg is Young's modulus of main girder, Ig is moment of inertia of main girder, and Lt is total length of bridge.

The relationship between the total span length and the relative stiffness ratio with respect to the bridges considered in the proposed study in shown in Fig. 6.1

6.3 Field Measurements of Cable-stayed Bridges

6.3.1 Scope

For the present, available filed data are extremely limited on the long-term behavior of the cable-stayed bridges. Namely, only two sets of data are available for use. Those are on 1) O Bridge and 2) KS Bridge. They consists of the time-dependent changes of the vertical deflections of the main girders and the cable tensions

6.3.2 KS Bridge

KS Bridge, shown in Fig. 6.2, is a cable-stayed bridge of multi-cable type, over the Ohkawa River in Osaka for pedestrians and bicycles and was completed in 1978. It has two continuous spans of 87.5m+40.65m, and has 20 LCR cables, the readers are recommended to see reference 3).

The cable forces were measured two times so far: on completion and three years and a half

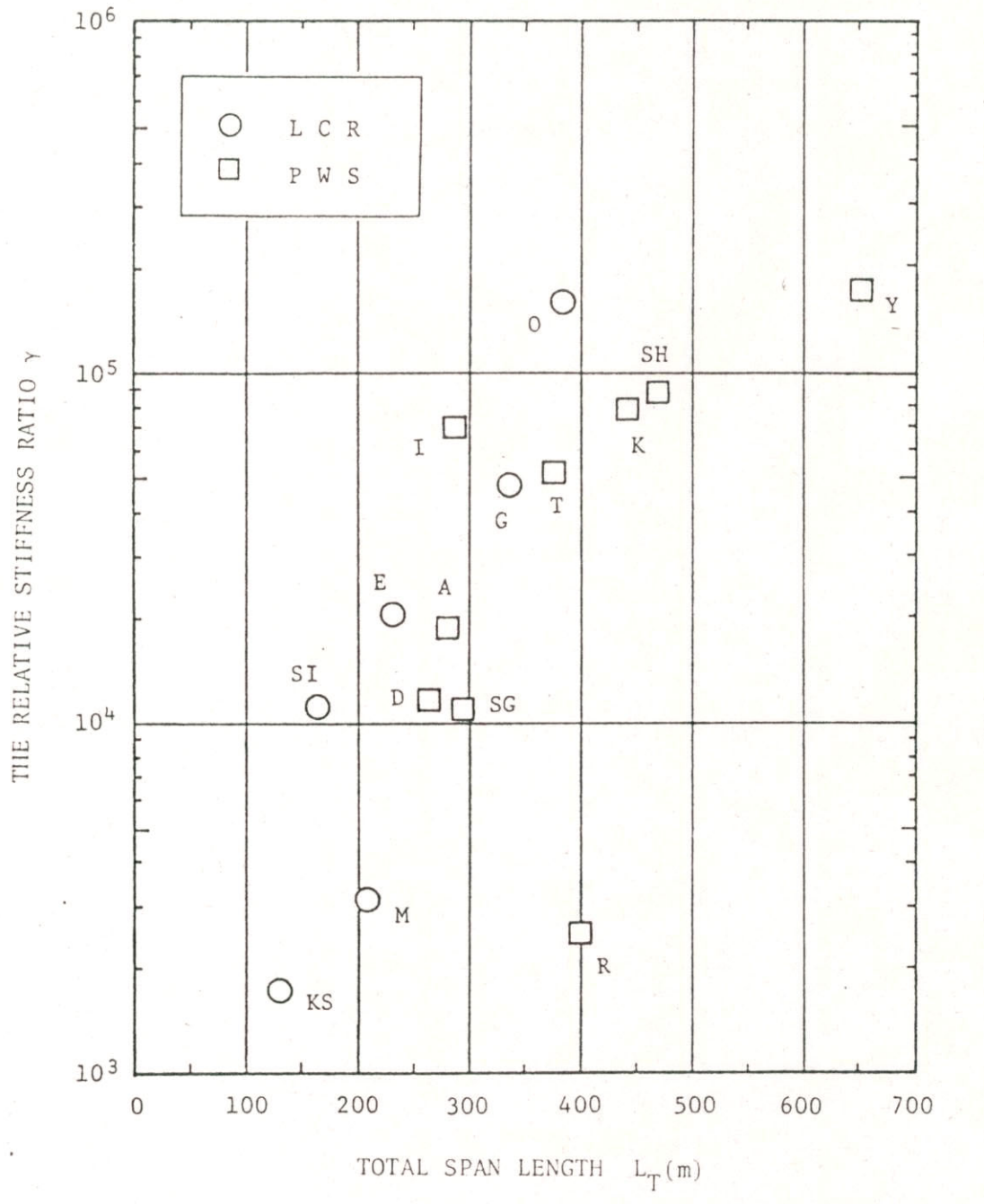

Fig.6.1 Relationship between total span length and the relative stiffness ratio

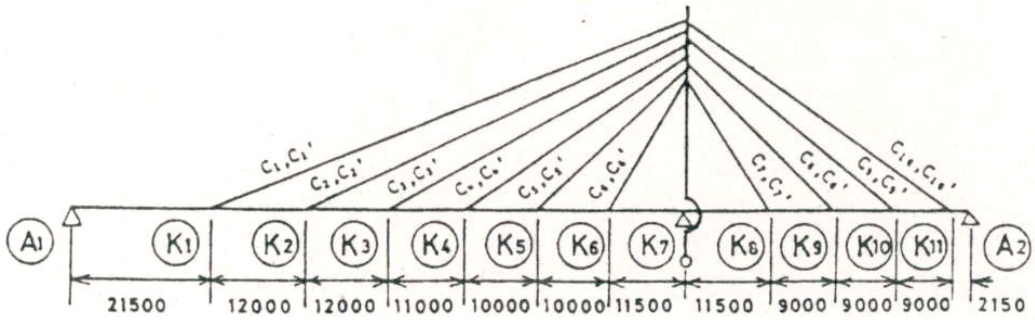

Fig.6.2 Dimensions of KS Bridge

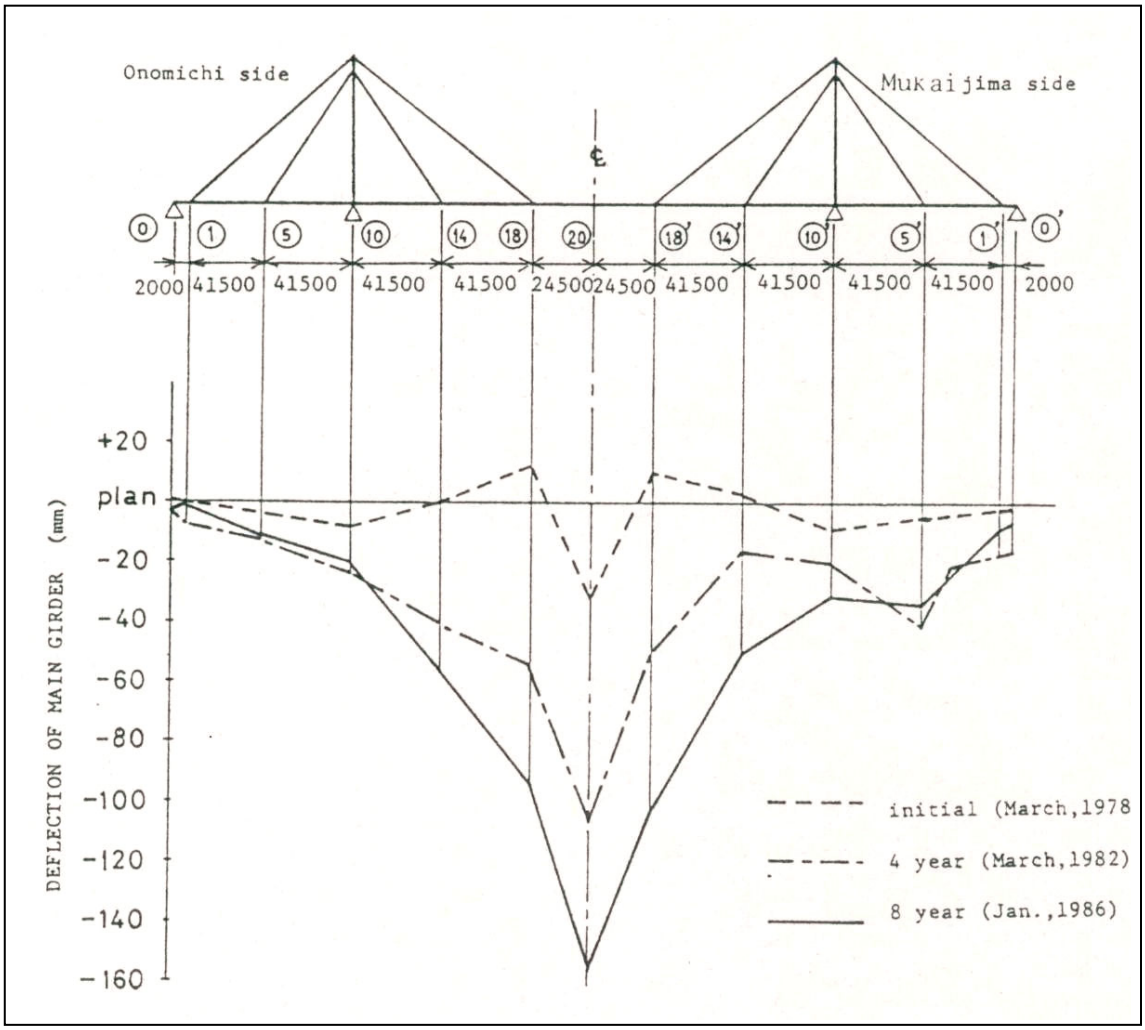

Fig.6.3 Measured deflection of O Bridge

afterward by the free vibration method using accelerometers and spectrum analyzer by Osaka Municipal Office and Kurimoto Steelwork. Some of the authors were fortunate enough to participate in the last measurement through the courtesy of Osaka Municipal Office.

The camber has been measured three times: on completion, one year and a half afterward, and three years and a half afterward, respectively.

6.3.3 O Bridge

O bridge has three continuous spans and the center span is 215 m. The cable alignment is radial type and 8 cables are connected at each stream side of the main girder. Each cable consists of 4 LCRs. The filed measurements were performed 8 times on the vertical deflections of the main girder. They were found to be significantly large even at the first field measurement and were finally decided to be re-tightened after 8 years from the completion. For detailed descriptions on the fabrication and erection of cables, the readers are recommended to see reference 8) and 9).

The bridge dimensions and the results at the completion, 4 and 8 years after the completion are shown respectively in Fig. 6.3. After 8 years from the completion, the deflection at the center span amounted to 158 mm below the original configuration.

6.4 Method of Structural Analysis for Cable-stayed Bridges

6.4.1 Linear Visco-Elastic Model of Cables

The linear visco-elastic model is adopted for convenience to the cables. From the fact that the maximum cable stresses do not amount to more than 30% of the breaking stresses of the cables, it may be quite reasonable to assume that creep may remain in the stage of the initial creep.

The linear visco-elasticity is defined by Boltzmann in 1-dimensional problem as follows:

$$\left.\begin{aligned} \sigma(t) &= \int_{-\infty}^{t} G(t-\tau)\frac{\partial e(\tau)}{\partial \tau}d\tau \\ e(t) &= \int_{-\infty}^{t} J(t-\tau)\frac{\partial \sigma(\tau)}{\partial \tau}d\tau \end{aligned}\right\} \quad \cdots\cdots (6.2)$$

Thus, the relationship between the stress and strain, that is, the constitutive equation can be expressed in terms of the convolution. Consequently, the governing equations derived from

this can be shown to take the form of Volterra's linear integral equations of first kind. Furthermore, Volterra's principle states that any problem of the theory of hereditary elasticity can be solved in exactly the same way as the corresponding problem in the normal theory of elasticity except that in the final result the elastic constants must be replaced by elastic operators. As a matter of fact, using Laplace transformation, and letting $\bar{f}(s)$ designate the Laplace transformation of function $f(t)$, then it is quite easy to show that Eq.(6.2) can be transformed into:

$$\bar{\sigma}(s)=\bar{E}(s)\bar{e}(s) \quad \cdots\cdots (6.3)$$

where $\bar{E}(s)=s\bar{G}(s)$, in which $\bar{G}(s)$ and $\bar{E}(s)$ is referred to as the relaxation function and the Young's modulus in the Laplace image space s, respectively.

The three-element model adopted in this study, slightly different from what is called "standard solid model" by Sonoda et al., is shown in Fig. 6.4.

It consists of elastic springs E_1 and E_2, and a dash-pot with the viscosity constant η. The stress-strain relationship is given by:

$$\dot{\sigma}+\lambda\sigma=E(\dot{e}+\mu e) \quad \cdots\cdots (6.4)$$

where $E=E_1$

$$\left.\begin{aligned}\lambda&=(E_1+E_2)/\eta\\ \mu&=E_2/\eta\end{aligned}\right\} \quad \cdots\cdots (6.5)$$

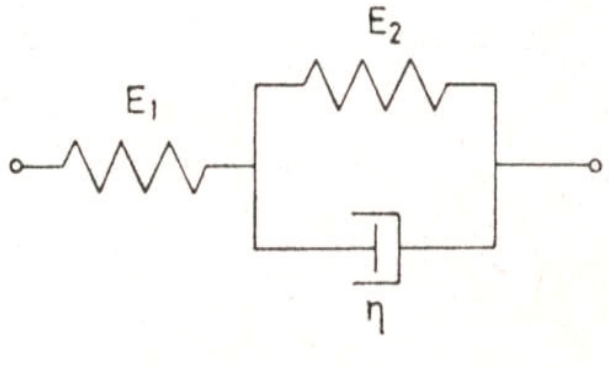

Fig.6.4 Three-element model for cable

and the dot implies the differentiation with respect to the time *t*, Eq.(6..4) can be transformed into the following, upon the Laplace transform assuming that $\sigma(+0)=Ee(+0)$:

$$\bar{\sigma}(s) = E\frac{s+\mu}{s+\lambda}\bar{e}(s)$$

$$= \bar{E}(s)\bar{e}(s) = s\bar{G}(s)\bar{e}(s) \quad \cdots\cdots (6.6)$$

where

$$\bar{E}(s) = E\frac{s+\mu}{s+\lambda} \quad \cdots\cdots (6.7)$$

$$\bar{G}(s) = E\frac{s+\mu}{s(s+\lambda)} \quad \cdots\cdots (6.8)$$

In case strain e(t) is known, then, from Eq.(6.6) it yields:

$$\bar{\sigma}(s) = E\left(\bar{e}(s) - (\lambda-\mu)\frac{\bar{e}(s)}{s+\lambda}\right) \quad \cdots\cdots (6.9)$$

In the case of the relaxation problem, that is when $e(t)=e(0)=e_0(t \geqq 0)$, $e(t)=0(t<0)$, it is easy to show that

$$\frac{\sigma(t)}{\sigma_0} = \frac{1}{1+\rho}(\rho + \exp(-\lambda t)) \quad \cdots\cdots (6.10)$$

where

$$\rho = E_2/E_1 \quad \cdots\cdots (6.11)$$

On the contrary, solving Eq.(6.6) for the strain, it can be seen that

$$\bar{e}(s) = \frac{1}{E}\left(\bar{\sigma}(s) + (\lambda-\mu)\frac{\bar{\sigma}(s)}{s+\mu}\right) \quad \cdots\cdots (6.12)$$

In the case of the creep problem, that is when $\sigma(t)=\sigma(0)=\sigma_0(t \geqq 0)$, $\sigma(t)=0(t<\sigma)$, it is also easy to show that

$$\frac{e(t)}{e_0} = \frac{1}{\rho}((1+\rho) - \exp(-\mu t)) \quad \cdots\cdots (6.13)$$

In actual cable-stayed bridges, cables are neither in the state of creep in a narrow sense of increasing strain on a constant stress, nor in the state of relaxation again in a narrow sense of decreasing stress on a constant strain, but it is reasonable to consider that both phenomena occur simultaneously.

The coefficient of the model may be determined from the creep test of ropes themselves. However, other factors such as the slips out of sockets or the deformation of bolts, and the settlement of the supports may affect the time–dependent behavior of cable-stayed bridges. Thus, it is difficult to determine the coefficients of cable model solely from the creep tests of the component wires.

In the proposed study, thereby, the coefficients will be determined on the basis of the data of cable tension measurements through the vibration tests can be considered to be relatively reliable. The elongation of cables, nevertheless, can not be calculated correctly merely from the camber measurements because towers deform simultaneously. In view of the fact that no data is available with respect to the tower, an attempt is made to determine the constants of the cable making the best use of the existing data.

When the actual phenomenon can be regarded as a relaxation problem, Eq.(6.10) can be solved as follows:

$$\lambda = -\frac{1}{t}\ln((1+\rho)\frac{\sigma(t)}{\sigma_0} - \rho) \quad \cdots\cdots\cdots\cdots\cdots\cdots\cdots\cdots\cdots\cdots\cdots\cdots\cdots\cdots \quad (6.14)$$

If the stress $\sigma(t_1)$, $\sigma(t_2)$ are given at two different time station t_1, t_2 and if λ remains constant, then,

$$\frac{1}{t_1}\ln((1+\rho)\frac{\sigma(t_1)}{\sigma_0} - \rho) = \frac{1}{t_2}\ln((1+\rho)\frac{\sigma(t_2)}{\sigma_0} - \rho) \quad \cdots\cdots\cdots\cdots\cdots\cdots\cdots\cdots\cdots \quad (6.15)$$

Thus, λ can be determined by letting ρ satisfy Eq.(6.15) and upon its substitution to Eq.(6.14).

On the other hand, when the actual phenomenon can be regarded as a creep problem Eq.(6.13) can be solved as

$$\mu = -\frac{1}{t}\ln((1+\rho) - \rho\frac{e(t)}{e_0}) \quad \cdots\cdots\cdots\cdots\cdots\cdots\cdots\cdots\cdots\cdots\cdots\cdots\cdots\cdots \quad (6.16)$$

If the strains of the cable $e(t_1)$, $e(t_2)$ are given at two different time stations t_1, t_2 and if μ remains constant, then,

$$\frac{1}{t_1}\ln((1+\rho) - \rho\frac{e(t_1)}{e_0}) = \frac{1}{t_2}\ln((1+\rho) - \rho\frac{e(t_2)}{e_0}) \quad \cdots\cdots\cdots\cdots\cdots\cdots\cdots\cdots\cdots \quad (6.17)$$

Therefore, μ can be determined by letting ρ satisfy Eq.(6.17) and upon its substitution

to Eq.(6..16). Unfortunately, since the sufficient relaxation data are not accumulated in view of the fact that the cable tensions have been measured only once after the completion of the bridge, the determination of the cable constants merely from the vibration tests will be found impossible. Thus, an attempt is made to determine the constants from the camber measurements assuming that the problem is the creep problem using only the data of cables that did not undergo significant change of the cable force, and the results were compared with the results from the tension measurements.

6.5 Formulation of Numerical Calculation for Cable-stayed Bridges

6.5.1 Scope

The long-term behavior of the cable-stayed bridges can be analyzed by finite element method. From the Volterra's principle, the stiffness matrix of linear visco-elastic cables can be superimposed to that of the linear elastic girders and towers in the Laplace image space s to form the global equilibrium equation of cable-stayed bridge. After solving this equation the final solutions will be obtained in the real time domain through the numerical Laplace inverse transformation.

6.5.2 Formulation by Finite Element Method

Since the girders and towers are linearly elastic, the stiffness matrix K_{ij} for a beam element is expressed as follows:

$$K_{ij} = \int_V B_{mi} E_{mn} B_{nj} dV \quad \cdots\cdots (6.18)$$

where B_{mi} or B_{nj}, E_{mn}, and V designate the strain matrix, the elastic modulus matrix, and volume of the element, respectively.

As cables are assumed to be linearly visco-elastic, the stiffness matrix is given by:

$$\overline{K}_{ij}(s) = \int_V B_{mi} \overline{E}_{mn}(s) B_{nj} dV \quad \cdots\cdots (6.19)$$

where E_{mn}(s) designates the elastic modulus in the Laplace image space and is represented from Eq.(6..8) as follows:

$$\overline{K}_{mn}(s) = \overline{E}(s) = E\frac{s+\mu}{s+\lambda} \quad \cdots\cdots (6.20)$$

Combining these stiffness matrices in the Laplace image space *s*, the equilibrium equation of the total bridge is given by

$$\begin{bmatrix} \overline{K_{11}}(s) & \overline{K_{21}}(s) \\ \overline{K_{21}}(s) & \overline{K_{22}}(s) \end{bmatrix} \begin{Bmatrix} \overline{w_1}(s) \\ \overline{w_2}(s) \end{Bmatrix} = \begin{Bmatrix} \overline{P_1}(s) \\ \overline{P_2}(s) \end{Bmatrix} \quad \cdots\cdots (6.21)$$

where K_{ij}, W_i, and P_i refers to the stiffness matrix, the nodal displacement, and the nodal forces, respectively. Moreover, subscript, 1 and 2 refers to the main girder and tower, respectively. In the proposed study, the forces consist of the dead load and the prestress force induced to the cables. The following equations hold the complete system:

$$(\overline{K'}(s))\{\overline{w'}(s)\} = \{\overline{P'}(s)\} \quad \cdots\cdots (6.22)$$

Similarly, for the system under erection:

$$(\overline{K''}(s))\{\overline{w''(s)}\} = \{\overline{P''}(s)\} \quad \cdots\cdots (6.23)$$

The total displacement and stress can be obtained as the sum of each system by the principle of superposition. Consequently, the displacements of girders and towers are obtained in the image space:

$$\begin{aligned} \{\overline{w}(s)\} &= \{\overline{w'}(s)\} + \{\overline{w''}(s)\} \\ &= (\overline{K'}(s))^{-1}\{\overline{P'}(s)\} + (\overline{K''}(s))^{-1}\{\overline{P''}(s)\} \end{aligned} \quad \cdots\cdots (6.24)$$

6.5.3 Numerical Laplace Inverse Transformation

The obtained solutions, nevertheless, constitute sets of numerical data in the image space *s*, and not in the real time domain *t*. It becomes necessary to apply the Laplace inverse transformation to the solutions so that they correspond to the real time *t*.

For successful execution of the numerical Laplace inverse transform, several considerations will be necessary. Regarding the choice of the interval to be subjected to the inverse transform, Izumi has proposed the following method: First, examine the variation of the Young's modulus in the image space s, and plot the value of $\overline{E}(s)$. Secondly, find the interval in which this value changes and use this interval for the inverse transformation for $\overline{f}(s)$. Finally, apply appropriate regression formula based on the least square procedure in the prescribed interval so that the solution satisfies the limit theorems.

At first, the non-dimentionization will be performed on time. The Laplace transformation is defined as follows,

$$\bar{w}(s) = \int_0^{\infty} \exp(-st) w(t) dt \quad \cdots\cdots (6.25)$$

Let us non-dimensionalize the expression in terms of a parameter, T:

$$t = T\bar{t},\ s = \bar{s}/T \quad \cdots\cdots (6.26)$$

Substitution of Eq.(6.26) in to Eq.(6.25) yields

$$\frac{\bar{w}(s)}{T} = \int_0^{\infty} \exp(-\bar{s}\bar{t}) w(T\bar{t}) d\bar{t} \quad \cdots\cdots (6.27)$$

The above equation shows that the Laplace transform of $w(T\bar{t})$ on t becomes $\bar{w}(s)/T$ and that the Laplace inverse transformation of $\bar{w}(s)/T$ on s becomes $w(T\bar{t})$. The parameter T is selected to be η/E, which is usually referred to as the delay time.

In the proposed study the solution of creep and relaxation is approximated as the sum of exponential functions.

$$w(T\bar{t}) = \sum_i^N a_i \exp(-\bar{b}_i \bar{t}) \quad \cdots\cdots (6.28)$$

where $\bar{b}_i = T b_i, \quad b_1 = 0$

Then the square error f can be formulated as:

$$f = \frac{1}{2} \sum_{j=1}^{k} \left(\sum_{i=1}^{N} \frac{a_i}{\bar{s}_j + \bar{b}_i} - \frac{\bar{w}(s_j)}{T} \right)^2 \quad \cdots\cdots (6.29)$$

where k refers to the number of the terminal points in the Laplace space, s. The values of a_i and b_i must be so determined as to satisfy the limit theorems and minimize function f. Now, letting $N=2$, a_i can be determined as:

$$a_1 = w_\infty, \quad a_2 = w_0 - w_\infty \quad \cdots\cdots (6.30)$$

Furthermore, from the condition that $\frac{\partial f}{\partial \bar{b}_2} = 0$

$$\sum \left(\frac{a_1}{\bar{s}_j} + \frac{a_2}{\bar{s}_j + \bar{b}_2} - \frac{\bar{w}(s)}{T} \right) \frac{1}{\left(\bar{s}_j + \bar{b}_2\right)^2} = 0 \quad \cdots\cdots (6.31)$$

The value of $\bar{b}_2$ which satisfies the above transcendental equation can be found through the Regula Falsi Method.

6.6 Numerical Illustrations of Cable-stayed Bridges

6.6.1 KS Bridge

The relative stiffness ratio is 0.17×10^4, which is much less than those for the other cable-stayed bridges.

Fig. 6.5 shows KS Bridge model and its model dimensions, respectively. KS Bridge was constructed in the following process, and the prestress was introduced by means of the jack-up and –down of the main girder. Thus, the analysis was made in conformity with the actual construction process:

1) Pre-dead Load: A temporary support is set up at point K4, the bridge girder is assumed to be three-span continuous.
2) Jack Up: The girder is jacked up by 700 mm at point A1; by 100 mm at point K4; while the tower is set back by 100 mm at its top. The cables having the prescribed lengths are fastened to the main girder without initial stresses.
3) Remove Temporary Support: Temporary support at point K4 is removed.
4) Jack Down: The girder is jacked down by 700 mm at point A1. Then, prestress forces are introduced into cables.
5) Post-dead Load: The post-dead load is applied to the completed bridge.

The pre-dead load of steel girders is 1.682 t/m. The weights of cables vary from 0.344 t to 1.044 t, and the post-dead load is calculated to be 0.447 t/m. Furthermore, Young's modulus

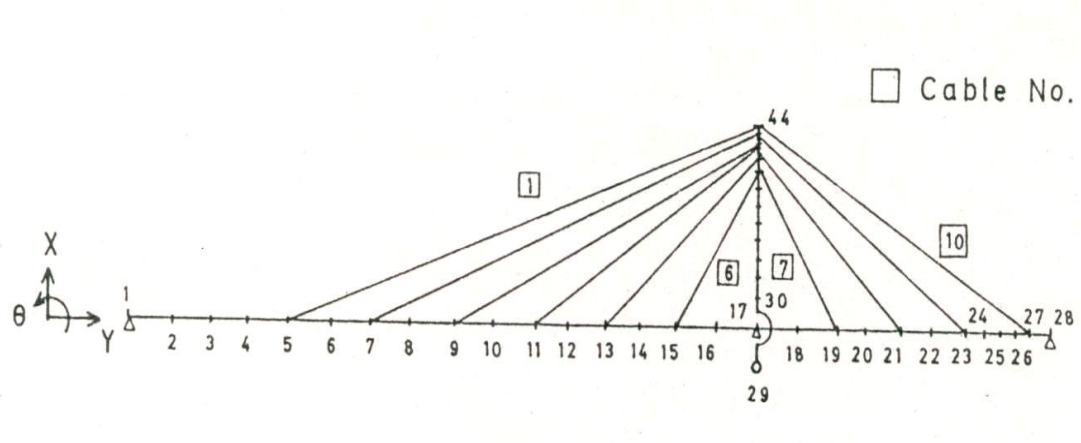

Fig. 6.5 Finite element model for KS Bridge

of girders and towers is E=2.1×10^6 kg/cm^2, and that of cables is Ec=1.6×10^6 kg/cm^2, respectively.

The coefficients, E_1, E_2, and η of three-element model for cables are determined based on the measured data in the following manner: Firstly, a spring constant E_1 is assumed to be the Young's modulus of cables, *Ec*. The vertical deflection of main girders was measured at 1.5 year and 3.5 years after the completion of the bridge. Then, the elongation and strain increments of cables are calculated from the measured data neglecting the set-back of towers. Visco-elastic constants are determined by Eq.(6.16) from the measured strains of cables obtained at different time stations with an appropriate modification made taking into account the settlement of the supports: ρ =5.0, μ =0.39; E_2=8.0×10^6 kg/cm^2, and η =20.5×10^6 year kg/cm^2.

Fig. 6.6 shows the relaxation of Cable 1 and Cable 10; whereas, Fig. 6.7 shows the creep deflection of the girder. Plotted also herein are the measured data. However, many discussions will be necessary with respect to whether the prediction of the future response is correct or not and how well it is considered to be fitted with measured data.

6.6.2 O Bridge

The relative stiffness ratio is 16.13×10^4, which is comparatively larger than the other bridges. The measurement of the deflection had been performed every one or two years after completion.

Upon substitution of the cable strains at two different time stations of 4 years and 8 years after the completion into Eq.(6.17), the coefficients are determined as: ρ =2.0, μ =0.109, E_1= *Ec*=1.6×10^6 kg/cm^2, E_2=3.2×10^6 kg/cm^2, and η =29.5×10^6 year kg/cm^2.

Fig. 6.8 shows the predicted change of the deflection at ⑭ and ⑱ plotted against the measured data taking into account only the dead load. The change of deflection after 4 years and 8 years are illustrated in Fig. 6.9, respectively. Again, discussions may be made whether the prediction is good or not. However, from the available set of data, this may be as much as what can be predicted. Besides, it can be seen that the simple application of the principle of least squares without regard to the structural model may result in the better fit to the measured value.

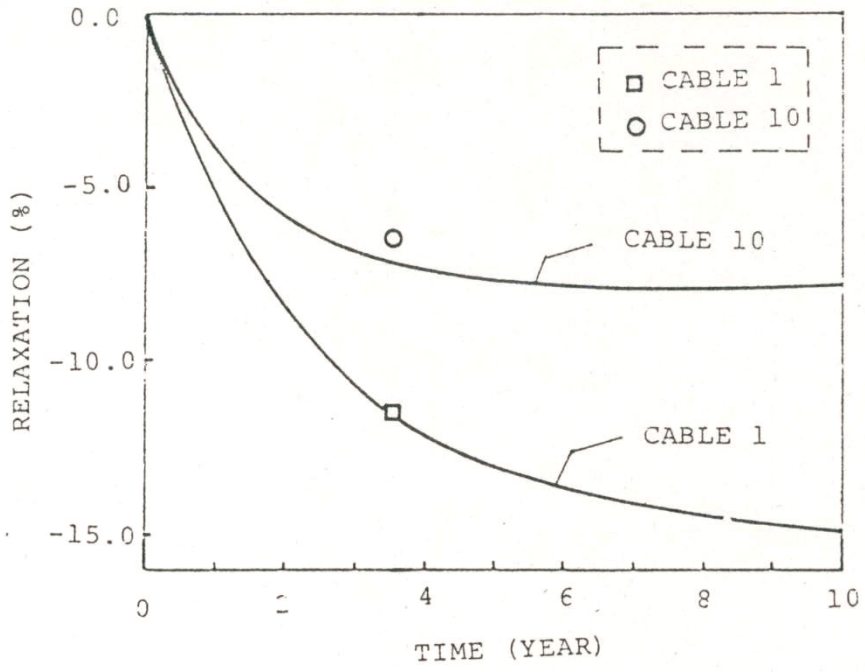

Fig.6.6 Relaxation of cable 1 and 10 in KS Bridge

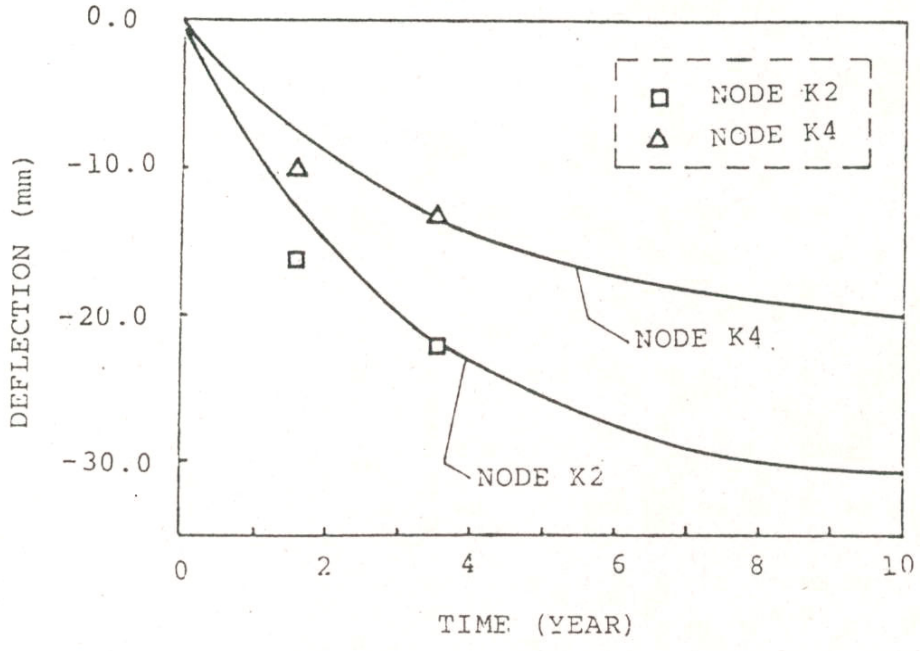

Fig.6.7 Change of deflection at node K2 and K4 on KS Bridge

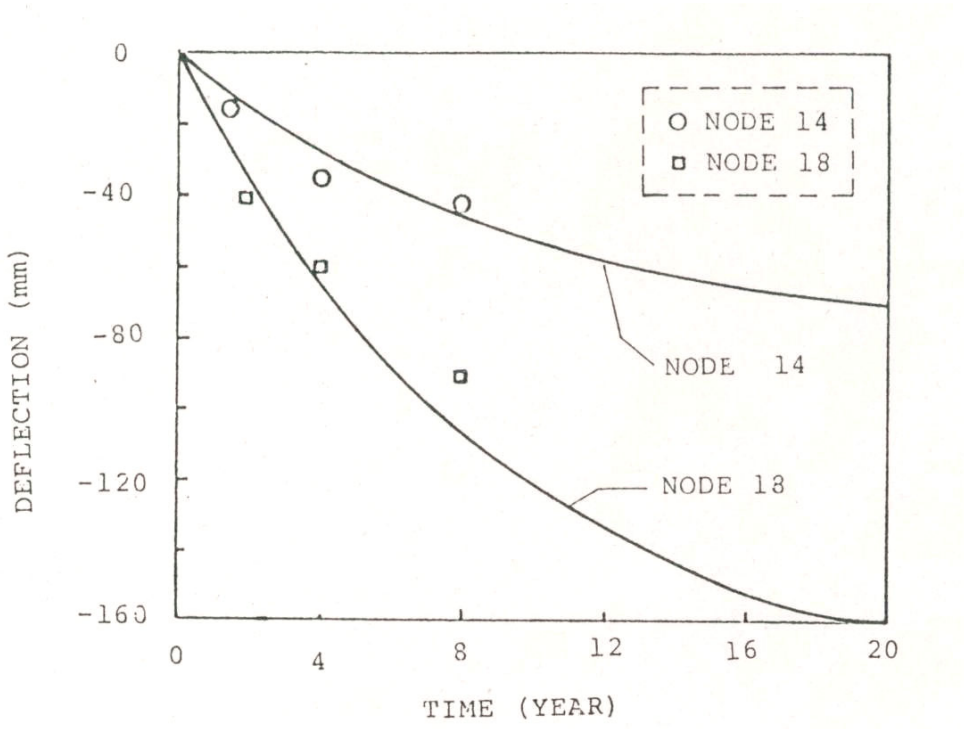

Fig.6.8 Change of deflection at node 14 and 18 on O Bridge

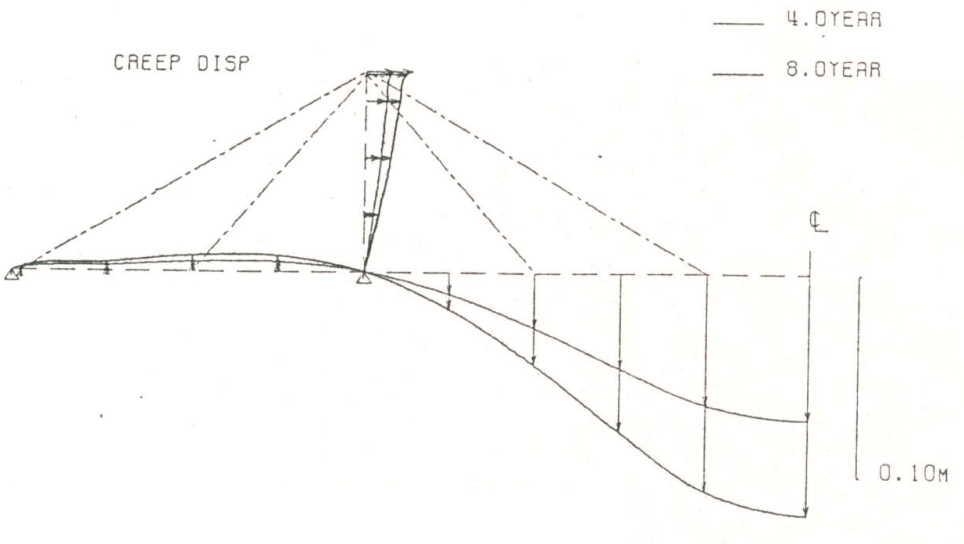

Fig.6.9 Change of deflection, O Bridge

6.7 Effects of Prestress and Relative Stiffness Ratio in Cable-stayed Bridges

6.7.1 Effect of Prestress

Sometimes the prestress is introduced to cables, either by using shim plates, by jacked-up and –down of the main girder or the saddle of cable anchors, although the magnitude of prestress itself is not so large as seen from Table 6.1. This is mainly to improve the bending moment distribution of the main girder. To find the effect of this prestress, a comparative analysis was performed on KS Bridge in both cases of with and without the prestress.

The relaxation of Cable 10 is shown in Fig. 6.10. The relaxation in case of prestress is 7.8 % after 10 years, compared with 5.5 % in case of non-prestress. Shown also in Fig. 6.11, is the increment of deflection at Point K2.

6.7.2 Effect of Relative Stiffness Ratio

Using the spring constant ratio: $\sigma = E_1/E_2 = 2.0$ which is found to be fitted for O Bridge, effect of the relative stiffness ratio is investigated.

Fig. 6.12 shows the relation between the relative stiffness ratio and the ultimate relaxation of cables considering only dead load. It may be obviously seen that the greater the relative stiffness ratio is, the less the relaxation of cables. The broken curve in this figure is a hyperbola obtained through the regression formula on the least square scheme.

Fig. 6.13 shows the relation of the relative stiffness ratio and the ratio of the ultimate creep strain to the initial strain. It may be observed that the greater the relative stiffness ratio is, the greater the ratio of creep strain becomes. Although Fig. 6.12 and 6.13 are obtained from very crude assumption of $\rho = 2.0$, they may be used know approximately how much creep and relaxation can be expected once the stiffness ratio is given.

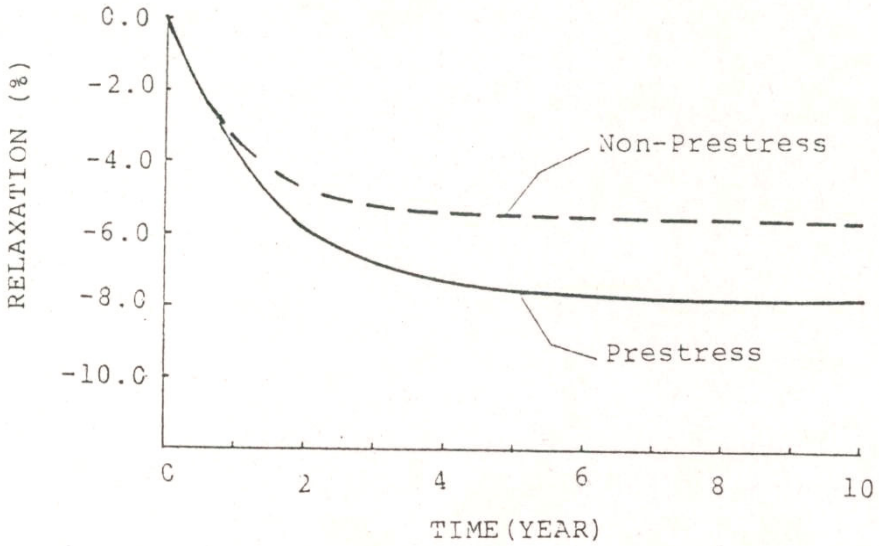

Fig.6.10 Tension change of cable 10

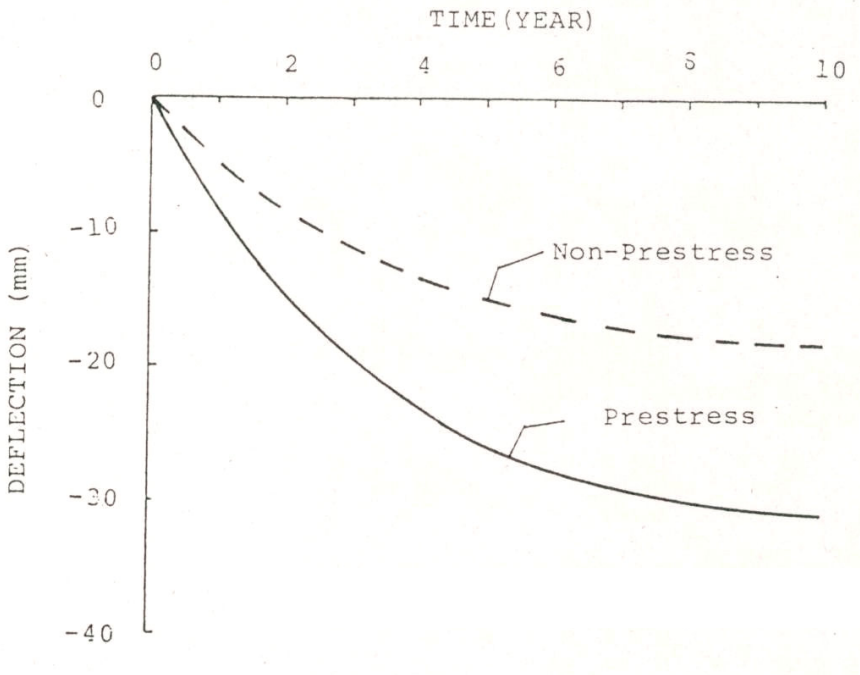

Fig.6.11 Increment of deflection at node K2

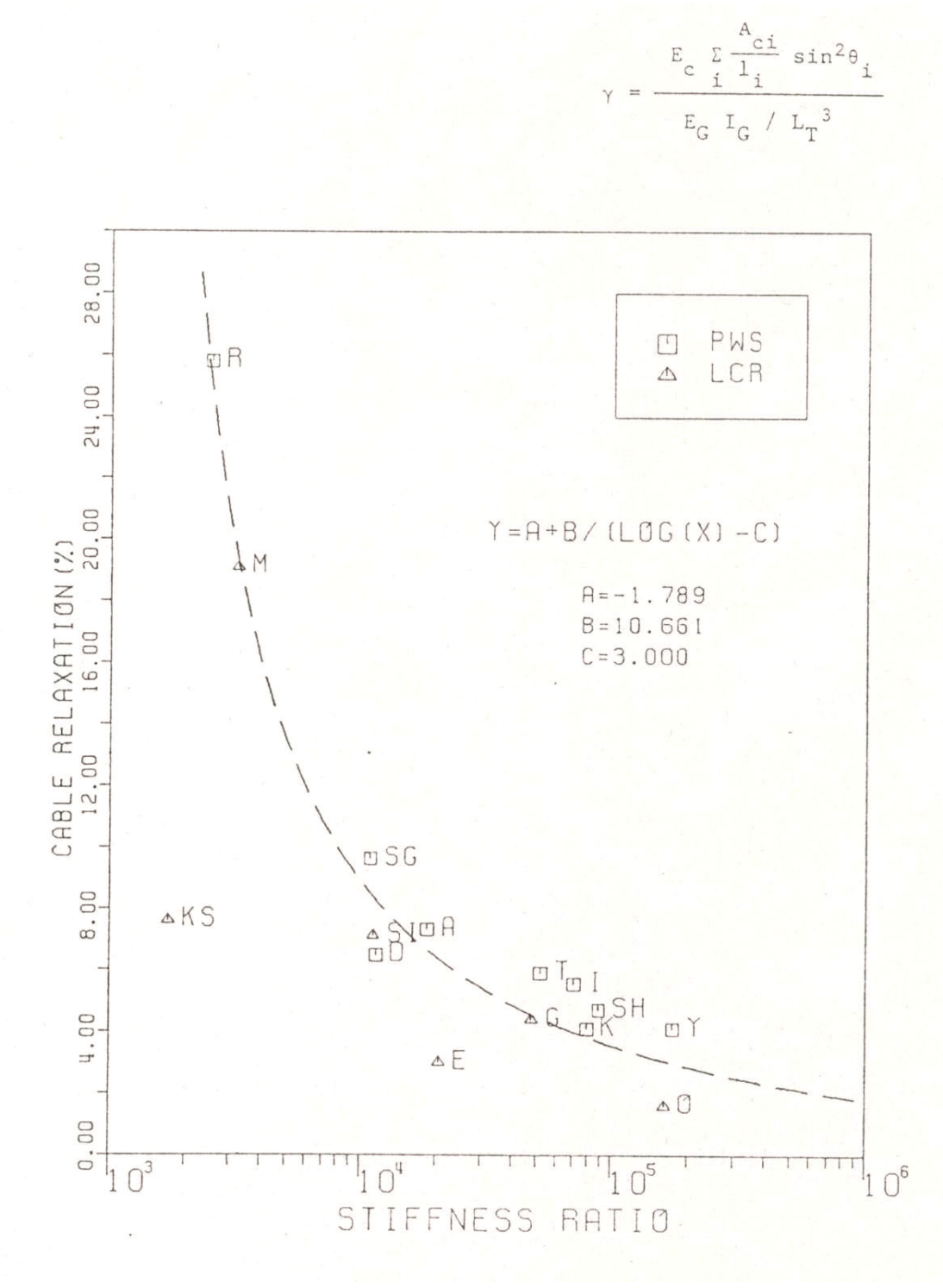

Fig.6.12 Relationship between relative stiffness ratio and relaxation

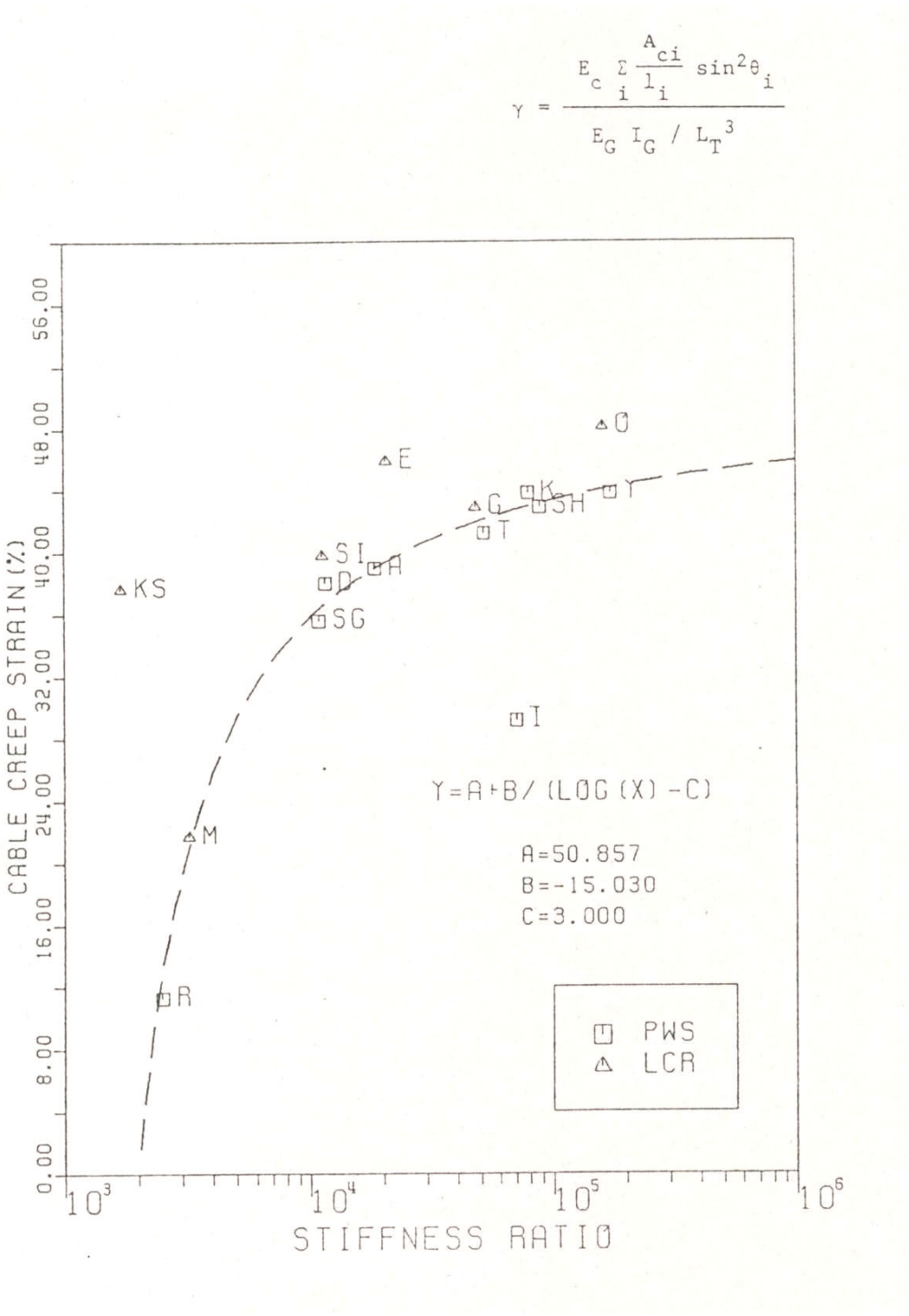

Fig.6.13 Relationship between relative stiffness ratio and ratio of creep strain to initial strain

6.8 Summary

The conclusion obtained from the proposed study can be summarized as follows:

(1) If changes of cables or cambers are measured at two independent time stations besides on the completion, the coefficients of cables model may be reasonably determined within the framework of the linear visco-elasticity.

(2) It is considered that creep and relaxation of cables tend to increase under influence of prestress. Thus, excessive prestress in comparison with other loads may not be beneficial.

(3) The greater the relative stiffness ratio becomes, the more the creep controls; on the contrary, however, the smaller the ratio becomes, the more the relaxation controls.

(4) At present, the available basic data on the time-dependent behavior of cable-stayed bridges is extremely limited. Thus, further accumulation of the basic data is highly recommended.

7. Proposal of Bridge Management System by Reliability Analysis

7.1 Introduction

Honshu-Shikoku Bridges are very important infrastructures, which were completed with plenty of costs, labors and periods in the twentieth century. These long-span bridges are national properties to be maintained in healthy conditions for a long time (Fig.7.1).

In the Honshu-Shikoku Bridge Authority, the design and construction of long-span bridges are reviewed and enhanced in the daily task. Currently, “the maintenance of long-span bridges” is a major task, which is unprecedented project in Japan. Especially, the basic policy of “the preventive maintenance” is introduced to the long-span bridges, which are appropriately inspected and repaired in order to extend their lives to more than 200 years.

For example, the high-durability coating systems for steel structures and the inspection methods for concrete structures are developed on the maintenance technologies, and the health evaluation methods for long-span bridges are studied.

However, “the bridge management system,” which inclusively consists of inspection, health evaluation, deterioration prediction and repair/reinforcement, has not constructed yet. In the daily maintenance work, the emergency repair is appropriately judged by bridge inspectors and evaluators. In this chapter, the current maintenance system is reviewed in order to make a future bridge maintenance system, and a new bridge maintenance system, which is based on the reliability analysis, is proposed.

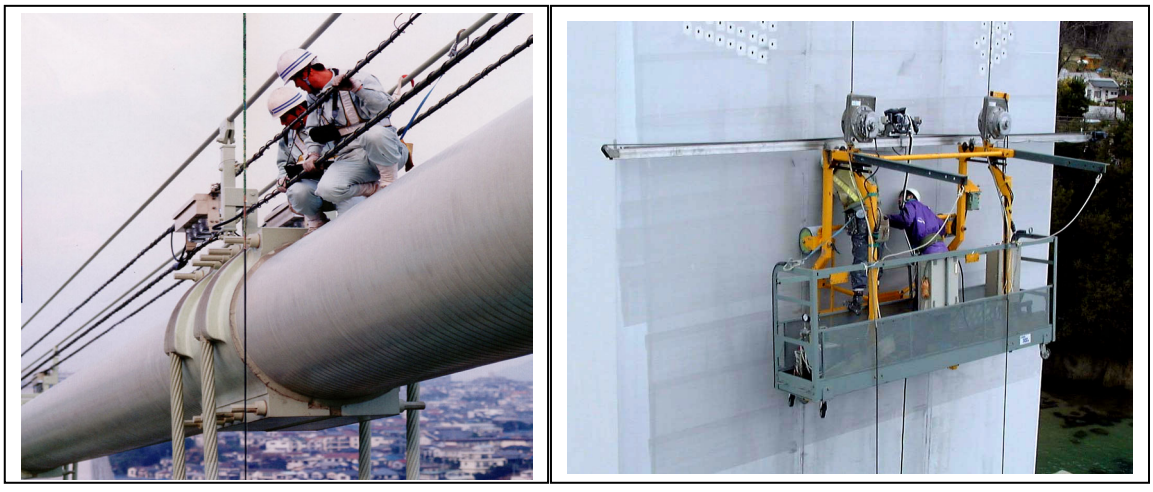

Fig. 7.1 Inspection and maintenance for long-span bridges

7.2 Examples of Bridge Management Systems

7.2.1 Bridge Management System in New York, USA

(1) Introduction

Dr. Kaito visited New York, USA as a researcher of the Colombia University from March 2001 to November 2001. He studied the bridge management system of New York City from the Dr. Yanev, who worked in Bridge Department, Transportation Bureau, New York City. There are 764 bridges (4,689 spans, 1,430,000 ㎡) in New York, and the average service life is 75 years. The organized maintenance is very important because of the aging bridges, the heavy traffic volumes, and anti-freezing agents in winter.

(2) Health Evaluation

Federal Highway Administration (FHWA) usually evaluates the bridge health conditions in 10 ratings. On the other hands, the New York City evaluates the bridge health conditions in 7 ratings. In USA, each bridge should be visually checked every two years. Based on the inspection results, the overall deterioration rating for each bridge is calculated, considering the weight factor of 1 to 10 for 13 members. Each bridge has the identification number and filed on each database, including the deterioration rating results and repair/reinforcement results. New York City introduced a special method called the flag engineering to visual check. In the flag engineering, several colors are used for immediate repair after visual check with respect to members and damages. The visual check is always carried out by more than two inspectors in order to enhance the reliability and objectivity of inspection and to reduce the human errors.

(3) Bridge Management System based on Health Evaluation

After appropriate maintenance the average deterioration rating was increased in 1992 to 2000. However, the larger the bridge is, the lower the average service life is. The average deterioration rating for approximately 700 bridges is calculated in 1994 (Fig.7.2). With appropriate maintenance the deterioration rating of 40-year-old bridge decreases to be rating 4 and constant. Without appropriate maintenance the deterioration rating of 55-year-old bridge decreases to be rating 2, which is equivalent to the service limit (Fig.7.3).

Based on the deterioration rating results, the deterioration rating can be predicted to decrease by 0.1 every year. The overall bridge deterioration prediction can be obtained by

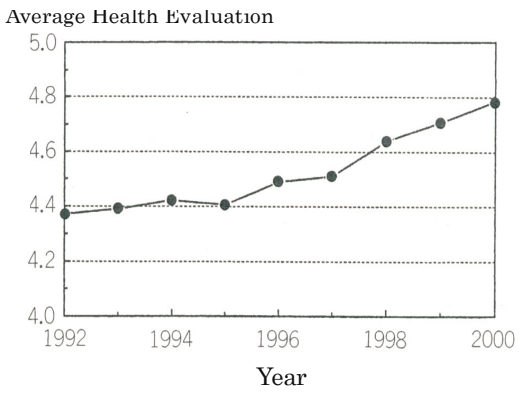

Fig. 7.2 Change of average health evaluation

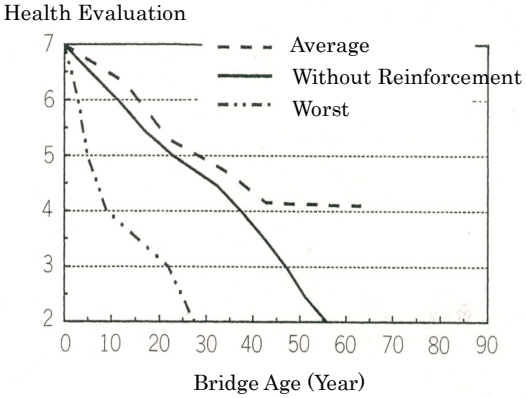

Fig. 7.3 Average deterioration curve in NY

weight average after calculating the deterioration prediction of each member, considering the effects of 15 maintenance works (0.0 to 1.0).

The life-cycle cost can be calculated for test estimation. In case of service limit, the bridge is assumed to repair, reinforce or reconstruct. If all maintenance work is done, the bridge service life will extend to be three times.

(4) Summary

The following items are very important; 1) standardization of inspection techniques, 2) identification of inspection method, 3) quantitative raring of deterioration, 4) electrical database, 5) public information, 6) effective use of database, 7) civic cooperation.

7.2.2 Bridge Management System in Germany

(1) Introduction

Prof. Izumo of Kanto Gakuin University explained the bridge management system in Germany. In European countries, the bridge management system, which is based on the bridge maintenance database, is now in an operational stage after collecting the exiting bridge information.

(2) Necessity of Bridge Management System in Germany

Federal government of Germany is the owner of federal highways and has the responsibility of maintenance and finance. Each local government has the responsibility of inspections and repairs of federal highways. The maintenance budget is estimated to increase because traffic volumes as well as truck loads are increasing. The bridge management system is developed so that the limited budget is required to efficiently enforce. This system provides the overview,

long-term aim/strategy for the federal government and the proposal of objective structures for the local governments.

(3) Concept of Bridge Management System

Practical use of bridge management system is scheduled to start by 2005. The bridge management system in Germany consists of the following seven modules; 1) database for highway network, 2) current data and evaluation, 3) damage analysis of objective structure, 4) repair plan, 5) cost/benefit analysis, 6) plan and execute, 7) management adjustment (Fig. 7.4).

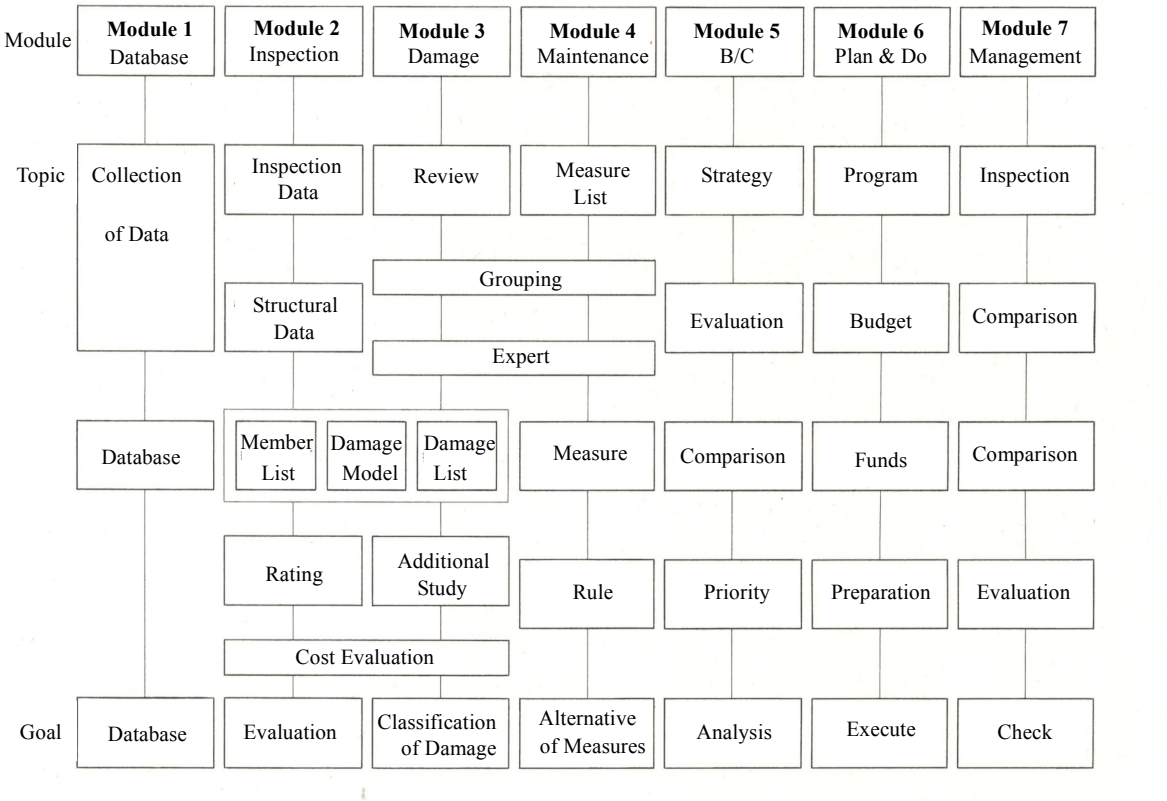

Fig. 7.4 Concept of bridge management system in Germany

(4) Database

According to the "ASB79" (statement on highway database), all highway data are collected and preserved. In addition, "SIB" (structural database), including related information, figures and photographs, are proposed and put in practical service. Currently, the federal government is developing a new system called the BISStra in order to improve the information processing conditions.

(5) Inspection and Investigation

Methods of inspection and investigation are prescribed in the DIN1076. The visual check and the yearly visual check shall be carried out four times per year and once per year, respectively. The basic inspection shall be carried out by inspectors by means of visual check every three years. Detailed investigation shall be carried out by experts by means of non-destructive tests every six years, and special investigation shall be carried out in case that a damage occurs, which has a possibility of influence on the structural safety.

The federal government made a guideline on inspection result process, which is called "RI-EBW-PRUEF" in 1998. In this guideline, the individual evaluation of the damaged structures are classified in the following three categories: 1) structural safety, 2) traffic safety, 3) structural durability, and the total evaluation the damaged structures are automatically calculated by means of quantitative manner.

(6) Construction of Bridge Management System

In the bridge management system, each local government has the following plan making processes: 1) damage, deterioration rating and evaluation, 2) structure overall evaluation, 3) decision of repair period, 4) emergence evaluation, 5) repair plan making, 6) repair plan evaluation, 7) priority of repair plan, 8) repair execution plan, and 9) budget to need.

On the other hand, the federal government has the following adjustment processes: 1) provision of network data, 2) comparison of target and result, 3) long-term cost estimation, 4) long-term deterioration rating, 5) statistical evaluation on special issue, 6) analysis and evaluation, and 7) effect of plan.

In addition, each local governments also has the following executing processes: 1) budget and plan making, 2) execution possibility, 3) plan decision, 4) execution, and 5) adjustment.

(7) Summary

The federal government and the local governments need to cooperate in all processes of plan, adjustment and execution. An objective process for plan decision, an integrated system and a maintenance method are needed.

9.2.3 Study on Bridge Management System in Japan

(1) Introduction

Prof. Miyamoto of Yamaguchi University and et al. studied the bridge management system

for concrete structures by using the Fuzzy theory. Since the concrete structures are slowly deteriorating in Japan, the concrete structures need the appropriate maintenance. In order to utilize the limited budget, the bridge management system is required. The bridge management system, which consists of visual inspection, deterioration evaluation, deterioration prediction and repair plan, is proposed in this study.

(2) Feature of Bridge Management System

The bridge management system is developed for existing reinforced concrete bridges. In the visual inspection, cracking, surrounding condition, traffic volume, etc., are considered. In the deterioration evaluation, an expert system, based on the Fuzzy theory, is introduced (Fig. 7.5). In the deterioration prediction, the durability valuation and strength evaluation are carried out by assumption of a third-power curve and a forth-power curve, respectively. In repair plan, effects of repair or reinforcement are expressed quantitatively.

(3) Application of Bridge Management System to real bridges

In order to ensure the precision of the bridge management system, a questionnaire survey to professional engineers on seven bridges is carried out. The survey results are summarized as follows.

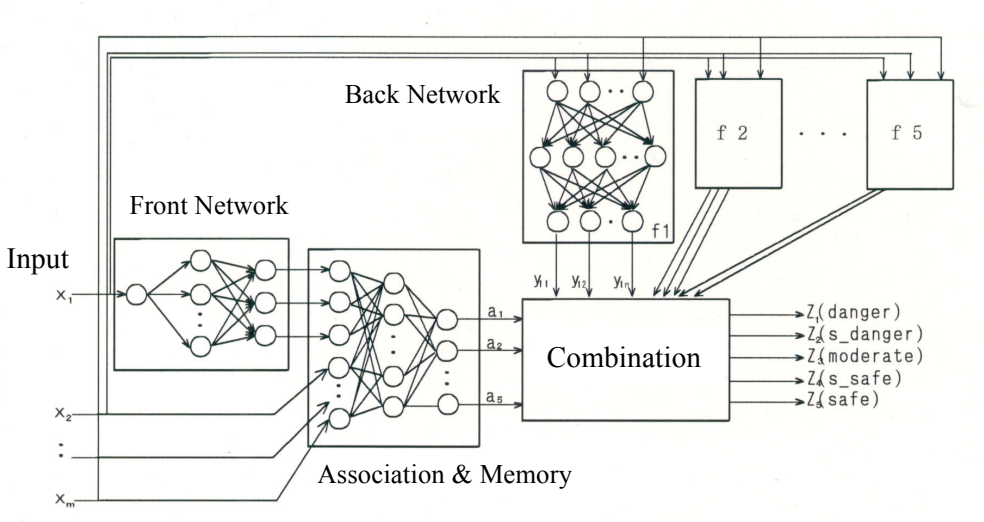

Fig. 7.5 Concept of expert system based on the Fuzzy theory

1) The visual inspection results by professional engineers are equivalent to real bridge conditions.
2) The deterioration evaluations results by professional engineers are almost equivalent to the deterioration evaluation results by the expert system.
3) The deterioration prediction results by professional engineers are longer than the deterioration prediction results by the expert system.
4) The repair plan results by professional engineers are almost equivalent to the repair plan results by the expert system.

(4) Summary

The bridge management system can be applied to real bridges as compared with the professional engineer's judgement and the expert system's judgement.

7.3 Current Maintenance System for Long-span Bridges

7.3.1 Inspection Method

In the inspection for long-span bridges of the Honshu-Shikoku Bridges, the periodical inspection is classified as follows.

1) Daily inspection: Structures are inspected by visual check from maintenance ways on long-span bridges every three months.
2) Basic inspection: Structures are inspected by visual check or finger check from maintenance ways or maintenance vehicles on long-span bridges every year or two years.
3) Detailed inspection: Structures are inspected by means of accurate measurement instruments every five years.

The results of the above-mentioned inspections have been kept on an electric database since 1998 in order to access the database to all bridge engineers.

7.3.2 Health Evaluation Method

Changes and disorders in the above-mentioned inspections are reported and evaluated by rating 1 to 5 in each structural member.

For superstructure, 1) floor system, 2) main girder, 3) main tower, and 4) main cable, are evaluated. For substructure, 5) anchorage, and 6) tower foundation, are evaluated. For others, 7) expansion joints, 8) bearing, 9) accessories, 10) coating system, and 11) pavement, are evaluated.

After the individual evaluation for each structural member, the overall evaluation is calculated in rating 1 to 5 by considering the individual weight of 4 to 10. The individual weights are 10 for the member 2) to 6), 8 for the member 1), 6 for the member 8), 5 for the member 9), and 4 for 7), 10) and 11), respectively.

The results of health evaluation for two bridges are shown in Table 7.1 to 7.3.

Table 7.1 Health evaluation results for two bridges from 1999 to 2003

Bridges	1999	2000	2001	2002	2003
AK Bridge	4.7	4.7	4.8	4.7	4.7
ON Bridge	4.1	4.1	4.1	3.9	3.9

Table 7.2 Health evaluation result of AK Bridge in 2003

AK Bridge (1998)	Health Evaluation in 2003		
Members	Weight (a)	Condition (b)	Weighted condition (a) ×(b)
Deck	8	5	40
Girder	10	5	50
Tower	10	5	50
Cable	10	5	50
Anchorage	10	5	50
Tower Foundation	10	5	50
Expansion Joints	4	4	16
Bearings	6	4	24
Accessories	5	3	15
Coating	4	4	16
Pavement	4	5	20
Total	81		381
Rating			**4.7**

Table 7.3 Health evaluation result of ON Bridge in 2003

ON Bridge (1985)	Health Evaluation in 2003		
Members	Weight (a)	Condition (b)	Weighted condition (a) ×(b)
Deck	8	5	40
Girder	10	5	50
Tower	10	5	50
Cable	10	3	30
Anchorage	10	4	40
Tower Foundation	10	3	30
Expansion Joints	4	4	16
Bearings	6	4	24
Accessories	5	3	15
Coating	4	2	8
Pavement	4	4	16
Total	81		319
Rating			**3.9**

7.3.3 Deterioration Prediction Method

In the steel structures of long-span bridges, many points for coating investigation are designated and the coating condition, including coating thickness, luster, choking, etc., are periodically checked. Based on the results of coating investigation, the average reducing speed in the coating thickness and the deteriorating curve of the coating thickness are obtained.

On the other hand, in the concrete structures of long-span bridges, the non-destructive tests are introduced, and the durability effects due to salinity or carbonation are checked by measuring the salinity density and the carbonated depth. In addition, the deterioration predictions are carried out, based on the results of the non-destructive tests.

7.3.4 Repair/Reinforcement Plan Method

Based on the coating deteriorating curves for the steel structures, partial repaint or overall recoating are proposed and carried out in the long-term maintenance program. Based on the deterioration predictions for the concrete structures, countermeasures are proposed and carried out in the long-term maintenance program.

7.3.5 Current Bridge Maintenance System

The above-mentioned processes are carried out in each long-span bridge, considering the completed year, the damaged member, the surrounding condition, etc. The current maintenance system for log-span bridges is shown in Fig. 7.6. An efficient maintenance system is required, based on the quantitative and rational judging criteria.

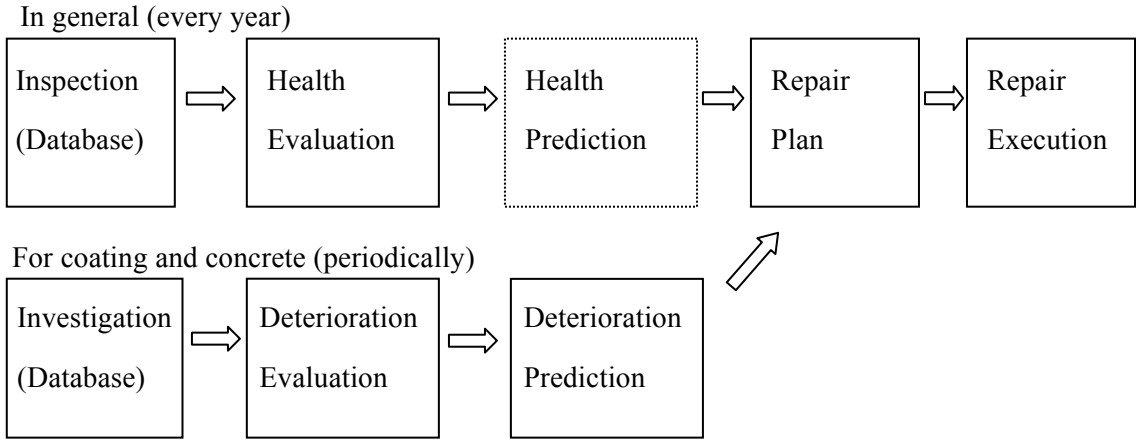

Fig. 7.6 Current maintenance system for log-span bridges

7.4 Long-span Bridge Management System by Conventional Method

7.4.1 Inspection Problem

Currently, the various inspection results are kept on an electric database of each operation office, these results should be kept on a common database in order to be easily accessed by each bridge engineer. The repair results are not necessarily kept on database of each operation office as well as on a common database. The investigation results, including the designated coating investigation for steel structures and the non-destructive tests for concrete structures, are required to make an electric common database.

7.4.2 Health Evaluation Problem

The objects of health evaluation are described as follows.

1) Compare the health evaluation results of various bridges in a short term.
2) Compare the health evaluation results of each bridge in a long term.
3) Accumulate the health evaluation results.
4) Make a budget and execute a repair work if an early repair is needed.
5) Make an appropriate repair plan for each bridge in each year.
6) Make the bridge management system in the near future.

The above-mentioned objects 1), 2), 3) and 4) have been almost achieved, and the objects 5) and 6) are required to solve immediately.

The method of health evaluation is revised every year, however the evaluations of changes or disorders are not necessarily quantitative and the results of health evaluation are easy to be variable. For instance, the weight for each member and the judgement of each condition depend on the engineering judgement, which includes the individual variation and lacks the objectivity.

The designated coating investigation for steel structures in every five year and the non-destructive tests for concrete structures in every five to ten years are required to consider their results in the health evaluation. How to evaluate the effect of repair or reinforcement is a future problem. For instance, the overall recoating obtains the rating after finishing the several-year recoating work.

7.4.3 Deterioration Prediction Problem

In ordinary inspections, visual checks are major inspection method, and the results cannot be considered in deterioration prediction. The coating deterioration prediction for steel structures and the concrete deterioration prediction for concrete structures, have no problem because those predictions are qualitative.

7.4.4 Repair/Reinforcement Plan Problem

How to reflect the health evaluation results to long-term repair plan is one of the most important problems. The results should be a major part of the bridge management system. Therefore, the health evaluation should be for the bridge management system. If possible, the health evaluation would be carried out for all bridges, including general steel bridges, reinforced concrete bridges and prestressted concrete bridges, and the bridge management system should be built for all bridges.

7.4.5 Bridge Maintenance System Problem

The inspection results and the investigation results could be evaluated as the same time. The problems of the health evaluation and the deterioration prediction in current bridge maintenance system are summarized as follows.

1) The weight for each member in the health evaluation method is not necessarily rational.
2) The structural safety in the health evaluation method is not necessarily clear.
3) The relation between the health evaluation and the deterioration prediction is unclear.
4) The process from the health evaluation to the deterioration prediction, the repair plan and the repair execution are not necessarily clear.

Consequently, the bridge management system, which is based on quantitative and rational judgement criteria, is required in order to maintain the long-span bridges appropriately in the limited budget. A draft for bridge management system of long-span bridges is shown in Fig. 7.7.

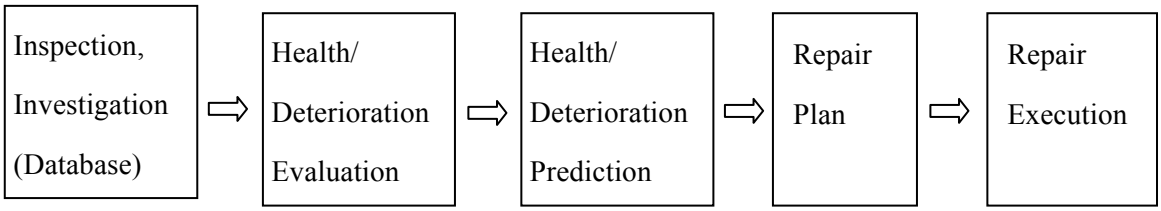

Fig. 7.7 Draft for bridge management system of long-span bridges

7.5 Proposal of Long-span Bridge Management System by Reliability Analysis

7.5.1 Proposal of Inspection

The inspection results, including the repair results, should be kept on a database of each operation office as well as on a common database. The investigation results, including the designated coating investigation for steel structures and the non-destructive tests for concrete structures, should be made as an electric common database.

7.5.2 Proposal of Performance Evaluation

In general, the performances of a structure are classified as the following major performances, 1) strength performance, 2) durability performance, 3) functional performance and others.

The reliability analysis can be applied to the strength performance, considering the resistances and the loads. The reliability index β and the probability of failure Pf can yield to the safety of the structure. In addition, the reliability analysis can be applied to the durability performance of steel structures, considering the coating thickness and the corrosion limit. The reliability analysis can be also applied to the durability performance of concrete structures, considering the salinity density and the corrosion limit. In general, the other performances are negligible to the safety of structure.

Based on the result of the above-mentioned consideration, the health evaluation for steel structures and deterioration evaluation can be revised to “the performance evaluation” by using the reliability analysis.

7.5.3 Proposal of Performance Prediction

The strength performance can be predicted by the reliability analysis, considering the time-dependent load and resistance. The durability performance can be predicted by the reliability analysis, considering the time-dependent corrosion limit and coating system.

Based on the result of the above-mentioned consideration, the health prediction for steel structures and deterioration prediction can be revised to “the performance prediction” by using the reliability analysis.

7.5.4 Proposal of Repair Plan

Based on the result of the above-mentioned consideration, the bridge management system can be obtained by means of the reliability analysis. The new bridge management system by

reliability analysis is shown in Fig. 7.8.

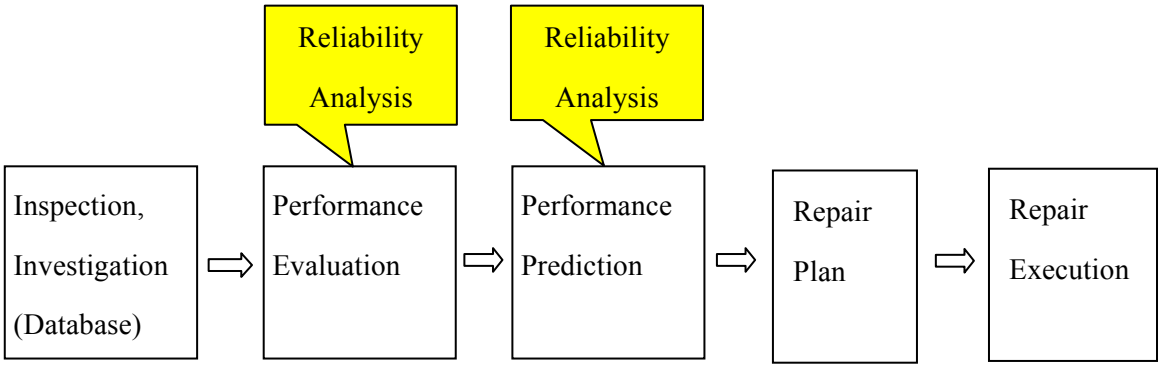

Fig. 7.8 New bridge management system by reliability analysis

7.6 Example of Long-span Bridge Management System by Reliability Analysis

Firstly, many examples of strength performance have been described in Chapter 4 and 5, considering the time-dependent load and strength. Application of reliability analysis is easily available to strength performance in the long-term maintenance.

Secondly, an example of durability performance is introduced in this section, considering the time-dependent corrosion and coating for steel structures. The coating investigation of ON Bridge in 1991-1998 is shown in Fig.7.9 (a) to (d), respectively. The normal distribution approximation is almost equal to the frequency of total coating thickness. And the log-normal distribution approximation is quite equal to the frequency of total coating thickness. The total coating thickness in designated criteria is 255 μm for polyurethane resin paint, which is dashed in Fig.7.9.

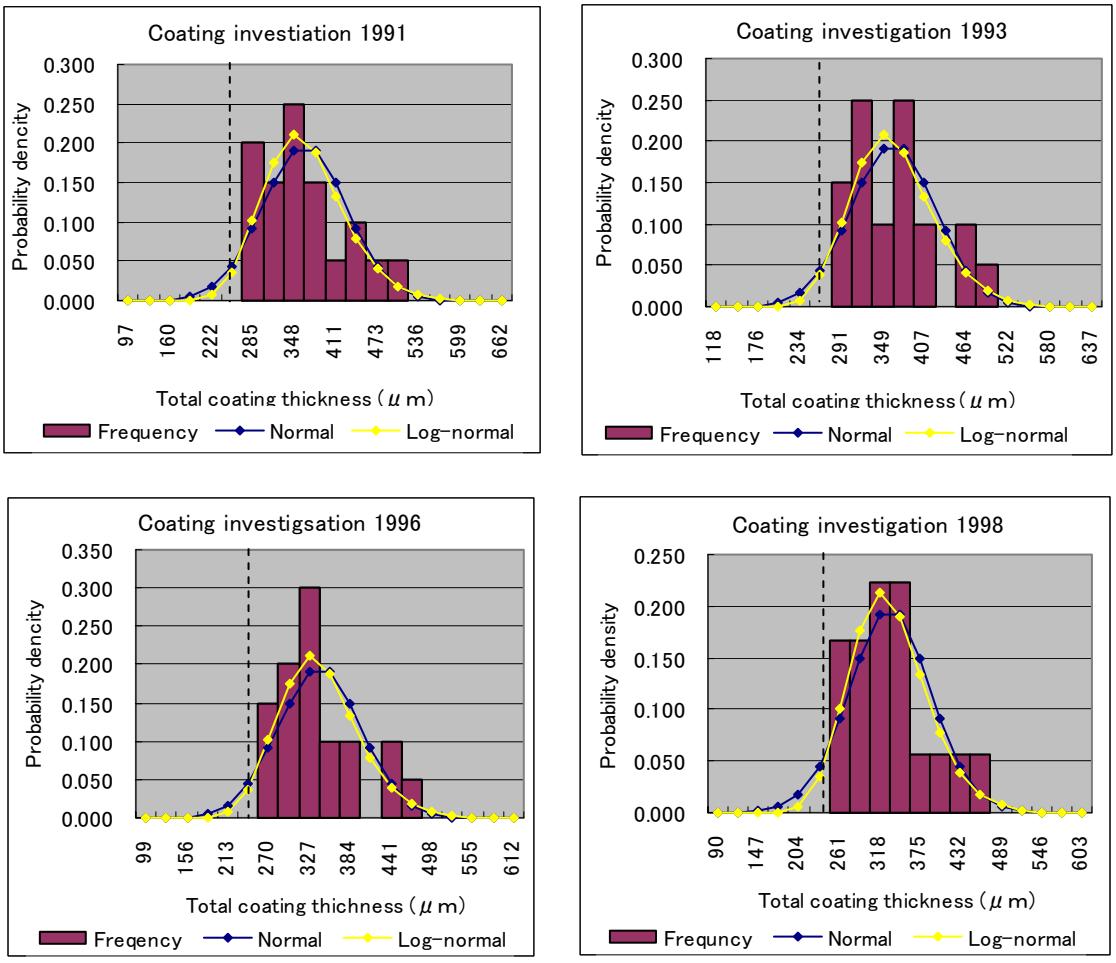

Fig.7.9 (a)-(d): Coating investigation of ON Bridge in 1991-1998

Changes of the normal distribution approximation and the log-normal distribution approximation in the total coating thickness are shown in Fig.7.10 and 7.11, respectively. These figures show the reduced average of total coating thickness and the increased variation of the total coating thickness according to the investigation year.

On the other hand, these figures also show the corrosion limits with the average of 135 μ m and standard variation of 30 μ m, which are dashed curves in Fig.7.10 and 7.11. The corrosion limit for polyurethane resin paint is supposed to occur as following assumption.

1) Corrosion occurs in a small area when the averaged total coating thickness is 195 μ m, where the sixth coating (upper paint) and the fifth coating (middle paint) disappear.

2) Corrosion occurs in a half area when the averaged total coating thickness is 135 μ m, where the four coating (lower paint) disappears.

3) Corrosion occurs in most area when the averaged total coating thickness is 75 μ m, where the third coating (lower paint) disappears.

The above assumption should be examined by means of accumulated data. However, the corrosion can be considered to occur when the total coating thickness becomes to less than the corrosion limit due to saline element, water, oxygen, and the other causes. The marginal coating thickness, which is the total coating thickness minus the corrosion limit, shall be calculated by the Monte Carlo Simulation. Therefore, the reliability analysis can be used for the durability performance as well as the strength performance.

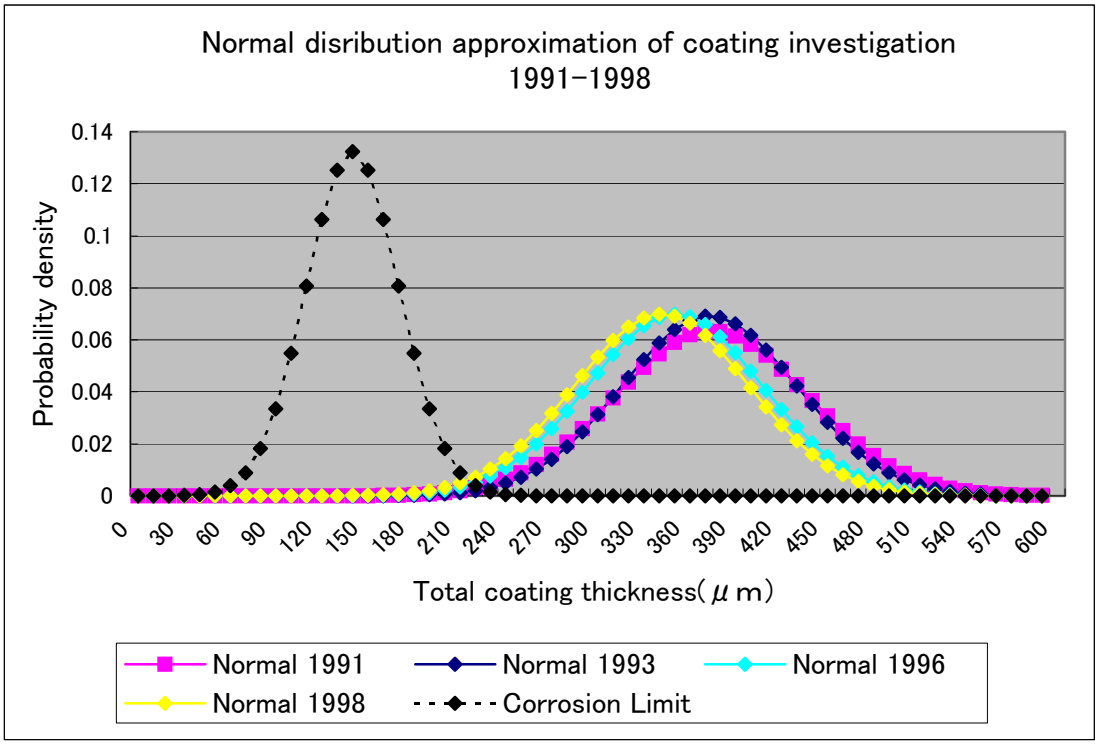

Fig.7.10 Normal distribution of corrosion and variable coating thickness

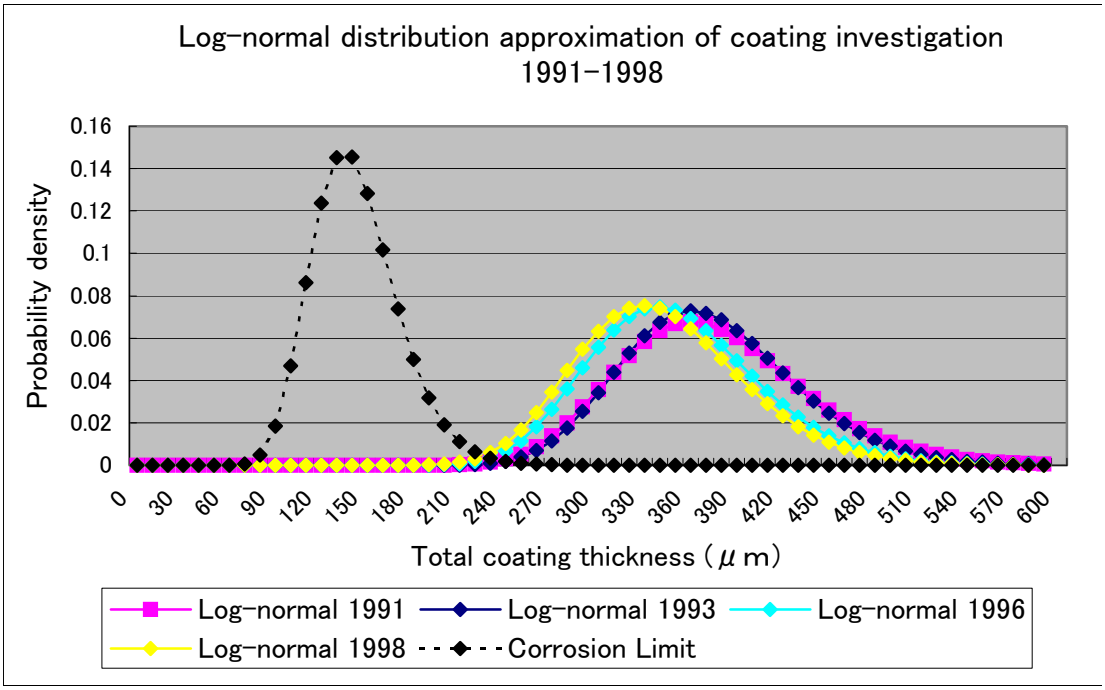

Fig.7.11 Log-normal distribution of corrosion and variable coating thickness

The reliability analysis for durability performance is carried out by application of the Monte Carlo Simulation to the corrosion limits and the total coating thickness as same as the load and resistance for strength performance.

The reliability index in the normal distribution approximation and the log-normal distribution approximation are shown in Fig.7.12. In the normal distribution approximation, the reliability index decreases from 3.57 in 1993 to 3.13 in 1998. In the log-normal distribution approximation, and the reliability index decreases from 3.67 in 1993 to 3.24 in 1998.

In addition, the failure of corrosion in the normal distribution approximation and the log-normal distribution approximation are shown in Fig.7.13. In the normal distribution approximation, the failure of corrosion increases from 0.0 in 1993 to 0.0008 in 1998. In the log-normal distribution approximation and the failure of corrosion increases from 0.0 in 1993 to 0.0004 in 1998.

Since the log-normal distribution approximation is equal to the frequency of total coating thickness, the analytical result of the log-normal distribution approximation is more precise than that of the normal distribution approximation. These results are tabulated in Table 7.4.

This approach can be available in application not only to the performance evaluation but also to the performance prediction. By using the deterioration curves for coating system described in the chapter 3, the reliability analysis can be carried out for the performance prediction.

Table 7.4 Results of reliability analysis for coating system against corrosion

	1993	1996	1998
Reliability Index			
Normal distribution	3.5708	3.2195	3.1295
Log-normal distribution	3.6722	3.4110	3.2411
Failure of Corrosion			
Normal distribution	0.0001	0.0004	0.0008
Log-normal distribution	0.0000	0.0001	0.0004

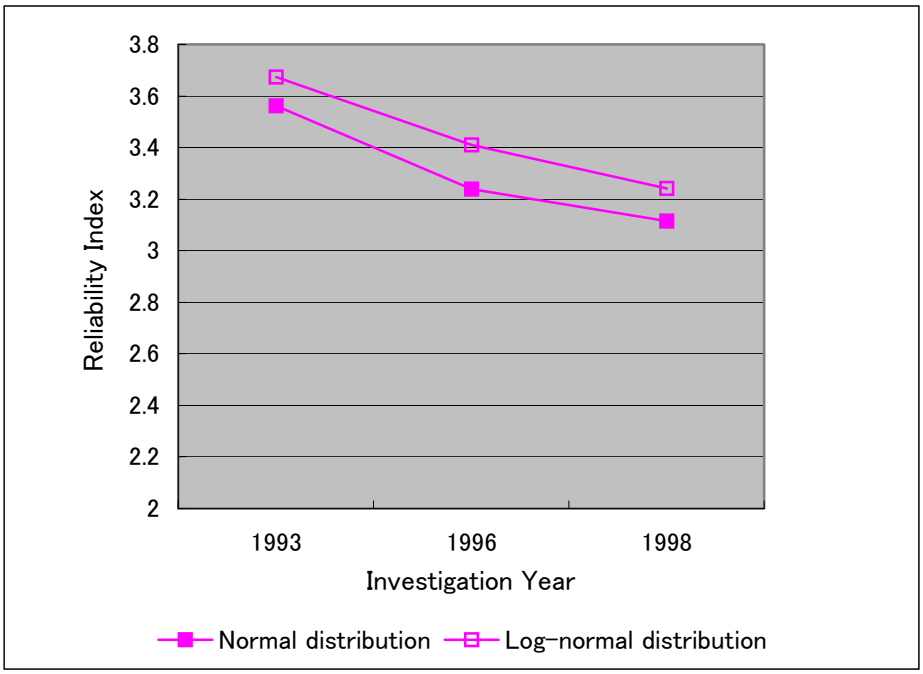

Fig.7.12 Reliability analysis of coating system against corrosion

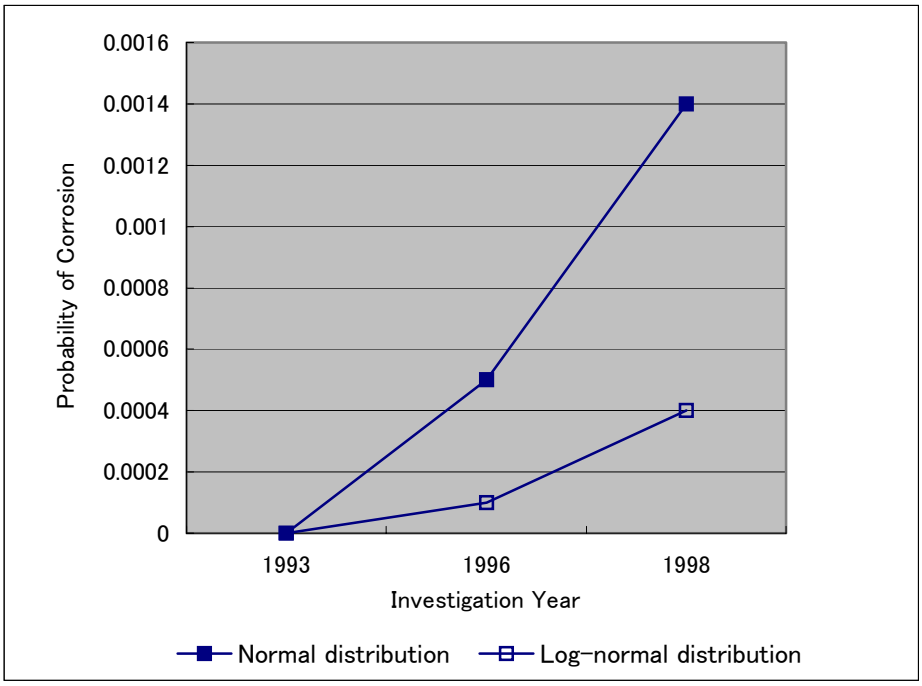

Fig.7.13 Reliability analysis of coating system against corrosion

Thirdly, the reliability analysis for durability prediction is carried out by application of the Monte Carlo Simulation to the corrosion limits and the total coating thickness as same as the load and resistance for strength performance.

The reliability index in the normal distribution approximation and the log-normal distribution approximation are shown in Fig.7.14. In the normal distribution approximation, the reliability index decreases from 3.04 in 2001 to 2.42 in 2010. In the log-normal distribution approximation, and the reliability index decreases from 3.23 in 2001 to 2.88 in 2010.

In addition, the failure of corrosion in the normal distribution approximation and the log-normal distribution approximation are shown in Fig. 7.15. In the normal distribution approximation, the failure of corrosion increases from 0.0013 in 2001 to 0.0083 in 2010. In the log-normal distribution approximation and the failure of corrosion increases from 0.0003 in 2001 to 0.0013 in 2010.

Since the log-normal distribution approximation is equal to the frequency of total coating thickness, the analytical result of the log-normal distribution approximation is more precise than that of the normal distribution approximation. These results are tabulated in Table 7.5.

The normal distribution prediction and the log-normal distribution prediction in the total coating thickness from 2001 to 2010 are shown in Fig.7.16 and 7.17, respectively. These figures show that the reliability analysis can be available in application to the performance evaluation as well as to the performance prediction.

Table 7.5 Results of reliability analysis for coating system against corrosion

	2001	2004	2007	2010
Reliability Index				
Normal distribution	3.0441	2.8653	2.6262	2.4195
Log-normal distribution	3.2254	3.0974	3.0070	2.8767
Failure of Corrosion				
Normal distribution	0.0013	0.0017	0.0036	0.0083
Log-normal distribution	0.0003	0.0005	0.0009	0.0013

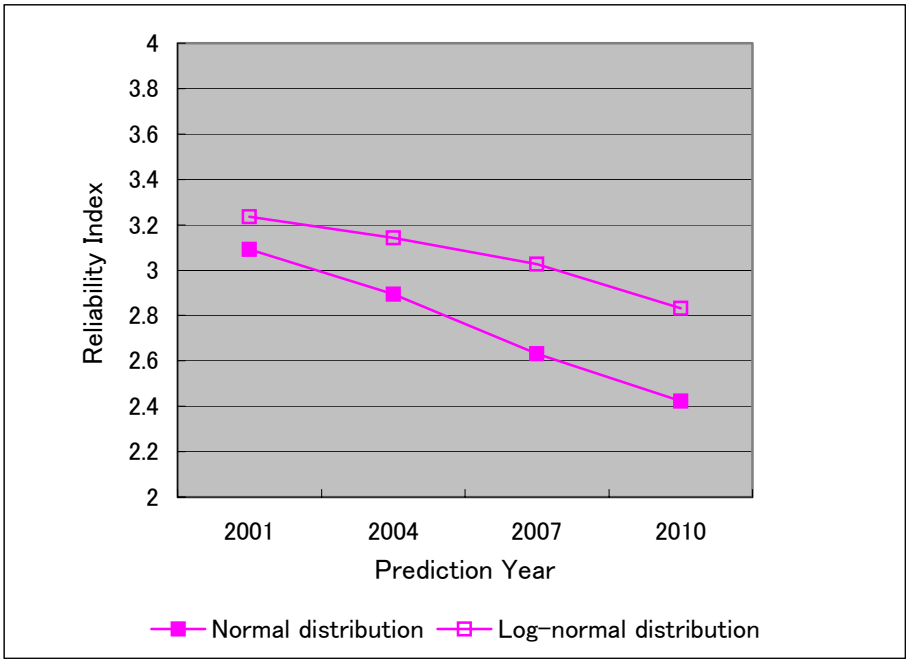

Fig.7.14 Reliability analysis of coating system against corrosion

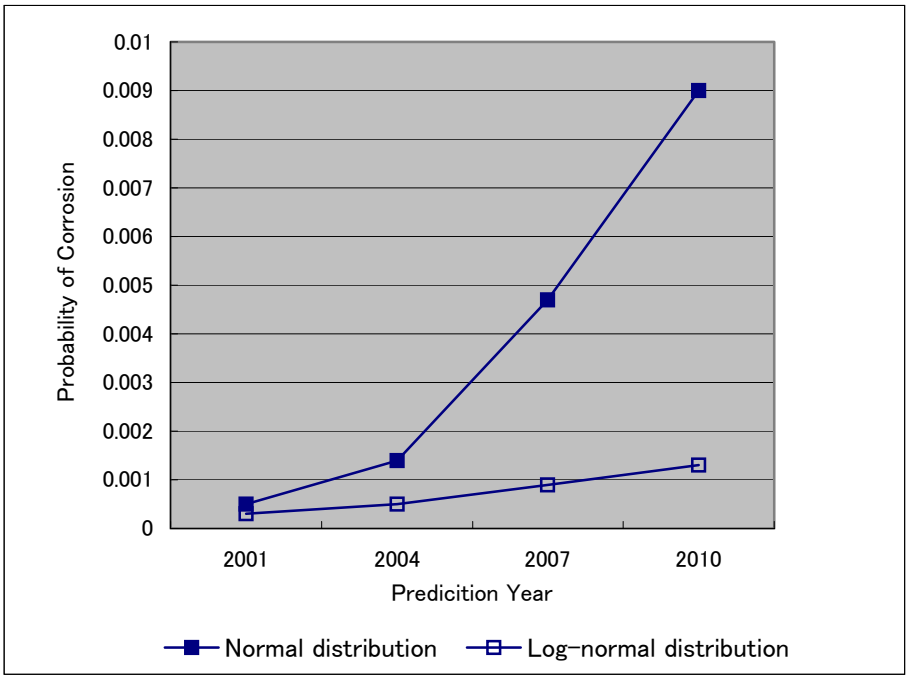

Fig.7.15 Reliability analysis of coating system against corrosion

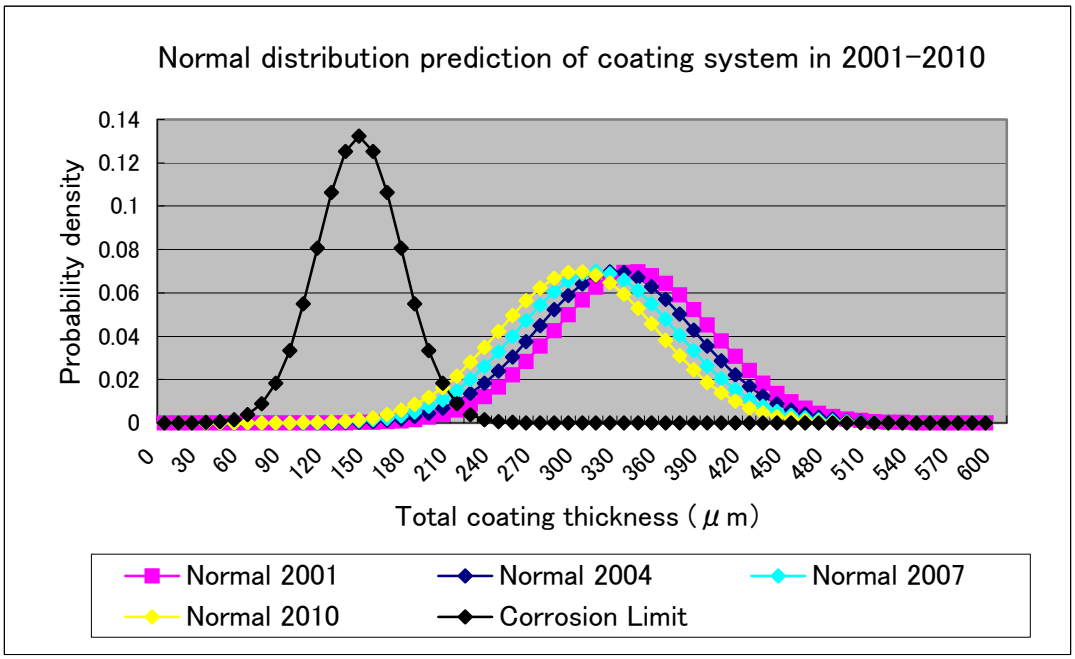

Fig.7.16 Normal distribution prediction of coating system

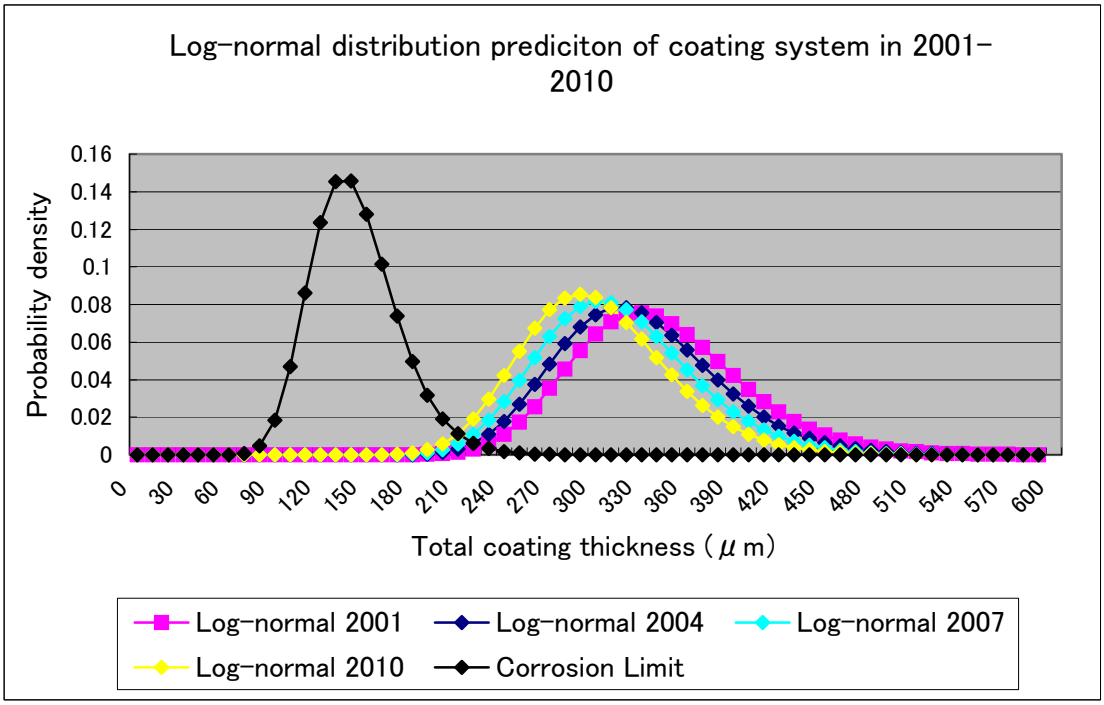

Fig.7.17 Log-normal distribution prediction of coating system

7.7 Summary

Examples of bridge management systems in foreign countries and Japan were reviewed. And the current bridge maintenance system for the long-span bridge was also reviewed.

By introduction of the reliability analysis to the bridge management system, the performance evaluation and the performance prediction for structures can be possible in terms of the reliability index and the probability of failure. This method can yields to the quantitative and rational repair plan for long-span bridges.

In future, the bridge management system will be applied to all bridges, including general steel bridges, reinforced concrete bridges and prestressted concrete bridges on the Honshu-Shikoku Highways.

8. Summary, Conclusions and Recommendations

8.1 Summary

In the second chapter, the basic theory on the reliability analysis was reviewed. The Monte Carlo techniques is very convenient for the reliability analysis even if the function has a complicated distribution, since the computer easily generates a lot of random numbers.

In the third chapter, the live load and the wind load were reviewed as increasing models of the time-dependent load. And the steel structures and the concrete structures were reviewed as aging models of the time-dependent strength.

In the forth chapter, the reliability analyses for various types of bridges (girder of steel deck plate, simply supported steel girder, three-span continuous steel girder, three-span continuous steel box girder, reinforced concrete girder) were carried out, considering the time-dependent load and strength. The results yielded that the safety reduces gradually against the increase of live load, but that the safety reduces rapidly against the corrosion of steel members.

In the fifth chapter, since the corrosions had been observed, the reliability analyses for the main cable and the suspender rope of suspension bridges were carried out, considering the time-dependent load and strength. The result yielded that the reliability index of the main cable is 8.0, which means no problem. And The result yielded that the reliability index of the suspender rope is more than 20.0 presently, and approximately 10.0 after 10 years. In addition, by using the entire model of suspension bridge, the representative members were checked by the reliability analysis against the increase of live load and wind load.

In the sixth chapter, the structural analysis for the creep and relaxation in cables of the cable-stayed bridges were carried out, assuming the visco-elasticity of the cable. The analytical results of many cable-stayed bridges yielded that the more the relative stiffness of the cable to the girder is, the more the creep occurs in cable, and that the less the relative stiffness is, the more the relaxation occurs in cable.

In the seventh chapter, the bridge management system by means of the reliability analysis was examined, which yielded the effectiveness of reliability analysis not only in the strength performance but also in the durability performance. For instance, the reliability analysis was applied to the problem of the decreasing coating thickness and the increasing corrosion.

Therefore, the bridge management system by means of the reliability analysis can be proposed in order to evaluate and predict the safety of bridge performance quantitatively and rationally.

8.2 Conclusions

The reliability analyses were carried out for the short-span bridges and the long-span bridges, considering the time-dependent load and strength in order to evaluate and predict the strength performance of steel structures and concrete structures. In addition, the reliability analysis was also applied to the durability performance of steel structures.

The conclusions of this thesis are summarized as follows.

1) In short-span bridges, the results of the reliability analyses considering the time-dependent load and strength yielded that the safety reduces gradually against the increase of live load, but that the safety reduces rapidly against the corrosion of steel members. The appropriate maintenance is need as usual because those bridges have low degree-of freedom.

2) In long-span bridges, the result of the reliability analyses considering the time-dependent load and strength yielded that the reliability index of the main cable is relative high, and that the reliability index of the suspender rope is very high at present. The appropriate maintenance is required against corrosion even though long-span bridges have high degree-of freedom.

3) The bridge management system by means of the reliability analysis (hereafter referred to as "reliability-based bridge management system") is effective of the evaluation and prediction not only in the strength performance but also in the durability performance. The reliability-based bridge management system is more quantitative and rational than the usual bridge management system.

4) The essential maintenance is major in the current maintenance works, but the preventive maintenance can be carried out by using the reliability-based bridge management system. This system can be applied to the short-span bridges as well as the long-span bridges.

8.3 Recommendations and Further Research

The long-span bridges, including the suspension bridges and cable-stayed bridges, have many structural members and detailed structures. The reliability analysis for all members of these bridges would be very complicated. Consequently, the reliability analysis should be

efficiently carried out for structural members to calculate the reliability. In addition, the evaluation of the performance increment after repair or reinforcement should be examined.

In order to solve these problems, the accumulated data for design, construction and maintenance of various bridges are required, and the maintenance method during the bridge lifetime should be examined, considering the life cycle cost.

References

[1] Japan Society of Civil Engineers: Safety and reliability in structures, 1976 (in Japanese)

[2] Gary C. Hart: Uncertainty analysis, load, and safety in structural engineering, 1982

[3] Robert E. Melchers: Structural reliability analysis and prediction, John Wiley & Sons, 1999

[4] Design Specification for Highway Bridges, Ⅰ Generals, Ⅱ Steel Bridges, March 2002, by Japan Road Association

[5] Traffic Investigation in the Seto-Ohashi Bridges, March 1991, by Honshu-Shikoku Bridge Authority, Second Operation Bureau

[6] Kiyohiro Imai, Dan M. Frangopol, "Experience with extreme loading specifications for winds and earthquakes used for reliability assessment of the Honshu-Shikoku Bridges: a brief retrospective", IAMBAS 2004, Kyoto, Japan

[7] Report on Stiffening Girder Construction of Akashi Kaikyo Bridge, April 1998, by Honshu-Shikoku Bridge Authority, First Operation Bureau

[8] Report on Coating Investigation of Ohnaruto Bridge, March 1999, by Honshu-Shikoku Bridge Authority, First Operation Bureau

[9] Eiichi Watanabe, et al., "Toward Effective Anti-Corrosion Strategy for Marine Steel Structures", Asian-Pacific Symposium on Structural Reliability and its Applications, October 12-14, 2003, APSSRA

[10] Takazawa,T., Hoashi,H., Furuya, K., Ogawa, K., "Corrosion Protection System of Cable and Non-destructive Inspection of Suspender Ropes in a Suspension Bridge," IAMBAS 2002, Barcelona, Spain.

[11] Fujiwara, M., et al., "Committee Report on Specification Standard for Long-span Suspension Bridges by Limit State Design Method", Honshu-Shikoku Bridge Authority, 1987. (in Japanese)

[12] Ishii, K., "Investigation of Suspender Ropes in the Ohnaruto Bridge," Honshu-Shikoku Technical Presentation, 2003 (in Japanese)

[13] DIN 1073: Stahleren Strassenbrucken, Berechnungsgrunglagen, 1974.

[14] Hitachi Zohsen: On creep of locked coil ropes in Onomichi Bridge, Kansai Research

Committee on Roadway Bridges, No. B-3, 1977 (in Japanese)

[15] Osaka Municipal Office: A report on the construction of Kawasaki Bridge, 1979 (in Japanese)

[16] Kurimoto Steelwork: Measurement on Kawasaki Bridge, 1981 (in Japanese)

[17] Nakai, M. et al.: Study on creep and relaxation of spiral ropes, Trans. JSME. Vol.41, No.343, 1975, pp.987-993 (in Japanese)

[18] Konishi, I.: Steel bridges, Maruzen, 1976 (in Japanese)

[19] Metropolitan Highway Public Corporation and Japan Society of Bridge Construction: Research report on cables for cable-stayed bridges, 1st Report, 1979 (in Japanese)

[20] Tamaru, S. et al.: On design of Onomichi-Ohashi Bridges, No.6, 1968 (in Japanese)

[21] Watanabe, T. et al.: On erection of Onomichi-Ohashi Bridges, No.8, 1968 (in Japanese)

[22] Rabotnov, Y.N.: Creep problems in structural members, Applied Mathematics and Mechanics, Vol.7, North-Holland Publishing Co., Amsterdam, 1969.

[23] Lee, E.H.: Stress analysis in visco-elastic bodies, Quart. Appl. Math., Vol.13, pp.183-190, 1955.

[24] Sonoda, K., Kobayashi, H., and Ishine, T.: Solutions for beams on linear-elastic foundation, Proc. of JSCE, No.247, 1976 (in Japanese)

[25] Yamada, N., and Kunieda, Y.: Laplace transform and operation calculus, Corona Co., 1970 (in Japanese)

[26] Churchill, R. V.: Operational mathematics, International Student Edition, McGraw-Hill, 1972

[27] Kusama, T., Mutsui, Y. and Yoshida, S.: Linear visco-elastic analysis by numerical inversion of the Laplace transform, Proc. of JSCE, No.292, pp.41-52, 1979 (in Japanese)

[28] Izumi, Y.: Fundamental study on efficiency of visco-elastic analysis for structures, unpublished M.S. thesis, Kyoto University, 1980 (in Japanese)

[29] Yamada, I.: Prediction of long-term behavior of cable-stayed bridges considering visco-elasticity of cables, unpublished M.S. thesis, Kyoto University, 1983

[30] Kiyohiro Imai, “Reliability Analysis of Geometrically Nonlinear Structures with application to suspension bridges”, Ph.D. thesis, Colorado University, U.S.A., 1999

Appendix A

Structural Members of Long-span Bridges

Superstructure of Suspension Bridge

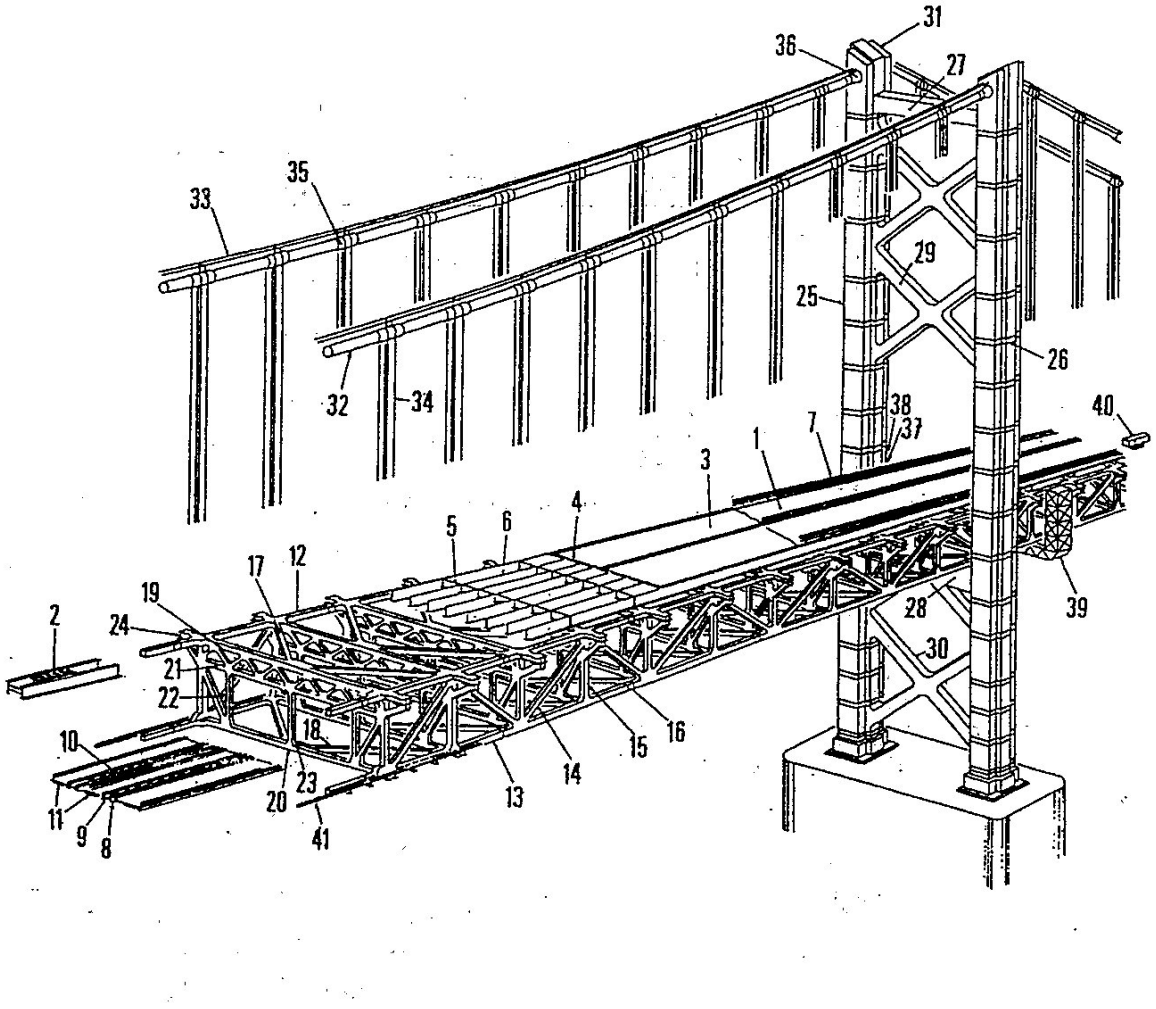

NO	吊橋上部構造の主な部材名称	names of major members of suspension bridge
1	舗　　装	pavement
2	グレーチング	grating
3	デッキプレート	deck plate
4	縦　リ　ブ	vertical rib
5	横　リ　ブ	lateral rib
6	縦　　桁	stringer
7	自動車防護柵	guard rail, clash barriers
8	縦　　桁	stringer
9	対　傾　構	cross frame
10	横　　構	lateral member
11	管　理　路	maintenance way
12	上　弦　材	upper main chord
13	下　弦　材	lower main chord
14	斜　　材	diagonal member
15	垂　直　材	vertical member
16	継　手　部	joint
17	上　横　構	upper lateral member, upper lateral bracing
18	下　横　構	lower lateral member, lower lateral bracing
19	上　弦　材	upper main chord, top chord
20	下　弦　材	lower main chord, bottom chord
21	中　弦　材	middle main chord
22	斜　　材	diagonal member
23	垂　直　材	vertical member
24	ハンガーブラケット	hanger bracket, suspender bracket
25	塔　　柱	tower shaft
26	継　手　部	joint, Horizontal splices
27	塔頂水平材	top horizontal shaft of tower, upper strut, lower portal beam
28	下部水平材	lower horizontal member lower strut, lower portal beam
29	上部斜材	upper diagonal member
30	下部斜材	lower diagonal member
31	サドルカバー	saddle cover
32	主ケーブル	main cable
33	ハンドロープ	hand rope
34	ハンガーロープ	hanger rope
35	ケーブルバンド	cable band
36	ケーブルプロテクター	cable protector
37	タワーリンク	tower link
38	ウインドシュー	wind bearing
39	検査車（外面）	inspection car (outside)
40	検査車（内面）	inspection car (inside)
41	検査車レール	inspection car rail

Anchorage of Suspension Bridge

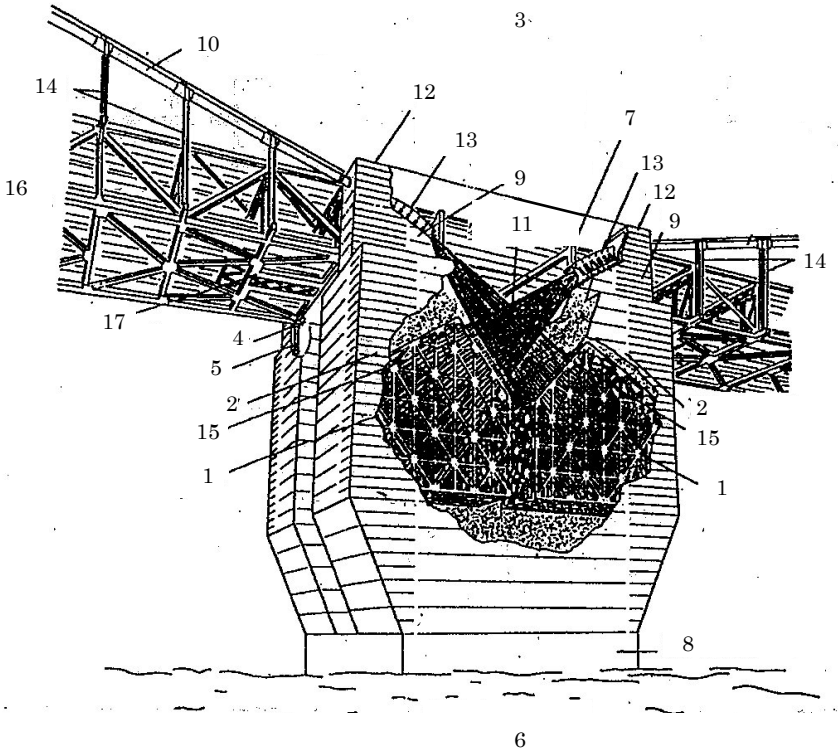

	吊橋アンカレイジ部の主な名称	names of major part of suspension bridge anchorage
1	アンカーフレーム	anchor frame
2	アンカーブロック	anchor block
3	アンカレイジ（ＢＢ４Ａ）	anchorage (BB4A)
4	ウインド沓	wind bearing
5	エンドリンク	end link
6	共用アンカレイジ	double anchorage
7	鋼製橋脚	steel pier
8	鋼製設置ケーソン	steel setting caison
9	サドルベント	splay saddle mount
10	主ケーブル	main cable
11	ストランド空中交差部	strand crossing in the air
12	ストランド防護壁	protector wall of strands
13	スプレーサドル	splay saddle
14	ハンガー下吊り部	section where lower chord is suspended
15	引　張　材	tension member
16	補鋼トラス	stiffened truss
17	補助縦桁（鉄道緩衝装置受け構造）	auxiliary beam for railway movement joint

Cable System of Suspension Bridge

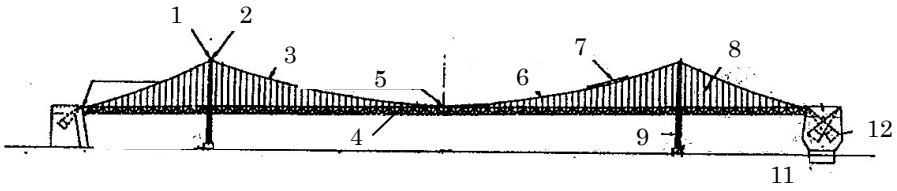

Splay Saddle

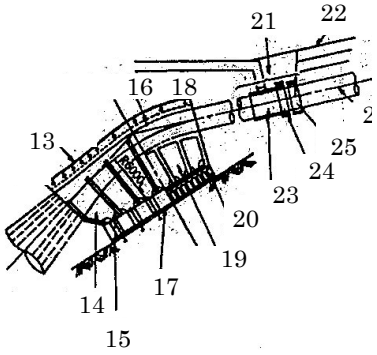

1	塔頂サドルカーバー	tower saddle cover
2	塔頂サドル	tower saddle
3	ケーブルバンド	cable band
4	補剛桁（トラス）	stiffening girder
5	センタースティバンド	center stay band
6	主ケーブル	main cable
7	ハンドロープ	hand rope
8	ハンガーロープ	hanger rope
9	主　　塔	main tower
10	上　　屋	shed
11	アンカレイジ	anchorage
12	アンカーフレーム	anchor frame

13	スプレーサドル	splay saddle
14	サドル外部	side wall of saddle
15	補強リブ	reinforcing rib
16	押え金物	pressing metal
17	底　　版	bottom plate
18	フィラー	filler
19	サドル鞍部	bottom plate of saddle
20	ローラー	roller
21	ケーブルプロテクター	cable protector
22	ハンドロープ	hand rope
23	ケーブルカバー	cable cover
24	ケーブルカラー	cable collar
25	端バンド	end band
26	主ケーブル	main cable

Tower Saddle

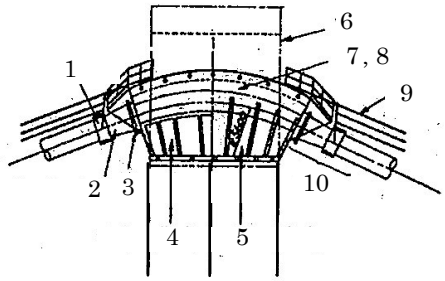

1	端バンド	end band
2	ケーブルカバー	cable cover
3	ケーブルカラー	cable collar
4	サドル鞍部	bottom plate of saddle
5	サドル外部	side wall of saddle
6	サドルカバー	saddle cover
7	押え金物	pressing metal
8	フィラー	filler
9	ハンドロープ	handrope, hand strand
10	ケーブルプロテクター	cable protector

Cable Detail

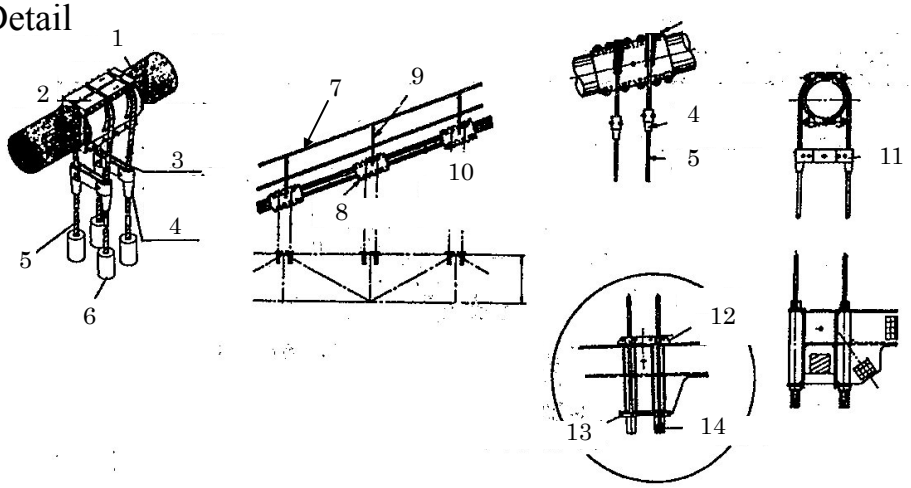

	ケーブル部詳細図	
1	主ケーブル	main cable
2	ケーブルバンド	cable band
3	ハンガーロープクランプ	hanger rope clamp, suspender clamp
4	ハンガークランプメタル	hanger clamp metal
5	ハンガーロープ	hanger rope, suspender rope
6	ソケット	socket
7	ハンドロープ	handrope, hand strand
8	ケーブルバンド	cable band
9	ハンドロープ支柱	hand rope pillar, hand rope stanchion
10	主ケーブル（ラッピングワイヤ）	main cable (wrapping wire)
11	クランプ	clamp, suspender clamp
12	ハンガーカラー	hanger collar
13	ロックプレート	locking plate
14	ソケット	socket

Center Stay

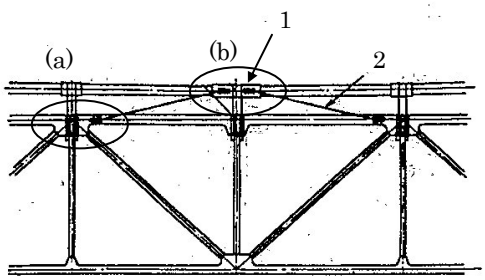

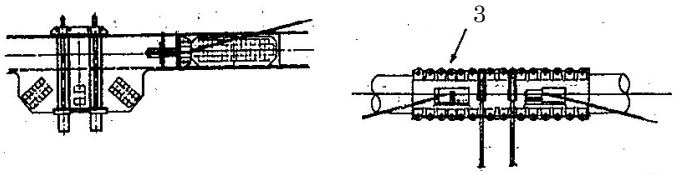

1	センターステイ	center stay
2	ステイロープ	stay rope
3	ステイバンド	stay band

Cable Anchor

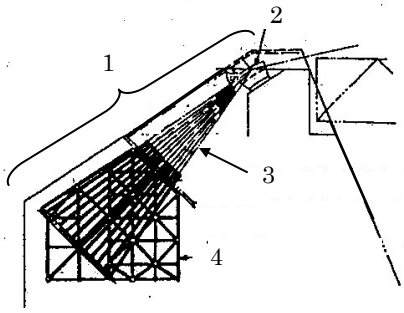

1	ケーブルアンカー部	cable anchor
2	スプレーサドル	splay saddle
3	ストランドケーブル	strand cable
4	アンカーフレーム	anchor frame

Girder

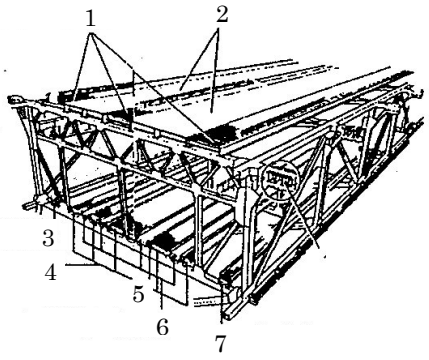

	桁	girder
1	オープングレーチング	open grating
2	鋼　床　版	steel floor
3	公団管理路	maintenance way of bridge authority
4	鉄道管理路	maintenance way of railroad
5	主構トラス	main truss
6	鉄道縦桁	stringer
7	ハンガーブラケット	hanger bracket

Expansion Joint

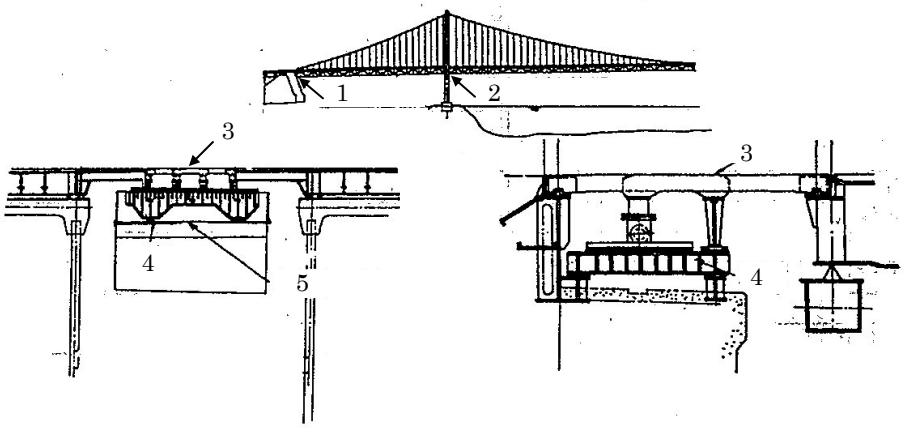

	伸縮装置	expansion joint
1	橋台部伸縮装置	expansion joint on anchorag
2	主塔部伸縮装置	expansion joint on main tower
3	櫛	comb
4	受桁	support girder
5	主塔水平材	horizontal member of main tower

Superstructure of Cable-stayed Bridge

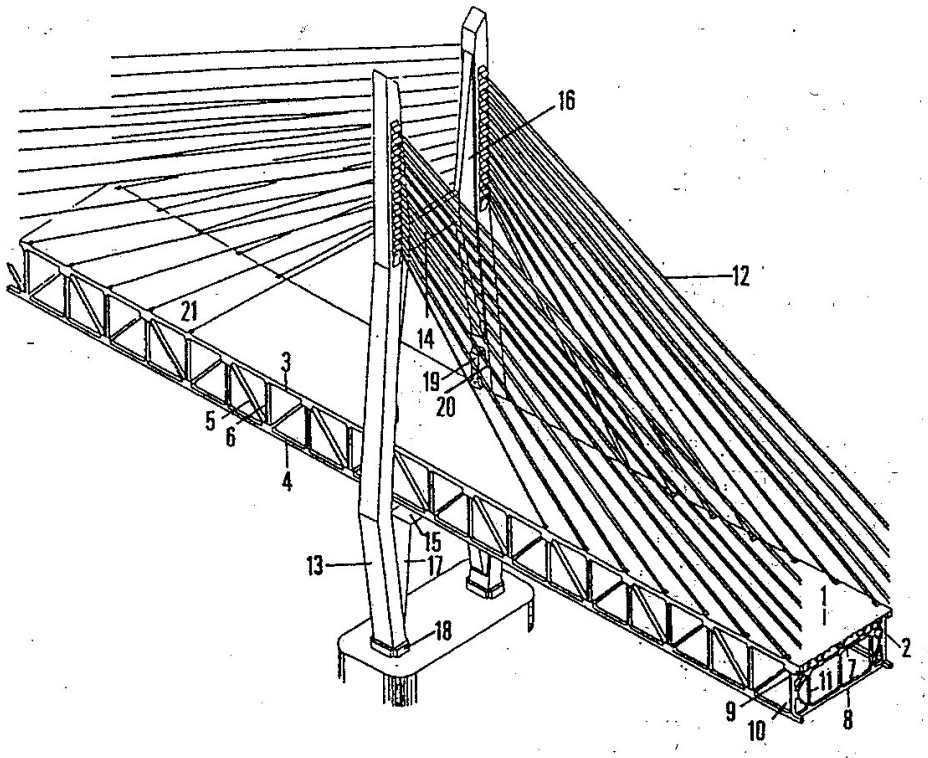

NO	斜張橋の主な部材名称	names of major members of cable-stayed bridge
1	デッキプレート	deck plate
2	縦　リ　ブ	vertical rib
3	上　弦　材	upper main chord
4	下　弦　材	lower main chord
5	斜　　材	diagonal member
6	垂　直　材	vertical member
7	中　弦　材	middle chord
8	下　弦　材	lower chord
9	小 組 斜 材	small diagonal member
10	斜　　材	diagonal member
11	垂　直　材	vertical member
12	ケーブル	cable
13	塔　　柱	tower shaft
14	上部水平材	upper horizontal member
15	下部水平材	lower horizontal member
16	上部ハンチ材	upper haunch member
17	下部ハンチ材	lower haunch member
18	塔　基　部	lower part of tower
19	タワーリンクブラケット	tower link bracket
20	タワーリンク	tower link
21	ケーブルカバー	cable cover

Cable System of Cable-stayed Bridge

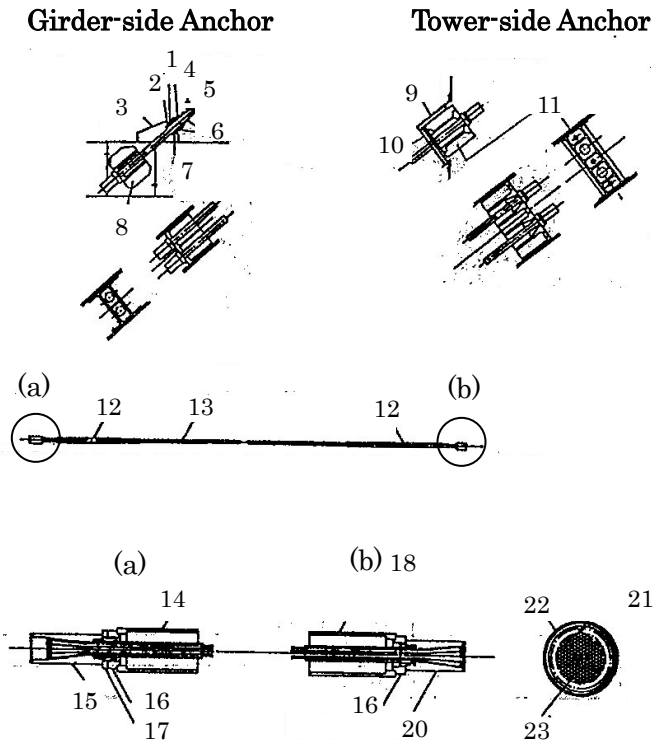

	斜張橋ケーブルシステム	cable-stayed bridge cable system
1	ゴムサポート	rubber support
2	充　填　材	grouting
3	ケーブルカバー	cable cover
4	止水カバーゴム	waterstop rubber cover
5	Ｐ　Ｅ　管	PE pipe
6	バ　ン　ド	band
7	鋼　　管	steel pipe
8	定着ブロック	fixing block
9	上面外板	upper outer plate
10	正面外板	front outer plate
11	定着ブロック	fixing block
12	オーバーラップＰＥ管	overlapping PE pipe
13	標準ＰＥ管	standard PE pipe
14	塔側定着ブロック	fixing block on tower
15	可動側ソケット	socket for adjustment side
16	座　　金	washer
17	シ　　ム	shim
18	固定側（主構側）アンカー	anchor of fixed side (bridge girder side)
19	桁側定着ブロック	fixing block of bridge girder
20	固定側ソケット	socket for fixing side
21	スペーサストランド	spacer strand
22	Ｐ　Ｅ　管	PE pipe
23	亜鉛メッキ鋼線７㎜	zinc galvanized wire ϕ 7㎜

Appendix B

THE AKASHI-KAIKYO BRIDGE

Design and Construction

of the World's longest Bridge

October, 1998

Honshu-Shikoku Bridge Authority

JAPAN

1. INTRODUCTION

On April 5, 1998, the Akashi-Kaikyo Bridge, the world's longest suspension bridge was completed over the Akashi-Kaikyo (straits) and opened to traffic. The Akashi-Kaikyo Bridge, which links Kobe City and Awajishima Island both in Hyogo Prefecture, has a main span of 1991 m and a total length of 3911 m and thus becomes the world's largest bridge, whose title had been hold by the Humber Bridge having a main span of 1410 m in England since 1981.

It was in May 1988 when real work at the site for the Akashi-Kaikyo Bridge began, and the work continued while overcoming many difficulty including an encounter with the Kobe Earthquake in January 1995. Also, engineers participating in the project have had to continue wide range of technical challenges in order to realize this enormous bridge. It is also noteworthy that no fatal accident was recorded in approximate 10 year's construction work.

The Akashi-Kaikyo Bridge has the following characteristics which will be discussed later into detail in Section 4.2;

① The bridge has a main span length of 1991 m and a total length of 3991 m (fraction in each length was due to the Kobe Earthquake) to meet such conditions as the waterway for navigation, the topography and geology at the straits, the land usage at both shores and so on.
② Two main piers were constructed as spread foundations by Laying-down caisson method at positions with great sea depth and strong tidal current. Also, big and deep foundations for the anchorages were constructed on reclaimed lands with various new technology. All foundations were well designed against severe earthquake with a newly established seismic design method. In addition, newly developed low heat type cement and concretes of various mix were used in actual construction.
③ The main towers made of steel reached 297 m above the sea level and were erected with high accuracy while oscillation by the wind was carefully suppressed.
④ The main cables, which were erected by Prefabricated Parallel Wires Strand method, were made of newly developed high strength galvanized wires, whose breaking strength was improved to 1800 N/mm^2.
⑤ The suspended structure was designed to be truss-stiffened, and its erection was carried out without disturbing heavy sea traffic reaching about 1400 ships per day. And, its aerodynamic stability was carefully checked in a newly constructed boundary layer large wind tunnel facility.

This report describes outline and the history of the Honshu-Shikoku Bridge Project, conditions as well as standards for the design of the Akashi-Kaikyo Bridge and the result , the construction of substructures as well as superstructures, related technical developments and facility for the bridge's operation and maintenance.

2. BACKGROUND AND HISTORY OF HONSHU-SHIKOKU BRIDGE PROJECT

2.1 Japanese Archipelago and Straits Crossings

The land of Japan consists of four main islands: Hokkaido, Honshu, Shikoku and Kyushu, from north to south. Transportation by ships and airplanes between those islands had been often interrupted from bad weathers as winds, waves or fogs. Also these mode required longer travel time and provided less capacity. To eliminate such inconveniences and to promote balanced development of the country, construction of fixed link to connect those islands has been in progress as shown in **Fig.-2.1.1**. Some crossings have already been completed and others are under construction. In addition, new strait-crossing projects are under investigation as will be mentioned in 2.1.4.

2.1.1 Kanmon Bridge & Tunnels

The Kanmon Straits between Honshu and Kyushu was connected by a railway tunnel in 1942, as the first strait crossing in Japan. A highway crossing with a suspension bridge was proposed by the Ministry of State of those days in 1937, however, it was changed to a tunnel plan due to opposition by the Japanese military. The construction of a highway tunnel began in 1941 but was suspended because of a defeat of the World War II. Finally, the tunnel was

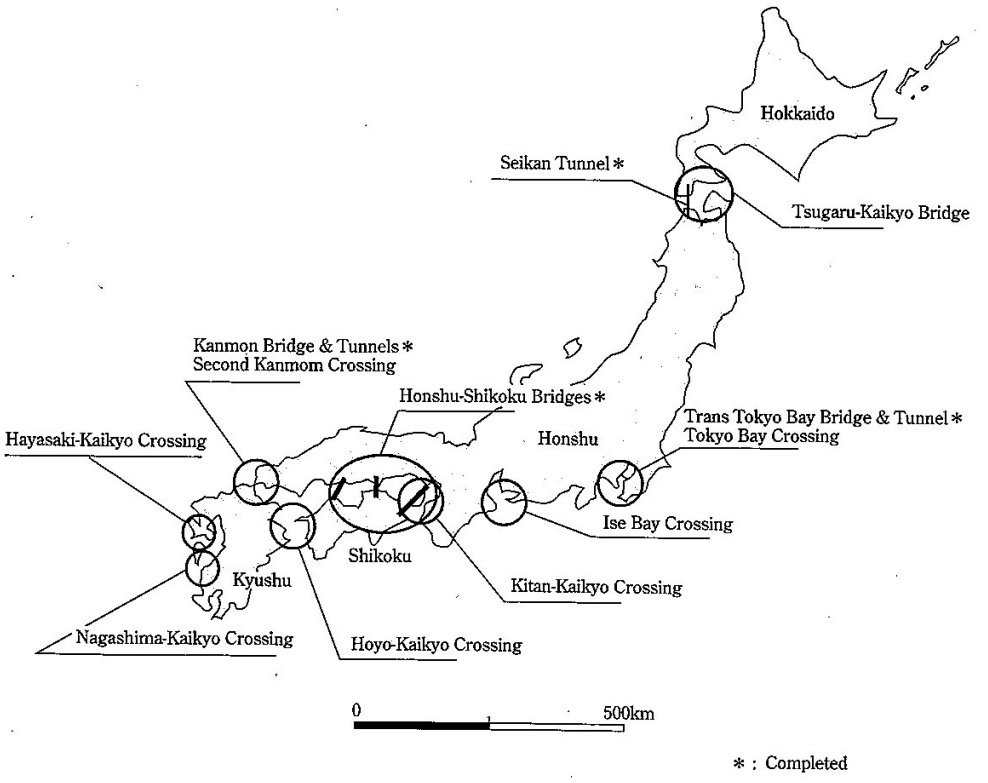

Fig- 2.1.1 Location of existing and future straits crossing

completed in 1958 for 2-lane highway. The tunnels played a significant role on restoration and development of the western part of Japan after the war.

Increasing demand realized the plan of a new additional crossing. The Kanmon Bridge, which is a part of the Kanmon Expressway and is a 6-lane highway suspension bridge, was constructed by the Japan Highway Public Corporation and completed in 1973. The New Kanmon Tunnel, which is a part of the Sanyo Shinkansen (bullet train) line connecting Osaka with Kyushu, was opened to traffic in 1975. The Kanmon Bridge was considered to be a pilot project for the Honshu-Shikoku Bridge Project from the viewpoint of long span bridge engineering.

2.1.2 Seikan Tunnel

The idea of connecting Hokkaido with Honshu by an underwater tunnel existed even before the World War II, and investigation of soil conditions under the Seikan Straits started in 1946, immediately after the war. After the Japan Railway Construction Public Corporation was founded in 1964, the corporation took over the investigation from the Japan National Railway (JNR) of those days and started digging of a survey tunnel. A decisive trigger of the tunnel construction was a sinking of the Toyamaru ferryboat by a typhoon in September of 1954, resulting in 1430 deaths. Peoples' strong demand to a stable and safe link accelerated movement toward construction of the tunnel.

The real construction work began in 1971. Though the construction encountered many difficulties, a main tunnel was pierced in March of 1985 and finally opened for service in March 13, 1988 as a part of the Tsugaru-Kaikyo Line for an ordinary railway. This year coincided with the year of completion of the Seto-Ohashi Bridges which will be discussed in 2.3 and 2.4.

2.1.3 Honshu-Shikoku Bridges

People have dreamed a fixed link between Honshu and Shikoku since old days like other strait crossings as the Kanmon and Seikan. A tragic accident that occurred in May of 1955, in which two ferries connecting Honshu and Shikoku collided each other and sank with 168 victims, undoubtedly identified need for the fixed link as nothing else could.

The JNR started a field investigation for the fixed crossing; at the same time, related local governments also started earnest researches. The Ministry of Construction (MOC) started another real investigation in 1959. After the Honshu-Shikoku Bridge Authority (HSBA) was founded in 1970 as a sole project execution body, the authority took over all these investigations previously done.

Though it was originally decided that three links between Honshu and Shikoku be simultaneously constructed, the construction was suspended due to the Energy Crisis in 1973. After the construction plan was changed, the construction of "one route and four bridges in the other two routes for local development" started. The construction of the rest of the routes and remaining bridges had been given permission one by one before the year of 1989.

The first bridge in the Honshu-Shikoku Bridges, the Ohmishima Bridge, was completed in 1979, and the first direct link between Honshu and Shikoku, the Seto-Ohashi Bridge, was put into service in 1988. The open of the Seto-Ohashi Bridge provided access of Shikoku not only to Honshu but also to the other two main islands of Japan.

2.1.4 Future projects

In order to strengthen transportation networks and meet future traffic demand in Japan, new strait crossings are under planning such as, from north to south, the Tsugaru-Kaikyo (straits) Bridge, the Tokyo Bay Crossing, the Ise Bay Crossing, the Kitan-Kaikyo Crossing, the Hoyo- Kaikyo Crossing, the Second Kanmon Crossing, the Hayasaki-Kaikyo Crossing and the Nagashima-Kaikyo Crossing. The MOC is now conducting investigations mainly on natural and socio-economic conditions for those projects while professional technical assistance has been made by the HSBA.

2.2 History of Honshu-Shikoku Bridge Project before 1970

A concept of a bridge across the Seto Inland Sea was evolved in the late 1880s, before modern civil engineering practices were established. In May of 1889, a local assemblyman Jinnojo Ohkubo, first advocated the idea of a bridge to cross the Inland Sea. In 1916, a senator Toranosuke Nakagawa, presented a bridge plan to a budget committee of the National Diet. These presentations were without any technical support, and nothing thus came of them. But, these facts illustrate that the concept of a bridge began to be discussed as early as the turn of this century.

A more definite idea was put forth by a civil engineer named Chujiro Haraguchi, a future mayor of Kobe City but in 1940 the project manager of a public works office of the Ministry of Interior then. He presented to a technical plan to build a bridge over the Naruto Straits between Awaji-shima Island and Shikoku, based on a study of the Golden Gate Bridge in the U.S.A. built in 1937. He intended in his plan to connect Tokushima in Shikoku with Kobe by the bridge and a ferry on the Akashi Straits, and to make it possible that people travel between two cities in two hours. Unfortunately, these preliminary activities for a bridge construction were halted by outbreak of the World War II.

The war brought devastation to Japan; nevertheless, the dream to bridge the Inland Sea had never disappeared. During those lean years, the Comprehensive National Land Development Law boosted local development which in turn accelerated the movement to link Honshu and Shikoku.

The tragic accident in May of 1955 strongly appealed the need for a bridge, because many of the 168 lives lost were boys and girls on excursion of junior high schools. That April, the former JNR just initiated a field investigation; at the same time, related local governments also started researches. By that time, Haraguchi as the mayor of Kobe City had progressed his idea to connect Tokushima with Kobe by bridges over the Akashi Straits as well as the Naruto Straits.

The MOC initiated investigation in 1959. Since that time, the MOC and JNR, which had been simultaneously conducting ongoing feasibility studies (the former was for highway and the latter was for railway), jointly entrusted their research results to the Japan Society of Civil Engineers (JSCE) so that the entire force of civil engineers in Japan could be mobilized. The JSCE thereupon established a technical committee to conduct extensive and comprehensive studies.

In 1967, JSCE issued a final report on the technical feasibility of the project and submitted it to both MOC and JNR. After evaluating the report, the MOC and the Ministry of Transport (MOT) jointly announced their official backing of the Honshu-Shikoku Bridge Project.

The Honshu-Shikoku Bridge Authority was then founded on July 1, 1970 based on a law as an execution body of the project. **Fig.-2.2.1** shows a concept and bridges of the Honshu-Shikoku Bridge Project.

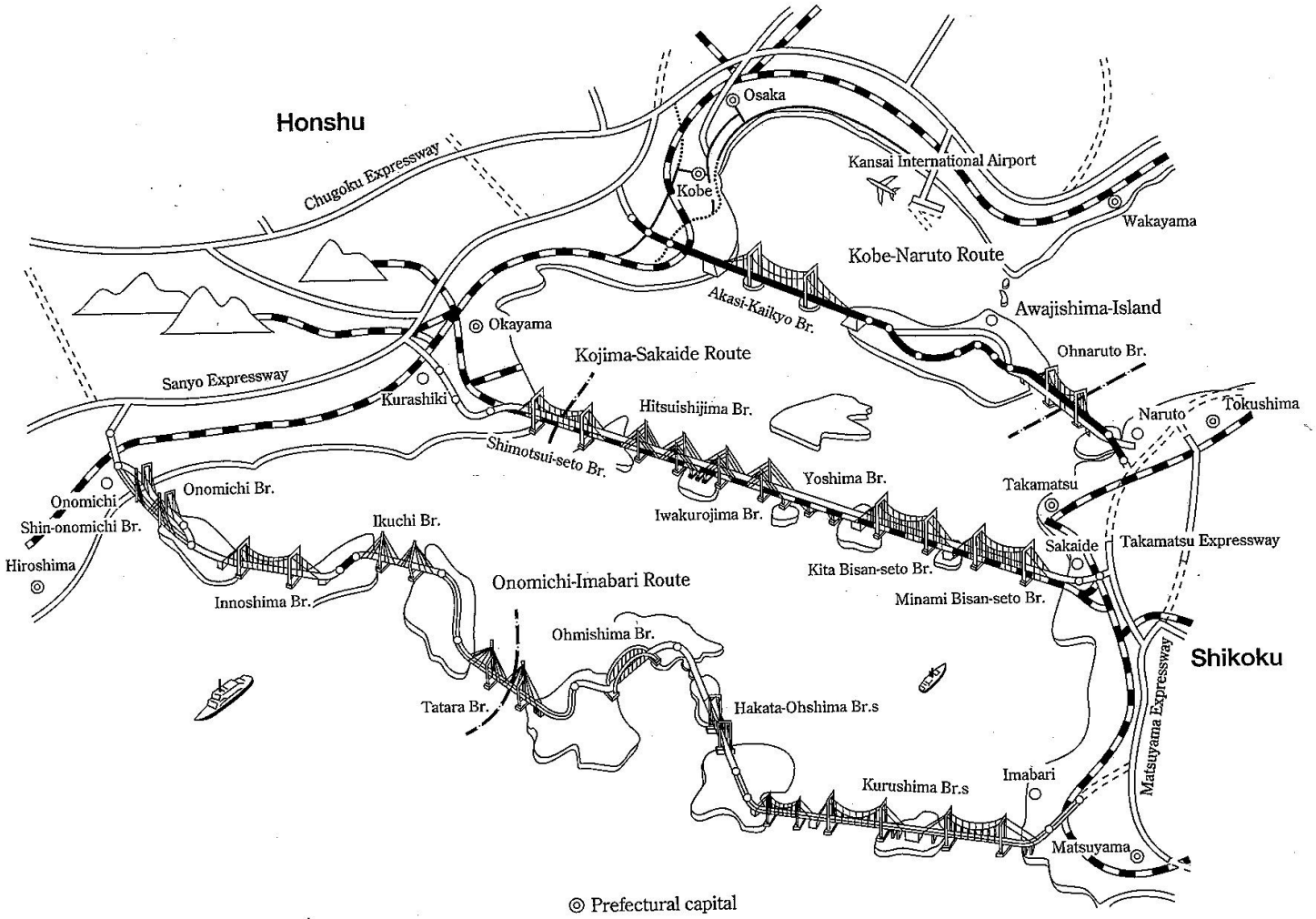

Fig-2.2.1 Three routes of Honshu-Shikoku Bridges

2.3 General Aspects of Honshu-Shikoku Bridge Project

2.3.1 Kobe-Naruto Route: Kobe-Awaji-Naruto Expressway

The Kobe-Naruto Route, the eastern route of the Honshu-Shikoku Bridge (HSB) Links, connects Kobe City in Hyogo Prefecture with Naruto City in Tokushima Prefecture, Shikoku via Awaji Island, and provides an 89 km, 4-lane (partially 6-lane) highway with a design speed of 100 km/h. About 45 km of the southern segment was opened to traffic in 1985, and the remaining northern segment including the Akashi-Kaikyo Bridge is now completed in 1998. This route greatly contributes to economic expansion of the area comprised of Osaka, Kobe, Awaji Island and eastern Shikoku.

Although the master plan previously determined by the national government intended to construct a double track bullet train line as well, its construction had been postponed by the government's policy with consideration of socio-economic situation of the railway sector in Japan. The Akashi-Kaikyo Bridge originally designed as a highway-railway combined bridge, therefore, was changed to be an only highway bridge.

This route contains two long span bridges: the Akashi-Kaikyo Bridge and the Ohnaruto Bridge.

The Akashi-Kaikyo Bridge, which spans the Akashi Straits between Kobe City and Awaji Island, is a 6-lane 3-span, 2-hinged truss-stiffened suspension bridge with a total length of 3911 m and a center span of 1991 m. Because of its record-breaking size, the Akashi-Kaikyo Bridge was carefully designed to withstand an earthquake with magnitude of 8.5 on the Richter scale as well as strong winds of 78 m/s, both which have approximately 150-year return period. The amount of materials used reached to 193,000 ton of steel for the superstructure and 1.4 million cubic meter of concrete for the substructure.

The Ohnaruto Bridge spanning the Naruto Straits known for famous eddying currents is a 3-span, 2-hinged truss-stiffened suspension bridge with a total length of 1629 m and a center span of 876 m. The bridge has a double decked structure with 6-lane on the upper level for vehicles and 2-track on the lower level for bullet trains in the future, however only four of the vehicle lanes are currently in use. A special feature of the bridge is that its foundations for the piers were constructed with multi-column foundation method in order to avoid adverse effect on the eddying currents. The bridge was designed to withstand winds of 88 m/s and earthquakes with the magnitude of 8 on the Richter scale.

2.3.2 Kojima-Sakaide Route: Seto-Chuo Expressway

The Kojima-Sakaide Route shown in **Fig.-2.3.1**,

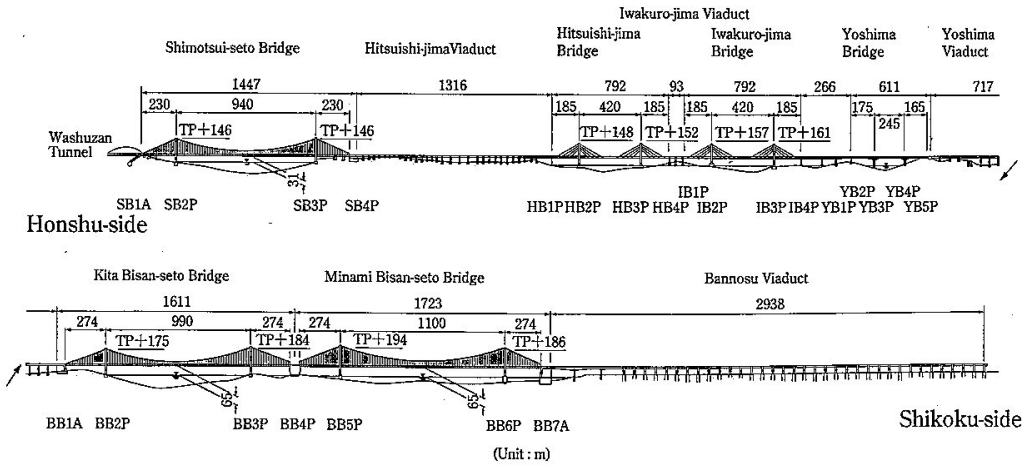

Fig.-2.3.1 Seto-Ohashi Bridges

the central route of the Honshu-Shikoku Bridge Links, connects Hayashima in Okayama Prefecture with Sakaide City in Kagawa Prefecture, Shikoku, and features a 37 km, 4-lane highway with a design speed of 100 km/h and a 32 km, 4-track railway (2 for ordinary and 2 for bullet trains). Currently, only two ordinary train tracks are in service and the bullet-train tracks are not installed yet.

This route was opened to traffic in April 10 of 1988 as the first direct link between Honshu and Shikoku. It contains six long span bridges: 3 suspension, 2 cable-stayed and one truss bridge over the 9.4 km straits, which are collectively known as the Seto-Ohashi Bridges.

Shimotsui-seto Bridge, which spans the Shimotsui Straits between Okayama Prefecture and the first island in Kagawa Prefectures, is a single-span truss-stiffened suspension bridge with cantilever extruded spans, a total length of 1447 m and a center span of 940 m. Its cable anchorage of the Honshu side was designed as a tunnel type anchorage embedded into the Wasyu Mountain in order not to affect aesthetics of the Seto Inland Sea National Park around the bridge. This bridge is also remembered as only one suspension bridge in the HSB project whose cables were erected with Aerial Spinning method.

Hitsuishi-jima Bridge and **Iwakuro-jima Bridge** are 3-span cable-stayed bridges with a continuos trussed girder, and each has a total length of 792 m and a center span of 420 m. Steel floor decks for vehicles were composite with the upper chord members of truss, thus sharing cable reaction. Couples of elastic supports were installed at each end of the girders to minimize seismic reactions.

Yoshima Bridge is a continuos truss bridge with a horizontal circular curve of a 1300 m radius and a S-shaped transition curve. The bridge is composed of 3 continuos spans (175 + 245 + 165 m) and 2 continuous spans (125 + 137 m). Quenched and tempered high strength steel HT780 (ultimate tensile strength = 780 N/mm^2) was used for the structural members.

Kita Bisan-seto Bridge and **Minami Bisan-seto Bridge** are both 3-span truss-stiffened suspension bridges with total lengths of 1611 m and 1723 m, and center spans of 990 m and 1100 m, respectively. Both two bridges have a continuous girder designed to raise runnability of the high speed trains. These bridges also required difficult construction of deep and large underwater foundations whose deepest bottom reached to 50 m below the water level. The cables for both bridges share a central anchorage.

2.3.3 Onomichi-Imabari Route: Nishi-seto Expressway

The Onomichi-Imabari Route, which includes ten long span bridges linking nine relatively large islands, is a 60 km highway from Onomichi City, Hiroshima Prefecture to Imabari City, Ehime Prefecture in Shikoku. Construction work on this route began in 1975.

The Ohmishima Bridge, the Hakata-Ohshima Bridges, the Ikuchi Bridge had been already completed by 1991, and 26 km in the total length of the highway has been opened to traffic. The remaining Tatara Bridge and Kurushima Bridges are now under construction and expected for completion in the spring of 1999, which fact means that this route will be also opened.

The sea and islands through which the Onomichi-Imabari Route runs form one of the most beautiful national parks with various natural treasures, scenic archipelagoes, a mild climate, and a valuable cultural heritage. This environment has been taken fully into consideration during the bridge planning and construction. Unlike the other routes, the bridges of this route provide a pedestrian and bicycle pass.

Onomichi Bridge and **Shin-Onomichi Bridge** are both steel cable-stayed bridges with the same center span of 215 m. The Onomichi Bridge, the first cable-stayed bridge with a center span exceeding 200 m in Japan, was constructed by the Japan Highway Public Corporation in 1968 and is now operated by HSBA. And, the Shin(New)-Onomichi Bridge is going to add additional 4 lanes for long distance rapid traffic to the existing 2-lane of the Onomichi Bridge, which has served mainly for local traffic.

Innoshima Bridge is a 3-span 2-hinged truss-stiffened suspension bridge with a center span of 770 m. This bridge, the first suspension bridge by HSBA, used cable strands each consisting of 127

wires to decrease the construction period as well as the size of the anchorage and utilized the steel decks to reduce the dead weight. Both were first challenge in large scale suspension bridges in Japan.

Ikuchi Bridge is a 3-span cable-stayed bridge with a center span of 490 m, which used to be the world's longest cable-stayed bridge. This bridge adopted steel girder for the main span and concrete girders for both side spans to compensate unbalanced main/side span length.

Tatara Bridge is a 3-span cable-stayed bridge with the world's longest center span of 890 m. Its box girder mainly consists of steel except end portions of both side spans which are PC boxes. The reversed Y-shaped towers are selected from the aesthetic point of view, and dimpled-surface stay cables are first adopted to prevent rain-wind-induced vibration.

Ohmishima Bridge is a single span 2-hinged steel solid rib arch bridge with a span of 297 m, and the first long span bridge constructed by HSBA.

Hakata-Ohshima Bridges consist of 2 consecutive bridges: the Hakata Bridge, a steel box girder bridge and the Ohshima Bridge, a single span box girder suspension bridge with a center span of 560 m, to which a box section was adopted for the first time in Japan for long span suspension bridges.

Kurushima Bridges consist of three suspension bridges (each center span, 600 m, 1020 m and 1030 m); they are consecutively arranged via two common anchorages. The bridges have streamlined box girders and are being constructed over rapid tide of the Kurushima straits.

2.4 History of Honshu-Shikoku Bridge Project after 1970

2.4.1 Preliminary investigation

The Honshu-Shikoku Bridge Authority established in July of 1970 made investigation on natural conditions and economic studies for HSB Project under the orders from MOC and MOT.

In 1970 and 1971, a meteorological observation towers were installed, and geological as well as soil conditions were investigated. Based on these data, preliminary design for determination of bridge type, span length, etc. and planning of construction method were made. In 1972, an approximate cost estimation regarding the preliminary design and socio-economic impact study were carried out. At the same time, investigations on design standard were continued based on the previous study done before 1970.

(1) Wind resistant design of long span suspension bridges

Various wind tunnel tests up to a 2000 m span length highway-railway combined suspension bridge were carried out, and its aerodynamic stability was investigated. Besides these, HSBA constructed a field test facility at a windy beach of the Boso Peninsular which could accommodate a large scale (1/10) model of a trussed girder in order to verify influence of natural gusty wind as well as Reynold's number on aerodynamic response, etc., and then refined the wind resistant design standard.

(2) Seismic design of long span suspension bridges

A more rational seismic design standard: a seismic design method for rigid foundations and a stability analysis method, were investigated with consideration that the foundations became inevitably huge in their size and were supported with relatively sound rock.

(3) Runnability of train on suspension bridges

When trains run on a suspension bridge, problems to be solved were such as running stability of trains on a flexible suspension bridge, angular bent

in the vertical plane and expansion or contraction of rails at both ends of the bridge. Runnability was investigated to determine how much angular bent the train could run over safely and smoothly. Model experiments and full scaled test runs were carried out on the to-be-abandoned Karikachi Line in Hokkaido as well as on the Sanyo Shinkansen Line before its official opening, and it was concluded that good running stability up to the speeds of 160 km/h for bullet trains and 120 km/h for ordinary trains was secured when the angular bent was restricted below 1/100. Rail joints absorbing up to plus-minus 60 cm of the expansion or contraction were also developed.

(4) Investigation of large scale underwater foundations

A design standard for huge underwater substructure was developed based on both large scale experiments and previously obtained results. Workability and quality of underwater concrete was confirmed through real sized experimental casting in the field and laboratory.

(5) Development of working platform on the sea

Working platforms, on which boring and the other works were to be done, were developed at first for the shallow and low speed current sea. For the case of the Akashi-Kaikyo Bridge, design and fabrication of a large scale working platform, which enabled to work in the deep (45 m) and fast current (4.5 m/s) sea, was begun.

(6) Seabed excavation method

Seabed excavating experiments to confirm efficiency of a gravity type and a rotary type excavation machines were carried out in the Naruto Straits and the sea near Kojima. Also, safe and harmless method for underwater blasting of granite was investigated.

(7) Navigation safety facility

Since the Honshu-Shikoku Bridges were planned in straits where many ships traveled, HSBA trusted navigation safety affairs to a committee, which studied circumstances of the navigation after bridging, ship collision protection facilities and bridge lighting and so on.

(8) Socio-economic study

Economic studies were carried out in order to estimate the traffic demand between Honshu and Shikoku, repayment conditions of the project and the socio-economic impact on the related areas. The HSBA took over the results of economic study and a traffic-volume estimation model between Honshu and Shikoku (Hon-Shi Model) from the MOC and MOT, then improved the model and the demand estimation. In addition, the traffic demand of inter-islands was analyzed with another model. Long term and short term socio-economic impacts were evaluated from the increase amount of regional production incomes by the project and also from the increase amount of productivity as well as income due to the project investment.

2.4.2 Preparation for construction and Energy Crisis

Preparation for commencement of the construction work was advanced while investigation and design were going on. The HSBA finally decided the commencement day to be November 25 of 1973.

But, the Energy Crisis, which was a sudden raising of the price of crude oil as a result of outbreak of the 4th Middle East War in October of 1973, brought skyrocketing prices in Japan. Consequently, the Honshu-Shikoku Bridge Project was suspended just 5 days before the scheduled commencement day as one of the policies taken by the Japanese Government for restraining consumer demand.

During this postponement, HSBA prepared for resumption of construction by developing new technology, re-studying of the design and construction methods and so on.

2.4.3 Toward resumption of construction

The HSBA had to wait for the resumption of construction until 1975. By that time, skyrocketing prices had become quiet. Local people and business sector began to insist upon the resumption of construction of the Honshu-Shikoku Bridge Project.

In these circumstances, it seemed appropriate to construct one route and a few bridges for local

development at first rather than to build all the three routes simultaneously. Following this idea, the Japanese Government finally decided in August of 1975 that the construction of one route, the Kojima-Sakaide Route, and three bridges: the Ohnaruto Bridge, the Innoshima Bridge and the Ohmishima Bridge be carried out.

After the preparation, construction of the Ohmishima Bridge started on December 21, 1975 as the first bridge of the project. Construction of the Ohnaruto Bridge and the Innoshima Bridge followed on July 2, 1976 and January 8, 1977, respectively.

The commencement of construction of the Kojima-Sakaide Route was approved in April of 1977 on condition that environmental assessment be carried out, because the route was located in the Seto-Inland Sea National Park. After carrying out environmental assessment, HSBA started the construction of the route on October 10, 1978.

Being added to the one route and three bridges, the Hakata-Ohshima Bridges were also decided to start the construction in January of 1979 based on the agreement among MOC, MOT and the National Land Agency. The ground was broken on March 21, 1981.

2.4.4 After one route and four bridges

After the Kojima-Sakaide Route and four bridges including the Hakata-Ohshima Bridges were completed by the year of 1988, the Honshu-Shikoku Bridge Project entered the second phase. The Akashi-Kaikyo Bridge, the Shin-Onomichi Bridge, the Ikuchi Bridge, the Tatara Bridge and the Kurushima Bridges, which were left at that time, were approved for construction. This means that the government decided to complete all the three routes as being previously determined.

The Akashi-Kaikyo Bridge, which was originally planned as a highway-railway combined bridge, was changed to a highway bridge by considering general situation of a bullet train network plan in Shikoku, and the official ground breaking ceremony was held in April of 1986 (real work began in May 1988). The ground for the Ikuchi Bridge was broken in 1986, and the bridge was completed in 1991.

The other bridges, the Tatara Bridge and the Kurushima Bridges, were approved for construction in 1990 and 1988, respectively. Both of them will be completed at the spring time in 1999. The Shin-Onomichi Bridge next to the Onomichi Bridge was decided for construction in 1993 and will be completed in 1999.

3. DESIGN CONDITIONS OF AKASHI-KAIKYO BRIDGE

3.1 Natural Conditions

3.1.1 Topography

The Akashi-Kaikyo is one of the famous straits in Japan and located between Kobe City on Honshu and Awaji-shima Island. The straits, linking the Osaka Bay and Harima-nada (nada is a vast open sea area in the Seto Inland Sea) has the minimum width of about 4 km, to which point the bridge has been constructed.

Topography beneath the straits is very complicated, and there are different topographical features between the 2P (Kobe-side pier) and 3P (Awaji-side pier). The 2P site showed similar to a marine terrace and a comparatively flat seabed while the 3P site showed complicated topographical characteristics with a steep rise and fall. The maximum water depth in the central part of the strait reaches approximately 110 m, while the Harima-nada in the west to the strait and the Osaka Bay in the east to the strait were 20 m to 30 m deep.

Both hinterlands are rather hilly, and narrow flat terrain is developed along the shore lines.

3.1.2 Wind

Since long span bridges are flexible, they require special consideration for wind action at the design stage. In addition, the Honshu-Shikoku Bridges are located in an area that frequently sustains typhoons. Therefore, it was required to conduct careful survey and research on wind characteristics at the bridge site.

An observation tower was constructed near the bridge site, and wind data observation began in 1964 for the purpose of establishing design criteria of the Akashi-Kaikyo Bridge. Twenty year long data (1964 to 1984) were collected, and mean wind speed, maximum wind speed, wind rose, turbulence intensity and scale, angle of attack, etc. were analyzed.

Fig.- 3.1.1 shows yearly maximum wind speed at 80 m above the sea level at the observation tower. Both two large values in 1964 and 1965 were recorded during typhoons. A basic wind speed, which is defined as a 10 minute averaged wind speed at 10 m above the sea level and has a 150-year return period, was estimated to be at 46 m/s based on extreme value analysis with the collected data.

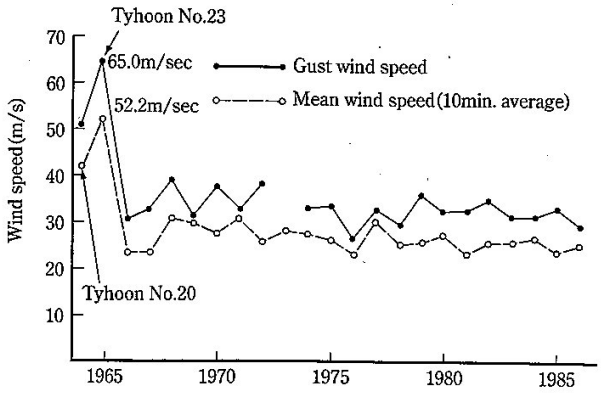

Fig.-3.1.1 Yearly maximum wind speed at Tarumi Observation Tower

3.1.3 Earthquake

Alike typhoons, earthquakes are likely to occur in Japan. Careful consideration for earthquakes is also required at the design stage of long span bridges. Historical earthquakes having a magnitude of more than 6 and a distance of less than 300 km were recorded as will be shown in Fig.-4.1.3.

Earthquakes that occurred in and around Japan are of three different types, some of which were disastrous. The types are classified with the area where earthquakes occurred; first, earthquakes along or off the coast of the Pacific Ocean; second, earthquakes in inland; and third, earthquakes off the coast of the Japan Sea. One of the features on the first type is of very large magnitude.

The design acceleration at the site was calculated by an attenuation equation by distance based on the records. Seismotectonic studies confirmed the existence of northeast-southwest faults in the area of the bridge and also indicated that there was no concrete evidence for the faults to move in the Quaternary period.

In earthquake analysis of long span bridges, phase lag may have a significant influence on the dynamic response. Therefore, an array observation system has been arranged around the bridge site to measure the phase lag.

The standard seismic motion for the design of the Akashi-Kaikyo Bridge was based on two types of response acceleration spectra as will be mentioned in 4.1.2 (2).

3.1.4 Marine conditions

The maximum current speeds at the 2P and 3P sites are very fast and approximately 3 to 3.5 m/s and 3.5 to 4 m/s, respectively. An observation near the site showed that mean wave height was 51.4 cm (standard deviation 21.8 cm) and the maximum wave height was recorded approximately 6 m during a typhoon.

Tidal level change was observed to be about 1 m.

3.1.5 Geological Conditions

The seabed consists of recent and upper Pleistocene deposits, Akashi Formation of the Pleistocene to Pliocene, Kobe Formation of the Miocene, and granite as shown in **Fig.- 3.1.2.**

The Akashi Formation is composed of semi-cemented gravel and sand, and contains a lot of decayed gravel. The Kobe Formation is made of weakly cemented soft rock with complicated alteration of thin sandstone and mud-stone layers.

Bearing layer is different at each foundation. Namely, 1A (Kobe-side anchorage) and 3P are founded on the Kobe Formation, and 2P is put on the Akashi Formation. On the other hand, 4A (Awaji-side anchorage) is designed to be rested upon weathered granite.

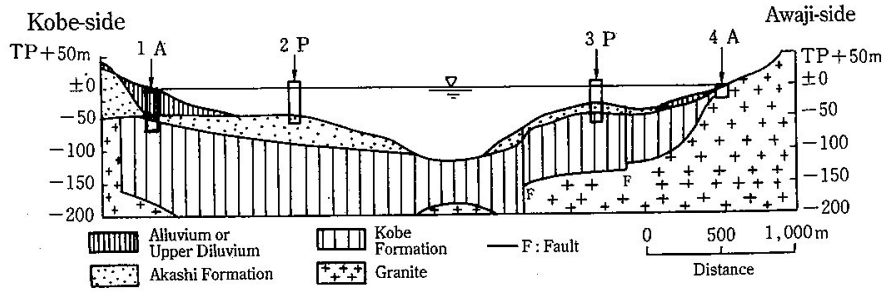

Fig.-3.1.2 Geological conditions beneath Akashi-Kaikyo Bridge

3.2 Social and Environmental Conditions

The Akashi Straits is designated as a statutory waterway with width of 1500 m where approximately 1400 ships pass daily. Eighty to ninety percent of those ships travel in the direction of east and west, which is perpendicular to the bridge axis. Fishing has been prosperous since old days.

The clearance under the deck was decided to be 65 m based on a report of the Port Council of the Ministry of Transportation.

The land usage in Kobe-side is largely different from that in Awaji-side. Kobe area is urban and densely populated while Awaji area is rural and less populated (see Photos-1, 2, 7, 10, 11, 12 and 17). Alignment of the route was decided with consideration of such conditions.

4. DESIGN

4.1 Outline of Design Standard

4.1.1 Wind resistant design

Because of its record breaking center span length, the Akashi-Kaikyo Bridge is a extremely flexible structure with low natural frequency (horizontal mode = 0.038 Hz, vertical mode = 0.064 Hz and torsional node = 0.140 Hz). This means that requirement for the wind resistant design is very demanding as shown in **Fig.-4.1.1**. Accordingly, the wind resistant design standard for the Akashi-Kaikyo Bridge was exclusively established in 1990. In this section, main contents of the standard is outlined.

(1) Flow of wind resistant design

Fig.-4.1.2 shows the flow of wind resistant design specified in the standard.

(2) Wind conditions to be considered

[Design wind speed]

As one of the important wind conditions to be considered in the design, basic wind speed is clarified in the standard. Based on field measurement data and wind tunnel test which was conducted to evaluate the effect of topography, the basic wind speed for this bridge was determined to be 46 m/s as being stated in 3.1.2.

In wind resistant design, vertical profile of wind speed has to be taken into account for determination of the design wind speed as being given in the next formula.

$U_Z = (Z/10)^{1/8} \cdot U_{10}$

where,

U_Z : design wind speed at the height of Z m,

and U_{10} : basic wind speed (46 m/s)

[Angle of Attack]

Another important wind condition is angle of attack. In the standard, angle of attack to be consid-

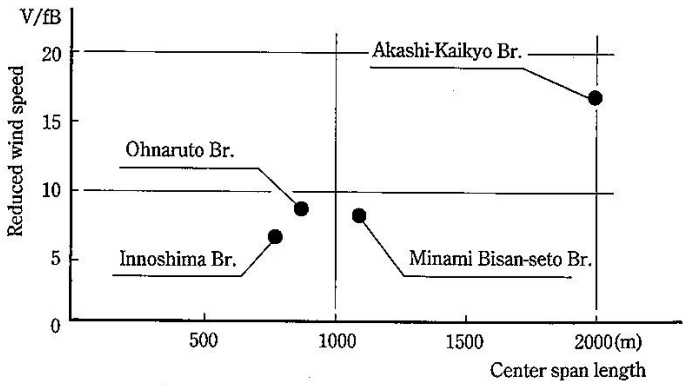

Note. V ··· Required flutter wind speed (m/s)
f ··· Torsional natural frequency (Hz)
B ··· Deck width (m)

Fig.-4.1.1 Required level of aerodynamic stability

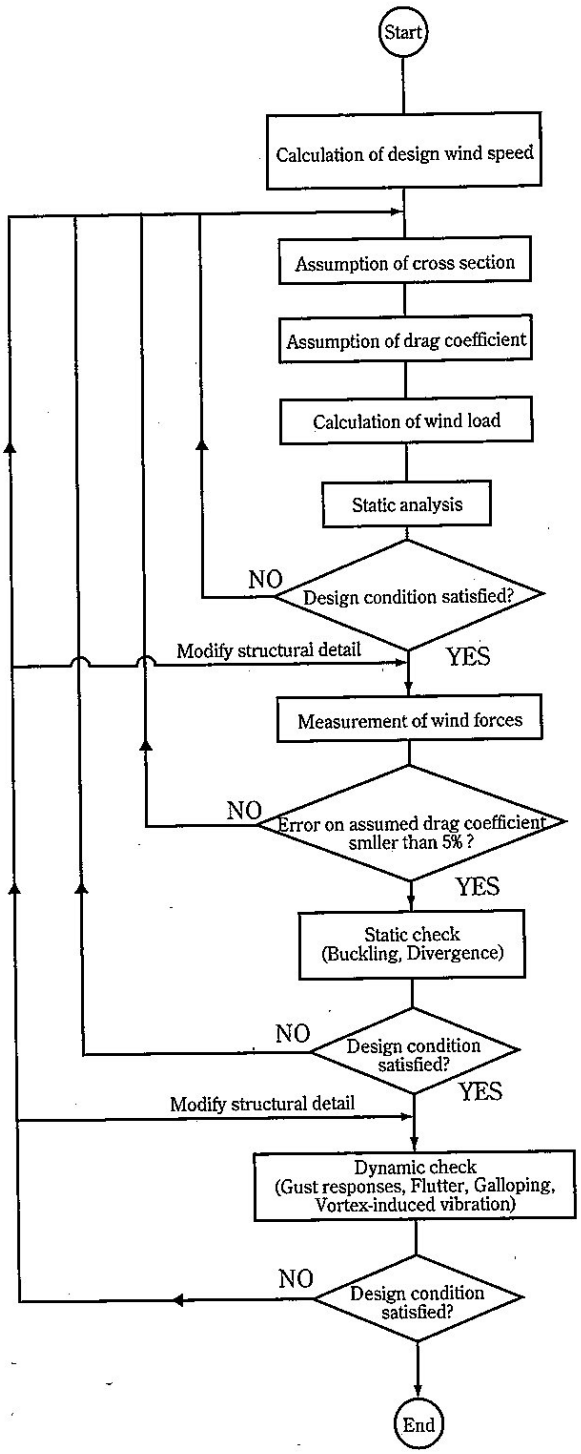

Fig.-4.1.2 Flow of wind resistant design

ered is specified as -3 to +3 degree. This range of angle of attack is determined by consideration of following three components, which can cause angle of attack to the natural wind.

- average inclination of the wind at the site
- static deformation of bridge girder due to wind load, and
- fluctuation in angle of attack by vertical turbulence.

[Turbulence intensity]

In evaluating the effect of gust response, turbulence intensity to be considered at the height of girder (80 m above the sea surface) is clarified as 10% for the main stream direction.

(3) Static design

Static design is to be conducted with the wind load given in the next formula.

$P_d = \mu_2 \cdot \rho \cdot U_z^2 \cdot C_d \cdot A_n/2$

where P_d : wind load
μ_2 : modification factor for gust responses (1.55)
ρ : air density
C_d : drag coefficient, and
A_n : profile area.

Important feature of this wind load is that effect of gust response is included in it. The factor was determined based on gust response analysis on preliminary design result of the Akashi-Kaikyo Bridge. In conducting the static wind resistant design, allowable stress can be increased by 1.50 for the girder as well as cable and 1.40 for the tower.

(4) Dynamic design

[Structural damping]

In conducting dynamic wind resistant design, structural damping have to be assumed. In the standard, they are given in **Table-4.1.1**.

These damping are determined from vibration test results carried out on existing long span suspension bridges.

[Gust responses]

As explained above, effect of gust response is to be considered as wind load. However, the modification factor 1.55 used in the formula is a conclusion of gust response analysis on a preliminary design result. It is accordingly required to conduct gust response analysis for final design, in which 3 components of wind load: drag, lift and moment, shall be taken into account. If the calculated stress exceed allowable stress more than 5 %, modification of the design must be done.

[Flutter, galloping]

As the amplitude of flutter and galloping abruptly increases when wind speed becomes high enough, it is required that the critical wind speed for flutter and galloping should not be less than the reference wind speed, which is to be calculated from the design wind speed by the following formula. As shown in the formula, a safety factor of 1.2 is introduced, and effect of fluctuation of wind speed over the 10 minutes averaged speed is taken into account as μ_F. This effect is evaluated on assumption that the flutter or galloping develops to destroy the bridge within 30 seconds.

$U_r = 1.2 \cdot \mu_F \cdot U_z$

where, U_r : reference wind speed for flutter and galloping, and
μ_F : modification factor for fluctuation of wind speed = 1.08

[Vortex induced vibration]

Effect of vortex induced vibration have to be evaluated from the viewpoint of users' comfort as well as safety of the structure against fatigue damage. In the standard, intensity of turbulence, which usually decrease the amplitude of vortex induced vibration, is clarified to be 5% for evaluation of effect of the vibration.

Table-4.1.1 Structural damping (logarithmic decrement)

	Bending mode	Torsional mode
Girder (Truss type)	0.03	0.02
Tower (Completed stage)	0.02	0.02
Tower (Free-standing stage)	0.01	0.01

[Wind tunnel test]

This standard is prepared on the premise that 2-dimensional rigid model wind tunnel tests are mainly to be conducted to evaluate the dynamic effect of wind. However, wind tunnel test with full aero-elastic model and various numerical analyses were also carried out for the bridge as will be mentioned in Section 6.1

4.1.2 Seismic design

(1) General

Conventional seismic design standard for Honshu-Shikoku Bridges established in March 1977 was mainly applicable to the foundations supported with granite or Izumi Formation, which were hard and old rock before the Oligocene or Cretaceous.

In this standard by which Ohnaruto Bridge and Seto-Ohashi Bridges were designed, the spectrum analysis with rigid model in 2-degree of freedom was specified to be done on the following conditions;

① ground spring was assumed to be a static one determined from plate bearing test,
② damping coefficient between the ground and foundation was constantly assumed to be 10 %, and
③ input seismic excitation to the analysis model was defined at the surface of bearing layer, but this was decided without consideration of the presence of foundation itself.

However in the case of Akashi-Kaikyo Bridge in which huge foundations were to be constructed upon softer and younger layers, a new seismic design standard had to be formed, because non-linearity of the bearing layer as well as dynamic interaction between the ground and foundation were judged to be not negligible. In the new standard, basic procedure is the rigid model in 2-degree of freedom as used to be, and stability check by time history analysis with FEM model is also requested.

(2) Input seismic excitation

Fig.-4.1.3 shows the distribution of earthquake epicenters and their magnitudes around the Akashi straits in the past 100 years. It can be seen from the

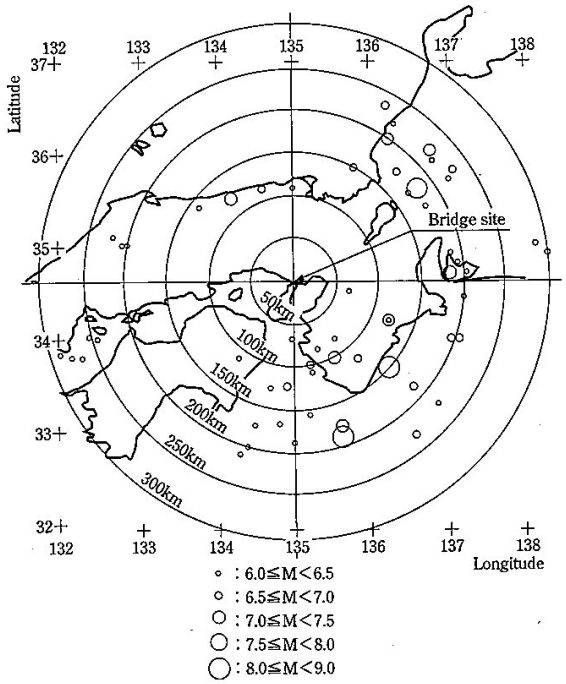

Fig.-4.1.3 Earthquake epicenters and magnitudes(1885-1979)

figure that several earthquakes with magnitude of 8.0 class in Richter scale occurred off the Pacific Coast (about 150 km south to the site) and that many earthquakes of magnitude 6 to 7 happened elsewhere in the region.

Assuming that the top surface of the Kobe Formation is exposed, the spectrum obtained as an envelope of the following two acceleration response spectra is defined as standard acceleration response spectrum (damping coefficient : h=0.05) which is as shown in **Fig.-4.1.4**.

① one from large scale plates boundary type earthquake: the acceleration response spectrum that is expected to give an influence to the construction site, and its magnitude and epicenter distance is assumed to be 8.5 in Richter scale and 150 km, and

② one calculated by statistical theory from historically recorded earthquakes which exceed magnitude 6.0 in Richter scale and had occurred during 1885 to 1979 within a radius of 300 km from the construction site. The acceleration response spectrum of this has a return period of 150 years.

Also in ground response analysis ("SHAKE") which will be mentioned later, a strong seismic motion wave recorded at Kaihoku Bridge by the Miyagi Prefecture Off-coast Earthquake in 1978 (maximum acceleration = 394 gal) is to be basically used.

(3) Seismic design procedure

Fig.-4.1.5 gives the flow chart of the seismic design procedure for the foundations specified in the standard for the Akashi-Kaikyo Bridge, and the procedure is based on the following concept.

① The response of the foundations is to be obtained through the response spectrum method with corresponding 2-degree of freedom system, which models both rigid foundation and ground springs to express the oscillation in rocking mode as well as swaying mode.

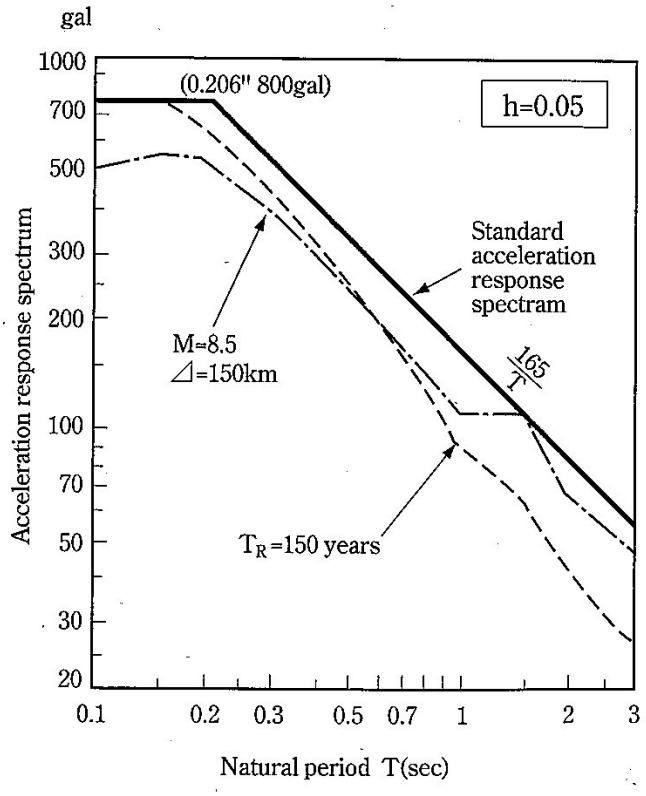

Fig.-4.1.4 Standard acceleration response spectrum

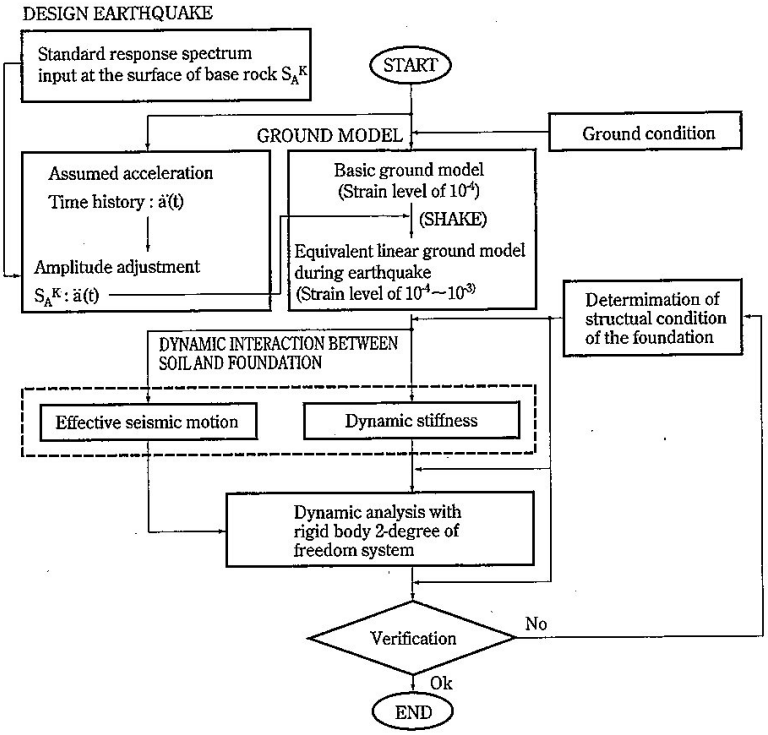

Fig.-4.1.5 Procedure for seismic design of Akashi-Kaiyo Bridge foundations

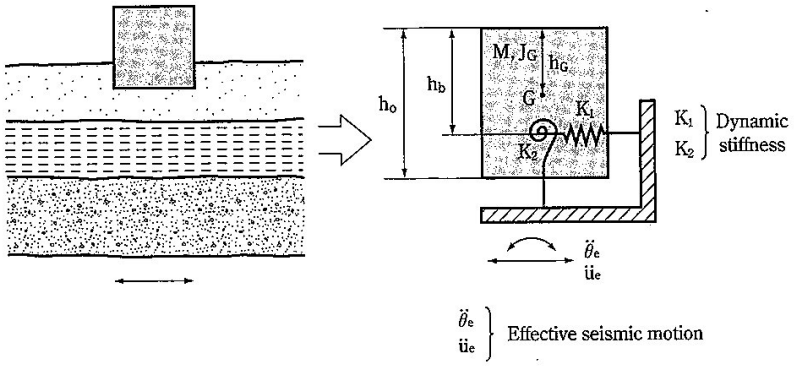

Fig.-4.1.6 Dymamic response analysis model

② The modes mentioned in ① should be established with consideration of dynamic interaction between the foundation and the ground (see **Fig.-4.1.6**), and

③ In order to evaluate the dynamic interaction, local ground condition around the foundations should be precisely taken into account.

(4) Dynamic interaction between foundation and ground

Recent progress in dynamic soil-structure interaction research shows that the interaction effect is

composed of two effects, i.e., effective seismic motion and dynamic stiffness (Fig.- 4.1.6).

Effective seismic motion, sometimes called the kinematic interaction effect, is defined as the response of massless foundations exposed to seismic excitation. The response of massless foundation against any seismic excitation is different from what is obtained on condition that no foundation exists on a free surface, because the presence of the foundation restricts the seismic excitation.

The response of a large scale foundation which is embedded into the ground is not only affected by vibration properties of the geological layer but differs depending on the configuration of the contact surface between the foundation and the ground because the foundation constraints the vibration of the ground. Accordingly, the ground response analysis: "SHAKE" is to be done with consideration of geological composition, their property such as S-wave speed, unit weight and dynamic Poisson's ratio and level of the strain generated beneath the foundation at the time of earthquake, in order to decide the effective seismic motion which is the input excitation in seismic design of the Akashi-Kaikyo Bridge.

On the other hand, the dynamic stiffness is introduced for consideration of effect of dispersion of vibration energy of the foundation into the ground, in the stead of conventional stiffness in which the ground spring is supposed to be a static one. In the dynamic stiffness, coupled oscillation between the foundation and the ground is taken into account, and the stiffness becomes variable by the frequency of oscillation.

(5) Stability check (verification)

The results of rigid model in 2-degree of freedom analysis is to be checked from the viewpoints of bearing, overturn and slide. In this, the shear strength of ground (C and ϕ) is to be obtained from CU (Consolidated but Undrained) test for the Kobe Formation and Akashi Formation because the loading speed during earthquake is too fast to disperse the pore water pressure. Those for the granite is to be based on CD (Consolidated and Drained) test because the pore water pressure in the granite is not originally high.

In the check of bearing, the response spectrum analysis gives the largest values for vertical force, horizontal force and moment all which must change their direction and magnitude in actual seismic motion, so FEM time history analysis is to be done for considering this point.

As for the check of overturn, stability would be confirmed if the response velocity of foundation due to earthquake was smaller than the potential energy expressed in terms of the energy.

The check of slide is to be done by ascertaining whether the safety factor is higher than 1.2 or whether accumulated slippage which is assumed to occur during the slippage safety factor being lower than 1.2 remains in harmless range to the bridge.

(5) Seismic design for superstructure

Because the natural periods of superstructure is very long: 16 sec. and 26 sec. in the vertical and horizontal direction, respectively, seismic input having long period components should be considered. Also, phase lag is to be taken into consideration because the distance between two anchorages reaches about 4 km.

The following three conditions were thus set in the design earthquake input for the time history analysis of the superstructure.

① Effective seismic motion acting separately to each foundation which has comparatively short period component.

② Seismic wave obtained by adjusting the amplitude of the recorded motion of the Tokachi Offshore Earthquake which has comparatively long period component. Amplitude adjustment is done so as to agree the response spectrum of the earthquake with that as shown in Fig.-4.1.4.

③ Seismic wave as same as ② but with consideration of the time lag for each foundations.

4.1.3 Design live load

Because the Akashi-Kaikyo Bridge is a part of the nationwide expressway system, its design live load which is specified as B-loading in "Design Specifications for Highway Bridges" issued by the Ministry of Construction, is basically same as the other bridges. The B-loading is determined mainly for bridges over which large vehicles weighing 25

ton (250 KN) frequently pass, and this contains TT-43 loading (trailer truck having the total weight of 43 ton and 4 axes) previously used for design of bridges in important network.

The design live load in Japan is classified into "floor loading (T-loading)" and "main structure loading (L-loading)"; the former is used in design of the deck and floor system whose influence line is short while the latter is applied to the main structure of a bridge such as main girder, truss, cable, tower and so on which have very wide influence line. And, the L-loading is often composed of a line load which is to be given to a limited area and distributing load which is to be given on wide area of the bridge.

Fig.-4.1.7 and **Table-4.1.2** show an image of the design live load for highway bridges in Japan as well as concrete value of the B-loading.

On a long span bridge like the Akashi-Kaikyo, however, it can be expected that possibility of full

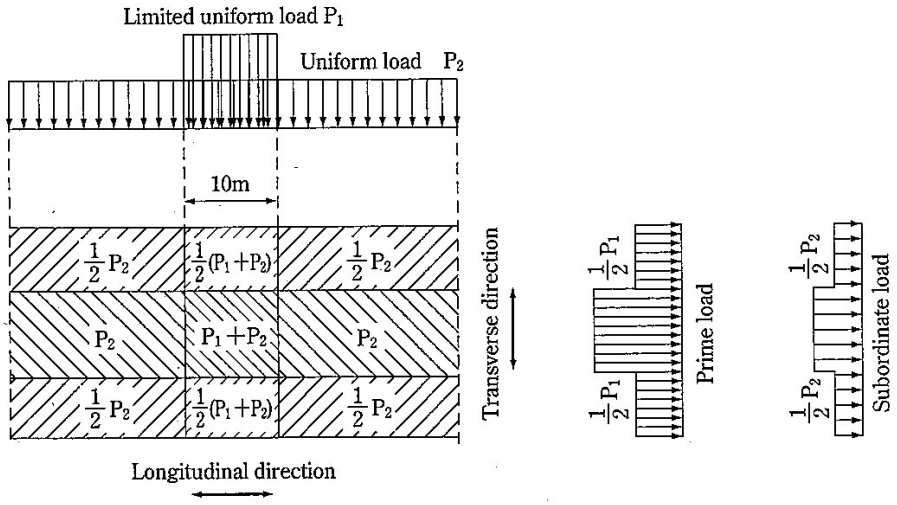

Fig.-4.1.7 Live load for Japanese highway bridge

Table-4.1.2 L-loading (B-loading)

Type		Span L (m)	Loading intensity
Prime load (Maximum loading width is 5.5 m)	Limited uniform load P_1 (up to 10 m in longitudinal direction)	$L \leqq 200$	For bending moment 1000 kgf/m² (10 KN/m²) For shearing force 1200 kgf/m² (12 KN/m²)
		$200 < L$	1200 kgf/m² (12 KN/m²)
	Uniform load P_2 (Other than above 10 m section)	$L \leqq 80$	350 kgf/m² (3.5 KN/m²)
		$80 < L \leqq 130$	430 - L kgf/m²
		$130 < L \leqq 500$	300 kgf/m² (3.0 KN/m²)
		$500 < L$	$300 \times [0.57 + 300/(200+L)]$
Subordinate load	p_1		Half of P_1
	p_2		Half of P_2

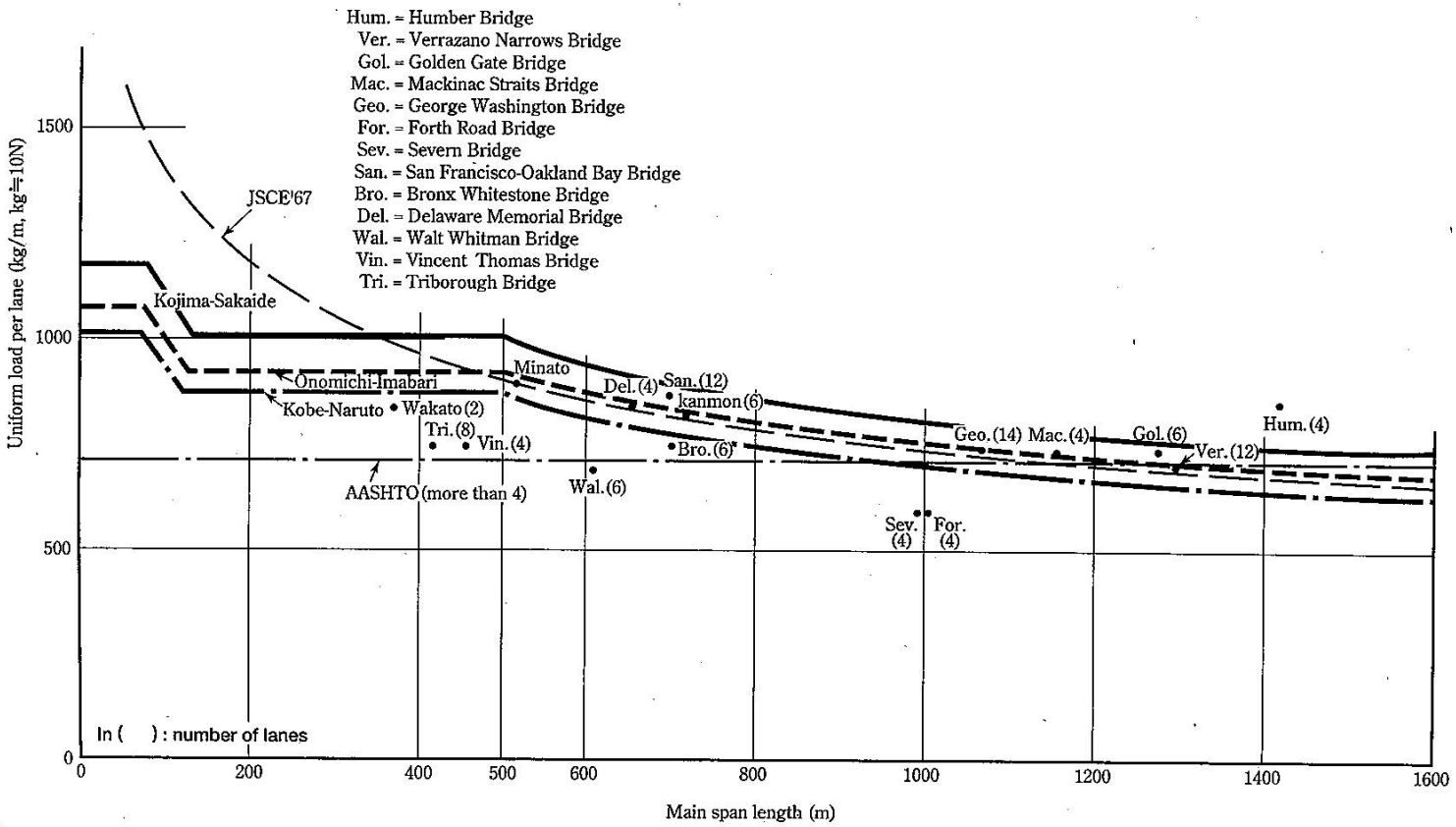

Fig.-4.1.8 Comparison of design live load per lane

loading of design live load, which is mainly specified for small span bridges, decreases. This natural tendency and reduction of the live load intensity had been pointed out and investigated probably since 1920's when the George Washington Bridge, the first bridge exceeding over 1000 m in span length, was in design stage.

The intensity of the distributing load for Honshu-Shikoku Bridges is specified to be decreased as the span length goes up as shown in Table-4.1.2 over the span range of 500 m, and this was determined mainly based on actual traffic surveys on heavy trunk roads.

Although the design live load in Japan is specified in bridge width basis, comparison with foreign bridges in lane basis which is equivalently converted is as shown in **Fig.-4.1.8**. Namely, no definite difference in tendency of the reduction is observed.

Table-4.1.3 Combination of various loads and increment of allowable stress

Combination of loads		Span>200m	Span≦200m
(1) Basic increment			
1	P	1.00	
2	D + L (F) + I (F)		
3[2]	P + T + SD[1] + E[1]	1.00	1.15
4[3]	W	1.50	1.20
5	D + W + T + SD[1] + E[1]	1.50 (1.35)[4]	1.35
6[5]	EQ	1.50	—
7[6]	D + EQ + L (EQ) + T + SD[1] + E[1]	1.50 (1.70)[4]	1.70
8	P + CO	1.70	
(2) Increment for erection stage			
9	ER (D + T)	1.25	
10	ER (D + T) + ER (W)	1.50	
11	ER (D + T) + ER (EQ)		

Marks:
P = D + L + T, D: Dead load, L: Live load, T: Influence of temperature change,
L(F): Live load to be considered for fatigue, I(F): Impact to be considered for fatigue,
SD: Influence of displacement of bearings, E: Error in erection, W: Wind load,
EQ: Influence of earthquake, L(EQ): Live load at earthquake = L/2,
CO: Collision of automobiles (Collision by ship is usually negligible)
ER(D+T): Dead load, temperature change, construction facility etc. during erection,
ER(W): Wind load during erection (usually W/2),
ER(EQ): Influence of earthquake deuring erection.

Notes:
1) Applicable to tower, stiffening girder and its bearings of suspension bridge as well as cable-stayed bridge.
2) SD shall not be considered to suspenders of suspension bridge.
3) Applicable to lateral bracing.
4) Applicable to other than main girder of any bridges other than suspension nor cable-stayed.
5) Applicable exclusively to lateral bracing of suspension or cable-stayed bridge.
6) For bridges having shorter span than 200 m, L(EQ) as well as combination of EQ and T can be neglected.

4.1.4 Combination of design loads and allowable stress

Specification about combination of the design loads and corresponding allowable stress is given in each design standard for such as superstructure, sub-structure, wind resistant design and so on. **Table-4.1.3** is quoted from the "Design Standard for Superstructure of Honshu-Shikoku Bridges, April 1989", which was examined and re-arranged for the Akashi-Kaikyo Bridge based on the experience at Seto-Ohashi Bridges up to 1100 m span length.

4.2 General Design of Akashi-Kaikyo Bridge

4.2.1 Basic design conditions

Though the basic design conditions of the Akashi-Kaikyo Bridge were discussed in Chapter 3, they are summarized as the following once again.

① The width of the straits is about 4 km, and its depth along the proposed bridge route reaches about 110 m.

② The natural conditions at the main pier site: water depth = 45 m, maximum tidal current = 4.0 m/s and maximum wave height = 9.4 m.

③ The wind condition: basic wind speed for design (defined as 10 minutes averaged speed at 10 m above the water level with a return period of 150 years) = 46 m/s and reference wind speed against flutter = 78 m/s

④ The geological condition: the base rock beneath the straits is granite, on which Kobe Formation (alternating layers of sand stone and mud-stone in the Miocene), Akashi Formation (semi consolidated sand and gravel layer in the late Pliocene and the early Pleistocene) and the alluvium layer are deposited.

⑤ The design earthquake: the one which occurs off the Pacific coast about 150 km away with the magnitude of 8.5 or the ones which are expected within radius of 300 km with a return period of 150 years, and

⑥ The social conditions: a waterway with 1500 m in the width and heavy sea traffic is designated amid the straits, and lands on both shores are highly utilized. The bridge is for 6-lane highway with design speed of 100 km/h.

4.2.2 Characteristics on design and construction

The Akashi-Kaikyo Bridge, therefore, has the following characteristics on design and construction (**Fig.-4.2.1, Photo-2 and 21**). However, its design is strongly influenced with the construction method, because design of a huge structure cannot but be done without consideration about the construction method and procedures.